

Non-linear block load corrections for dry docking

Thesis

Bart Jacobse

DAMEN SCHELDE NAVAL SHIPBUILDING



Non-linear block load corrections for dry docking

Thesis

by

Bart Jacobse

to obtain the degree of Master of Science
at the Delft University of Technology,
to be defended publicly on Tuesday July 9, 2021 at 10:00 AM.

Student number: 4738403
Project duration: September 1, 2020 – July 9, 2021
Thesis committee: Dr. A. Cicirello, TU Delft, Daily supervisor & Chair
Dr.Ir. G.J.P. Ravenshorst, TU Delft, Committee member
Ir. P. van der Male, TU Delft, Committee member
Dr. G. Lavidas, TU Delft, Committee member
Ir. W. Smalcerz, Damen Schelde Naval Shipbuilding, Industrial supervisor

This thesis is confidential and cannot be made public until December 31, 2023.

An electronic version of this thesis is available at <http://repository.tudelft.nl/>.

Abstract

Damen is designing more and more slender hull forms, which leads to a small dock block contact area, and therefore a high load on the block bed. Dry docking is achieved by using multiple blocks located along the longitudinal length of the ship. Dock blocks are constituted by several layers, normally three or more. The configuration of the block bed (concrete in combination with hard- and softwood) creates the support of the vessel with non-linear behaviour. This study focuses on a prediction of the block load in the dry dock, taking into account non-linear material behaviour of the timber layers.

Nowadays, the approach to predict the dock block load makes the assumption of linear-elastic behaviour of the timber layers. The loads produced can cause a non-linear behaviour of each block, which might lead to an over-stress failure of one or more blocks. The assumption of linear-elastic behaviour possibly results in wrong load distributions, which eventually leads to a re-distribution of the loads on the other blocks. In turn this can force other block failures and ultimately this produces damages of the hull forms. The consequences of a poor dry docking analysis are potentially catastrophic. A docking failure can lead to extensive ship and dock damage, disruption of docking schedules, and loss of the ship to active duty until repairs can be made.

Two set of models are conducted to predict the load on a dock block and evaluate the influence of the non-linear behaviour. The Timoshenko beam theory with multiple springs is used to calculate the load on every single dock block location. The load on every particular location is used in the model for a single dock block formed by elastically connected beams. A double Winkler foundation system represents the interaction of the stacked block layers and dictates the non-linear behaviour. Non-linear material properties are captured by the secant modulus of the top layer.

A test campaign pointed out that for each layer of nominal identical specimens a large variability in material properties is noticed. Material properties found in the literature were different from those obtained during experiments. Moisture content has a significant influence on linear and non-linear effect, with the Young's modulus and yield point being shifted to lower values. The variability in material behaviour and moisture content must be considered when predicting the block load. Moisture content variability lead to changing block bed load distributions. Underestimation of the moisture content can lead to large differences in the single dock block analysis.

With the good matching in the validation work, this research confirms the reliability of a double Winkler system to prescribe non-linear material behaviour of a single dock block. Although the analysis of a single dock block matches results obtained from finite element models, further research is still needed. The model of a Timoshenko beam on spring supports gives reasonable results, but underestimates the load in case of local increased stiffness caused by a transverse bulkhead. Optimization on this particular section is needed to get more realistic results.

Preface

This graduation thesis is a result of my research work in section offshore and dredging engineering at TU Delft.

The research was carried out in the DVU Group (Dynamics, Vibration and Uncertainty Group) in collaboration with Damen. Firstly, I want to give my appreciations to my chairman and daily supervisor Dr.A.Cicirello for the opportunity to work together for the last nine months. Dr.Cicirello helped me a lot with explaining her theories and giving valuable advice to me. She helped me to find the direction of the research instead of getting lost in the abundant calculations. I am grateful for the patient supervision and positive advice on my work from Ir.W.Smalcerz for countless times. He is always willing to share the knowledge on this topic and his valuable experience with me. His interest and insistence on this project motivate me to get through all the challenges in the process. I would like to thank Dr.ir. G.J.P. Ravenshorst who helped me on the test campaign and gave me a lot of insight in testing and material characterization.

My family deserves a particular note of thanks. Working in isolation in this time of pandemic was sometimes difficult and challenging. I would not have been able to complete this work without their unconditional encouragement and support. My deepest gratitude goes to my girlfriend. She is the only one that I can turn to for consolation at my tough moments. I am thankful for her patience to accept all the ups and downs in the last 9 months.

Last but not least, I would like to consider the three years in TU Delft as the most successful decision in my life so far. Working together with fellow students in this excellent academic environment was a special experience.

*Bart Jacobse
Delft, July 2021*

Contents

Abstract	iii
Preface	v
List of Figures	xi
List of Tables	xv
1 Introduction	1
1.1 Theoretical background	1
1.2 General objective & Research questions	1
1.2.1 Problem Statement	1
1.2.2 General docking information	2
1.2.3 Dry docking procedure	2
1.2.4 Objectives	3
1.2.5 Research Questions	4
1.3 Project Scope and Boundaries	4
1.4 Thesis outline	5
2 Review of dock blocks and materials used	7
2.1 Dock type and block overview	7
2.2 Variability in dock block configurations	10
2.2.1 Amels	10
2.2.2 Ritthem	11
2.2.3 Schiedam	11
2.2.4 Stellendam	11
2.3 Material characterization	12
2.3.1 Orthotropic nature of wood	12
2.3.2 Elastic properties	13
2.3.3 Common Properties	14
2.4 Material characterization analysis	15
2.5 Material characteristic values used at DSNS	16
2.6 Conclusion	18
3 Review of dock block static analysis: block loads and non-linear response	19
3.1 Block model methodology: to predict the deformation of the individual material layers	19
3.1.1 Empirical methods (for single dock block)	19
3.1.2 Numerical studies (for single dock block)	19
3.1.3 Analytical study: Euler-Bernoulli beam theory (for single dock block)	20
3.1.4 Analytical study: Winkler Foundation (representing floor-block interaction)	22
3.2 Ship model methodology: block load response as consequence of docking on multiple blocks	24
3.2.1 Empirical methods (for ship model)	24
3.2.2 Germanischer Lloyd SE	24
3.2.3 Crandall's trapezoidal method	24
3.2.4 Lloyd's register	25
3.2.5 Results of empirical studies	25
3.2.6 Numerical studies (for ship)	28
3.2.7 Analytical studies (for ship model)	29
3.2.8 Beam theory as interaction between ship and dock block	30

3.3	Conclusions	33
3.3.1	Block model methodology	33
3.3.2	Ship model methodology	33
4	Modelling of dock block and ship behaviour	35
4.1	Modelling of single dock block	35
4.1.1	Classical beam theory and introduction of the interaction parameter	35
4.1.2	Solution approach for a single dock block: double Winkler method	39
4.1.3	Parametric study for interaction foundation modulus	41
4.1.4	Final dock block deformation evaluation	41
4.2	Modelling of ship behaviour	42
4.2.1	Euler-Bernoulli model approach for ship	42
4.3	Conclusion	44
4.3.1	Single dock block model	44
4.3.2	Ship model	44
5	Validation of single dock block model and ship model	45
5.1	Validation of single dock block model	45
5.1.1	Validation of neglecting the Timoshenko shear effect for the single dock block model	45
5.1.2	Validation of limit case scenarios for the single dock block model	47
5.1.3	Validation of the boundary conditions for the single dock block model	48
5.1.4	Validation of the uniform distributed load for the single dock block load	49
5.1.5	Validation of single dock block with FE model	50
5.1.6	Validation of single dock block model with case study results	51
5.2	Validation of ship model with case study on a patrol ship (PS).	53
5.2.1	Validation of the ship model by using the Euler-Bernoulli theory	53
5.2.2	Validation of the Timoshenko shear effect in the ship model	54
5.2.3	Validation of the ship model by using the Timoshenko theory	55
5.2.4	Validation the Timoshenko theory with the existing tool from Bedert.	56
5.2.5	Timoshenko theory with optimized input parameters	57
5.3	Conclusions.	58
5.3.1	Conclusion for the model of a single dock block	58
5.3.2	Conclusion for the ship model	58
6	Characterization of the material properties of the dock block layers	59
6.1	Why testing?	59
6.1.1	Importance of testing	59
6.2	Studies on compression tests perpendicular to the grain.	60
6.3	Test requirements, limitations and preparation	61
6.3.1	Test dimensions and size effects	62
6.3.2	Dimension check	63
6.3.3	Moisture content	63
6.3.4	Density	64
6.3.5	Expected failure mechanism during compression of a stacked dock block	64
6.3.6	Specimen status	65
6.3.7	Statistical terms.	65
6.4	Compression test procedure.	66
6.4.1	Creep test on material combinations	66
6.4.2	Test overview and flowchart	66
6.5	Individual material test results	66
6.5.1	Young's Modulus in linear range (individual material test)	66
6.5.2	Young's Modulus in non-linear range (individual material test).	69
6.5.3	Yield point (individual material test)	71
6.6	Material combination test results	72
6.6.1	Young's Modulus in linear range (material combination test).	72
6.6.2	Young's Modulus in non-linear range (material combination test)	73
6.6.3	Yield point (material combination test).	73

6.7	Creep test results	73
6.8	Secant modulus	75
6.9	Conclusions	76
7	Effect of material variability on dry docking solutions	77
7.1	Validation of model with test results	77
7.2	Solution approach to check material variability	78
7.3	Material variability effect of moisture content on the obtained models	79
7.3.1	Material variability effect of moisture content on the obtained models in worst case scenario	81
7.4	Material variability effect of different material layers on the obtained models	82
7.4.1	Material variability effect of different material layers with linear properties	83
7.4.2	Material variability effect of different material layers on the obtained models with non-linear material properties	84
7.5	Conclusion	86
8	Conclusions and Recommendations	87
8.1	Conclusions	87
8.2	Recommendations	89
A	Common strength properties	91
B	Modelling of dock block and ship behaviour	93
B.1	Derivation of the expression for the deformation of the beam on elastic foundation	93
B.2	Matlab script for single dock block model	96
B.3	Matlab script for complete model	101
B.3.1	Run file for the model.	101
B.3.2	Input file for the model	104
B.3.3	Reaction force file for the model	106
B.3.4	Strain file for the model.	110
B.3.5	ODE file for the model	113
C	Validation	115
D	Test results	123
	Bibliography	145

List of Figures

1.1	Over-stress failure due to a minimized contact area in the fore of the ship. Complete failure of the softwood is the consequence of the small contact area. (DAMEN yard, Ritthem)	2
1.2	Flow diagram of the thesis	6
2.1	Graving dry dock (Damen yard, Schiedam)	7
2.2	Floating dry dock (Damen yard, Stellendam)	8
2.3	Sketch of single dock block (bottom is hardwood and the top is a softwood)	9
2.4	Overview of ship on multiple dock blocks, here the concrete is introduced to increase a sufficient height.	9
2.5	Transverse view (or section)	9
2.6	Longitudinal view	9
2.7	Larger effective contact area by placing a steel plate on the dock block. Here the 45° method, used at DSNS, is introduced.	10
2.8	Amels dock block (photo)	10
2.9	Amels dock block (sketch)	10
2.10	Ritthem dock block (photo)	11
2.11	Ritthem dock block (sketch)	11
2.12	Schiedam dock block (photo)	11
2.13	Schiedam dock block (sketch)	11
2.14	Stellendam dock block (photo)	12
2.15	Stellendam dock block (damage)	12
2.16	Direction of load in relation to direction of annual growth rings: 90° or perpendicular (R), 45°, 0° or parallel (T). [29]	13
2.17	Three principal axes of wood with respect to grain direction and growth rings [32]	13
2.18	Force-Displacement relation where the first region is denoted as elastic behaviour, and the second region to plastic behaviour.	14
2.19	Stress-Strain relation where the slope of this curve results in the Young's modulus. Stress and strain are related to the force displacement parameters.	14
2.20	Stress-Strain curve pinewood [41]	17
3.1	Finite Element analysis of single dock block (overview)	20
3.2	Dock block modelled as a component that is designed to support transverse loads ($q(x)$), that is, loads that act perpendicular to the longitudinal axis of the beam. The beam supports the load by bending only and lead to a deformation $W(x)$ along this longitudinal axis.	20
3.3	(a) Beam undergoing transverse motion and (b) differential element of the beam subject to the shear force, bending moment and external load [36]	21
3.4	Beam on elastic foundation representing the interaction (springs) of the timber layers with the rigid concrete foundation.	22
3.5	Double Winkler foundation: k_{d1} is the interaction between the individual timber layers, k_{d2} is the interaction between the rigid ground and the bottom timber layer.	23
3.6	Crandall's principle [47]	24
3.7	Crandall's principle with interrupted keel bearing [47]	25
3.8	Lloyds's register principle [33]	25
3.9	YN18801 yacht fully meshed in FEM software (NX9 Siemens) while standing on dock blocks [16]	26
3.10	Dock block reactions retrieved by FEM for the YN18801 [16]	26
3.11	Dock block reactions retrieved by FEM for the Germanischer Lloyd principle [16]	27

3.12 Dock block reactions retrieved by FEM for the Crandall principle [16]	27
3.13 Dock block reactions retrieved by FEM for the Lloyds Register principle [16]	28
3.14 Finite Element Model of Damen Patrol Ship	29
3.15 Beam theory on multiple spring representing the interaction between the dock blocks and the ship	30
3.16 Principle of beam theory	31
3.17 Dock block reactions retrieved by FEM for the Euler-Bernoulli principle [16]	32
3.18 Dock block reactions retrieved by FEM for the Timoshenko principle [16]	32
4.1 Sign convention for: Displacements, applied loads and internal forces when using beam theories	35
4.2 Euler-Bernoulli boundary conditions (W =deflection, ϕ =slope, M =moment and V =shear) [36]	37
4.3 Euler-Bernoulli boundary and interface conditions for a partly uniform distributed load (load is located between abscissa x_{q1} and x_{q1})	37
4.4 Characterization of interaction parameter k_d for the deflection diagram of a pinned-pinned boundary condition	38
4.5 Illustration of the model representing two material layers with a double elastic foundation connecting them	39
4.6 Segmentation view of ship model with 3 springs representing the dock blocks located at x_1, x_3 and x_4	43
5.1 Deflection graph to check the influence of the Timoshenko shear deflection for a pinned-pinned boundary condition	46
5.2 Limit case 1 for double elastic foundation beam deflection and pinned-pinned boundary conditions	48
5.3 Limit case 2 for double elastic foundation beam deflection and pinned-pinned boundary conditions	48
5.4 Limit case 3 for double elastic foundation beam deflection and pinned-pinned boundary conditions	48
5.5 Limit case 4 for double elastic foundation beam deflection and pinned-pinned boundary conditions	48
5.6 Deformation graph for Free-Free boundary conditions with two elastic layers	49
5.7 Deformation graph for Pinned-Pinned boundary conditions with two elastic layers	49
5.8 Pinned-Pinned boundary conditions - partly uniform distributed load between $x_{q1} = 100$ and $x_{q2} = 700$ with total block length of 800	50
5.9 Pinned-Pinned boundary conditions - partly uniform distributed load between $x_{q1} = 300$ and $x_{q2} = 900$ with total block length of 1200	50
5.10 Validation of the deformation of a stacked block with FE software (FEMAP) for a practical configuration	51
5.11 Patrol ship weight distribution	53
5.12 Validation of the ship model reaction force with the Euler-Bernoulli theory	54
5.13 Deflection curve for the 5 segments with Euler-Bernoulli	55
5.14 Deflection curve for the 5 segments with Timoshenko ($G=0.1$)	55
5.15 Deflection curve for the 5 segments with Timoshenko ($G=1$)	55
5.16 Deflection curve for the 5 segments with Timoshenko ($G=100$)	55
5.17 Validation of the ship model reaction force with the Timoshenko theory	56
5.18 Validation of the ship model reaction force with the Bedert report	57
5.19 Validation of the ship model reaction force, Bedert vs Jacobse	58
6.1 Block dimensions with respect to the load perpendicular to the grain	62
6.2 Cracking failure mechanism	65
6.3 Compression failure mechanism	65
6.4 Total force displacement - SON	67
6.5 Total stress strain - SON	67
6.6 Linear force displacement range - SON	68
6.7 Linear stress strain range - SON	68

6.8	Stress-Strain for ALN and ALO - linear range	69
6.9	CV vs MC for E-modulus in the linear range	69
6.10	Non-linear force displacement range - SON	70
6.11	Non-linear stress strain range - SON	70
6.12	Stress-Strain for ALN and ALO - non-linear range	71
6.13	CV vs MC for E-modulus in the non-linear range	71
6.14	SON yield point	71
6.15	Displacement time graph for creep	74
6.16	Secant modulus for SON	75
7.1	Deformation picture as result of compression a combination of Azobe and Spruce	77
7.2	Deformation picture as result of compression a combination of Oak and Spruce	77
7.3	Influence of moisture content variability with respect to the dock block reaction force	80
7.4	Influence of moisture content variability with respect to the dock block strain for softwood	81
7.5	Influence of moisture content variability with respect to the dock block strain for hardwood	81
7.6	Influence of moisture content variability with respect to the dock block strain for softwood in a worst case scenario	82
7.7	Influence of moisture content variability with respect to the dock block strain for hardwood in a worst case scenario	82
7.8	Influence of different material layers on dock block reaction force response	83
7.9	Influence of different material layers on dock block softwood strain response	84
7.10	Influence of different material layers on dock block hardwood strain response	84
7.11	Influence of different material layers on dock block reaction force response with non-linear softwood properties	85
7.12	Influence of different material layers on dock block softwood strain response with non-linear softwood properties	86
7.13	Influence of different material layers on dock block hardwood strain response with non-linear softwood properties	86
B.1	Matlab code for single dock block pressure and deflection 1	96
B.2	Matlab code for single dock block pressure and deflection 2	97
B.3	Matlab code for single dock block pressure and deflection 3	98
B.4	Matlab code for single dock block pressure and deflection 4	99
B.5	Matlab code for complete analyse - Runfile page 1/2	101
B.6	Matlab code for complete analyse - Runfile page 2/2	102
B.7	Matlab code for complete analyse - Inputfile	104
B.8	Matlab code for complete analyse - Reaction force file page 1/3	106
B.9	Matlab code for complete analyse - Reaction force file page 2/3	107
B.10	Matlab code for complete analyse - Reaction force file page 3/3	108
B.11	Matlab code for complete analyse - Strain file page 1/2	110
B.12	Matlab code for complete analyse - Strain file page 2/2	111
B.13	Matlab code for complete analyse - ODE file	113
C.1	Dockplan for a patrol ship	121
D.1	Flowchart for test plan	124
D.2	Test overview individual material tests	125
D.3	Test overview material combination tests	126
D.4	Test overview creep tests	127
D.5	ALN force displacement graph	128
D.6	ALN stress strain graph	128
D.7	ALN stress strain graph for elastic range	128
D.8	ALN stress strain graph for plastic range	128
D.9	ALO force displacement graph	129
D.10	ALO stress strain graph	129
D.11	ALO stress strain graph for elastic range	129
D.12	ALO stress strain graph for plastic range	129

D.13 AOO force displacement graph	130
D.14 AOO stress strain graph	130
D.15 AOO stress strain graph for elastic range	130
D.16 AOO stress strain graph for plastic range	130
D.17 RAN force displacement graph	131
D.18 RAN stress strain graph	131
D.19 RAN stress strain graph for elastic range	131
D.20 RAN stress strain graph for plastic range	131
D.21 RPN force displacement graph	132
D.22 RPN stress strain graph	132
D.23 RPN stress strain graph for elastic range	132
D.24 RPN stress strain graph for plastic range	132
D.25 RSN force displacement graph	133
D.26 RSN stress strain graph	133
D.27 RSN stress strain graph for elastic range	133
D.28 RSN stress strain graph for plastic range	133
D.29 SON force displacement graph	134
D.30 SON stress strain graph	134
D.31 SON stress strain graph for elastic range	134
D.32 SON stress strain graph for plastic range	134
D.33 SSN force displacement graph	135
D.34 SSN stress strain graph	135
D.35 SSN stress strain graph for elastic range	135
D.36 SSN stress strain graph for plastic range	135
D.37 Compression of Azobe (RAN)	136
D.38 Compression of Oak (AOO)	136
D.39 Compression of Oak (SON)	136
D.40 Compression of Pine (RPN)	136
D.41 Compression of LVL (ALN ALO)	136
D.42 Compression of Spruce (RSN)	136
D.43 Compression of Spruce (SSN1)	136
D.44 Compression of Spruce (SSN2)	136
D.45 AOOALN and AOOALO force displacement graph	139
D.46 AOOALN and AOOALO stress strain graph	139
D.47 RANRPN force displacement graph	139
D.48 RANRPN stress strain graph	139
D.49 RANRSN force displacement graph	140
D.50 RANRSN stress strain graph	140
D.51 SONSSN force displacement graph	140
D.52 SONSSN stress strain graph	140
D.53 Compression of Azobe and Pine (RAN RPN)	141
D.54 Compression of Azobe and Spruce (RAN RSN)	141
D.55 Compression of Oak and LVL (AOO ALN)	141
D.56 Compression of Oak and LVL (AOO ALO)	141
D.57 Compression of Oak and Spruce 1 (SON SSN1)	141
D.58 Compression of Oak and Spruce 2 (SON SSN2)	141
D.59 Force displacement graph for creep	142
D.60 Creep 1 AOO1D ALN3C	143
D.61 Creep 2 AOO6A ALO1D	143
D.62 Creep 3 AOO5B ALO1E	143
D.63 Creep 4 AOO5A ALN4C	143
D.64 Creep 5 AOO6C ALO3D	144
D.65 Creep 6 SON2B SSN1D	144
D.66 Creep 7 RAN2D RSN2D	144
D.67 Creep 8 AOO2D ALO1E Fail	144

List of Tables

2.1	Characteristic values according to EN 338 [12] and Centrum-hout [51]	14
2.2	Young's modulus pinewood test	17
2.3	Material properties based on Amels' experience	17
4.1	Boundary and interface conditions for Euler-Bernoulli beam (Pinned-Pinned)	38
4.2	Characterization of interaction parameter k_d	38
4.3	Boundary and interface conditions	43
5.1	Difference between deflection of Euler-Bernoulli theory and Timoshenko theory for numerical application	46
5.2	Results for boundary condition scenarios	49
5.3	Results for boundary condition scenarios - partly uniform distributed load	50
5.4	Validation results for FE analysis compared to the single dock block model	51
5.5	Material deformation for both the existing tool as the new tool	52
5.6	Evaluating the maximum allowable strain for the softwood, hardwood and blockload tool	52
5.7	Spring reaction forces for model with 5 segments	55
5.8	Shear area for a patrol ship according to [7]	56
5.9	Inertia and shear area for a patrol ship according to [7]	57
6.1	Results from Nobel [39]	60
6.2	Results from Dolganov [17]	61
6.3	Results from Ali et al. [5]	61
6.4	Dimensions of structural timber according to norm EN 408	62
6.5	Test sample dimensions	63
6.6	Material labels	63
6.7	Maximum sample dimensions	63
6.8	Ratios of wet to dry bearing stresses [35]	64
6.9	Moisture content and density	64
6.10	Young's Modulus (E_{\perp}) perpendicular to the grain in the linear range	68
6.11	Young's Modulus (E_{\perp}) perpendicular to the grain in the non-linear range	70
6.12	Yield point and CV for material specimen on individual compression tests	72
6.13	Young's Modulus (E_{\perp}) for material combinations in the non-linear range (w.r.t analytical approach)	72
6.14	Young's Modulus (E_{\perp}) for material combinations in the linear range (w.r.t analytical approach)	73
6.15	Yield point for material specimen on combination compression tests	73
6.16	Creep test results	74
6.17	Second modulus values	76
7.1	Displacement results for combination of Azobe (RAN) and Pine (RPN)	78
7.2	Young's moduli for case study: hardwood, softwood and equivalent	79
7.3	Yield strain point for specimens with different moisture content	80
7.4	Input values for the effect on different material layers with linear characteristics	83
7.5	Input values for the effect on different material layers with non-linear characteristics	85
C.1	Weight distribution per frame and location for the patrol ship	116
C.2	Weight distribution per frame and location for the patrol ship	117
C.3	Input values for deflection calculation of dock block material layers	118
D.1	Characteristic values for individual materials	137

D.2 Yield point values for individual materials 138

List of Symbols

Physics Constants

Δ	Displacement (in Force-Displacement relation)	[m]
ϵ_{\perp}	Strain perpendicular to grain	[-]
ϵ_{\parallel}	Strain parallel to grain	[-]
κ	Timoshenko shear coefficient	[m]
ν	Poisson ratio	[-]
ω	Moisture content (MC)	[%]
\bar{x}	Mean value in statistics	[-]
σ	Standard deviation	[-]
σ	Stress	[N/m ²]
ρ	Density (characteristic value)	[kg/m ³]
A	Cross-sectional area of keel block	[m ²]
A_{eff}	Effective contact area	[m ²]
b	Specimen or beam width	[m]
b_{keel}	Keel width	[m]
CV	Coefficient of variance	[%]
d	Distance of plate floors adjacent to the transverse bulkheads	[m]
d_{KB}	Spacing between the dock blocks	[m]
E_{\perp}	Modulus of Elasticity perpendicular to grain	[N/m ²]
E_{\parallel}	Modulus of Elasticity parallel to grain	[N/m ²]
E_a	Apparent Modulus of Elasticity	[N/m ²]
E_{eq}	Equivalent modulus of elasticity	[N/m ²]
E_{sec}	Secant modulus of elasticity	[N/m ²]
E_s	Modulus of elasticity for the ship	[N/m ²]
F	Applied Load	[N]
F_{\perp}	Applied Load perpendicular to grain	[N]
f_m	Bending strength	[N/m ²]
$f_{c,\perp}$	Compressive strength perpendicular to grain	[N/m ²]
$f_{c,\parallel}$	Compressive strength parallel to grain	[N/m ²]
$F_{cap,max}$	Hydraulic test machine capacity	[N]

G	Shear modulus	$[N/m^2]$
g	Gravitational Constant	$[m/s^2]$
h	Specimen or beam height	$[m]$
I	Moment of Inertia	$[m^4]$
I_s	Area moment of inertia of ship	$[m^4]$
K	Dock block stiffness	$[N/m]$
k_d	Dock block interaction parameter	$[N/m^2]$
l	Specimen or beam length	$[m]$
m_0	Mass of of the oven dry test slice	$[kg]$
m_1	Mass of the test slice before drying	$[kg]$
N	Number of tests	$[-]$
P	Block pressure	$[N/m^2]$
q	Nominal keel block load	$[N/m]$
W	Deformation (of beam/timber)	$[m]$
W_s	Total ship displacement	$[m]$
W_{KB}	Weight distribution over keel block	$[N/m]$
x_b	Keel block location in reference to the start of the keel	$[m]$
x_f	Ship location in reference to the start of the keel	$[m]$
x_s	Ship section location in reference to the start of the keel	$[m]$

Acronyms

ASTM American Society for Testing and Materials. 64

DSNS Damen Schelde Naval Shipbuilding. 1, 4

FEM Finite Element Method. 3

LR Lloyd's Register. 25

MOE Modulus of Elasticity. 12

Introduction

1.1. Theoretical background

“Damen Schelde Naval Shipbuilding” (DSNS) is specialized in the design of naval ships and complex commercial vessels. DSNS is designing more and more slender hull forms, especially in the aft of a ship where the propeller performance is optimized. The complexity is even more increasing while the hull forms are getting more complex and the proliferation of unusually shaped appendages such as sonar domes make the application of traditional docking methods more difficult. Due to slender hull forms the contact area between the keel of the ship and the dock blocks are minimized which increases the occurring loads during dry docking. This minimized contact area and consequent increased load can lead to dock block failure, and ultimately this produces damage of the hull. A smaller contact area results in higher local pressure on the dock block, and increasing failure possibility due to this load concentration.

Dry docking is achieved by using multiple blocks located along the longitudinal length of the ship. Dock blocks are constituted by several layers, normally three or more. Due to the configuration of the block bed (concrete in combination with hard- and softwood), the support of the vessel is created with non-linear behaviour. So, the wood pressure has to be within the limits of the soft- and hard wood. Moreover, this information is needed to estimate the docking loads correctly, especially in the fore- and aft end of the vessels. Additionally, the characterization of the block configuration is an important factor to consider.

1.2. General objective & Research questions

1.2.1. Problem Statement

The consequences of a poor dry docking analysis are potentially catastrophic. Dock block failure while a ship is dry docked can cause not only loss of life, but also enormous economic losses. A docking failure can lead to extensive ship and dock damage, disruption of docking schedules, and loss of the ship to active duty until repairs can be made. At DSNS they make use of a linear approach [7], hereby the assumption of linear-elastic deformation is made. During dry docking, the loads produced can cause a non-linear behaviour of each block, which might lead to an over-stress failure of one or more blocks (Figure 1.1). This leads to crushing and damage to the hard wood. Besides the non-linear material behaviour, the existing model does not take into account the interaction between individual material layers. As the soft wood is a relative cheap material the damage is not of importance (sacrificial material), the damage at the hard wood however is expensive and should be prevented, but in the end it can lead to a loss of stability as well. The block failure leads to a re-distribution of the loads on the other blocks, which can lead to more block failures.



Figure 1.1: Over-stress failure due to a minimized contact area in the fore of the ship. Complete failure of the softwood is the consequence of the small contact area. (DAMEN yard, Ritthem)

1.2.2. General docking information

The origin of dry-docking comes from the early Egyptians, who were the first to repair their vessel by docking their ships. Floating their ships into shallow basins, and build a dam at the entrance. All this was done by slaves who also scooped the water out using containers and waterwheels [26]. In this section a basic understanding is provided of how a dock is designed, and a summary of the materials mostly used for typical dock block configurations is provided. Insight in the dock type, the dock procedure and the dock block materials are fundamental for this in-depth analysis. By starting with a general overview of the docking procedure and material properties, and ending with specific dock block material parameters, the full spectrum is described.

1.2.3. Dry docking procedure

Dry docking is usually used for ship maintenance or repair and is therefore a very important procedure. The first objective of docking is to show the parts of a vessel that are submerged underwater for a protracted time. So as to urge to the present position a strict dock plan for every vessel is dispensed following these steps [1] [2] :

- Phase 1: Pre-docking preparation
The process of dry docking of a ship must be planned meticulously. Days before a ship is to be dry docked, the dock master will prepare a docking plan, taking into consideration all the minute details of the structure of the ship, i.e. hull structure of the ship, locations of the drain plugs, and echo sounders beneath the ship to not damage them during docking the ship.
- Phase 2: Preparing a docking plan
The process of dry docking of a ship must be carefully planned to be executed with ease. Dock masters and designers take aid of a series of sketches and detailed calculations about the ship's height, weight, and structure. The docking plan explains a way to successfully dock the ship and how to simply undock it. It also reduces the danger of a ship capsizing during undocking. From the docking plan the dock master wants to know:

- Hull structure so he/she can arrange the blocks to support the ship's hull
- Locations of transducers for log and echo sounders so these do not come beneath blocks
- Location of sea chests and drain plugs for the identical reason
- Phase 3: Understanding the stability conditions
It is imperative for the ship to be stable while docking. The weight distribution of the ship that is to be docked has to be calculated accurately. Since almost the complete weight of the ship is borne by the keel blocks, the slightest error in the calculations of the stability conditions can lead to a mishap. Hence, the stability condition of the ship is analyzed perfectly before the particular process begins.
- Phase 4: Arrival dry-docking port
The ship must adhere to any or all the stability conditions on its arrival to the dry-docking port. The propeller of the ship also has to be immersed and also the ship must have the smallest amount ballast. It is best to avoid dry docking if there is an opportunity of a rough weather. The cleaners and dock master then board the vessel.
- Phase 5: Docking of the vessel
Once the ship has successfully achieved the pre-docking conditions, the ship is to be tugged into the dock since its engine is not available. When the ship is inside the docks, the ship is moored and made secure. The crew then takes over and starts pumping out dock water, running the ballast pump, and removing the drain plugs, amongst other cleaning procedures.

1.2.4. Objectives

Taking the aforementioned into account, the main objective of this thesis is to:

Define 'non-linear block load corrections for dry docking' and represent this in a model to predict and verify reliable loads.

Finding these non-linear corrections would make it possible to analyse the problem, and to overcome the limitations inherent in existing methods. In doing so it is aimed to achieve:

- Literature Study:
 - To develop an understanding of dry docking
 - To relevant material behaviour and areas for improvement, to identify important parameters
 - To identify solution approaches, and gaps in current models
- Test block specimens that are used in the yards of Damen, and verify these with the literature values. In case there is information regarding FEM¹ analysis found in the literature this can also be used as validation.
 - Investigate the non-linear properties of the materials
- Generation of knowledge and insight in the physics involved in dock block loading leading to an improved model strategy
- Develop a methodology to quantify the load acting on the dock blocks in terms of non-linear behaviour
- Application of the proposed methodology:
 - Each individual block position
 - Individual block deformation
 - Validation of the proposed approach

¹The finite element method (FEM) is the most widely used method for solving problems of engineering and mathematical models. Typical problem areas of interest include the traditional fields of structural analysis, heat transfer, fluid flow, mass transport, and electromagnetic potential. The FEM is a particular numerical method for solving partial differential equations in two or three space variables (i.e., some boundary value problems) [3]

1.2.5. Research Questions

From the problem statement and the associated objectives, the following research questions arises:

How does non-linear material behaviour influence the drydock block load and how can this be predicted?

To answer this question the following sub-questions are formulated:

- What materials are involved in dock blocks and what properties influence the load acting on the block and how is this calculated and distributed?
- How should one model the interaction between the individual material layers to get a representation of the physical compression effect?
- How should one model the interaction between the ship and the dock block to get a realistic but still practical result?
- What are the similarities and differences between the test results and the theoretical values of mechanical properties?
- What affect has the non-linear material behaviour in the obtained tool with respect to the linear tool used at the DSNS engineering?

1.3. Project Scope and Boundaries

This thesis is intended to achieve the objectives and answer the questions posed above, here validation is among the scope of the project. Included in this thesis scope are material characterization and a model development to account for the dock block loads. To get a realistic result one should account for non-linear material behaviour, ships overhang, uniform weight distribution and non-rigid ship hull. Possible earthquakes or extreme wind conditions are neglected for this study. The study of the block load corrections is at the situation where the vessel is already docked, this means that there is a static equilibrium. The so-called critical period, when the ship is in the docking phase and the aft of the ship touches the first dock block, resulting in a change of the metacentric height is not in the scope of this thesis. The weight distribution of the ship is given as an input by DSNS and is known. The model is based on a dry dock with the assumption that the dock floor is endless rigid. Full scale testing of a ship on dock blocks is a rather difficult and expensive process and therefore no possibility.

For linear material behaviour a model is developed, this to make an estimation of the block loads in an early stage (Bedert [7]). This tool makes a good estimation for the mid-ship but is inaccurate at the fore and aft of the ship (due to the overhang). Material properties in literature are obtained by testing, however, these results are not applicable in the described docking situation. Average values in literature such as the Wood Handbook [32] do not account for large specimen with possible imperfections (knots, splits etc.), besides the load direction is almost always parallel to the grain (instead of the perpendicular load on dock blocks).

To verify and validate the literature study on materials a test case with frequently used specimens from the yard will be set up. This test is focused on the non-linear behaviour, here the Young's modulus (perpendicular to the grain) is the most important parameter. Variability of material properties need to be included in the obtained model to evaluate different scenarios. The innovation in this thesis is to get an encompassing insight in the parameters involved when dry docking a ship, and to capture compression interaction phenomena with mathematical expressions. In order to get to this insight a model will be developed in which these parameters are implemented. Validation will be done by literature analysis, and a showcase on a DSNS vessel. A final analysis will be done by comparing results of the model (with non-linear phenomena) and the dock block tool used at DSNS. FE results are known at Damen and also considered for validation.

1.4. Thesis outline

The way to go about attaining the objectives and answering the research questions is visualized in the flowchart in figure 1.2.

- The introduction (chapter 1) where the problem is defined, the objectives, research questions and scope are formulated.
- Chapter 2 is focused on the literature study and a full gap identification of the dock block. Here the functionality of the block, the configuration with different layers and materials of these layers are described. Yard investigation is described to show the variability of different configurations and different materials within the company Damen.
- Chapter 3 gives a review of the dock block static analysis. The first objective in this chapter is to identify the different solution approaches regarding the individual block layer deformations on one single dock block. Second objective is to see how the ship resting on a sequence of blocks interact and how this model should predict the consequent loads on the single dock block. Finally, the gap identification for both blocks lead to a conclusion on the shortcomings and an preliminary concept of the new models.
- Chapter 4 gives a full description of the preliminary concepts described in the model review. Here all the important mathematical expressions, assumptions and derivations are explained.
- Chapter 5 is the validation of the obtained models from chapter 4. Using limit cases and validation for both block configuration as ship model will be discussed and evaluated.
- Chapter 6 gives the needed input data for both models. Studying the input values lead to necessary tests which are discussed and characterized. After a material characterization the results are discussed, and a conclusion on the variability is given.
- Chapter 8 gives a critical review on the work done, here conclusions are summarized and recommendations for future work are explained.

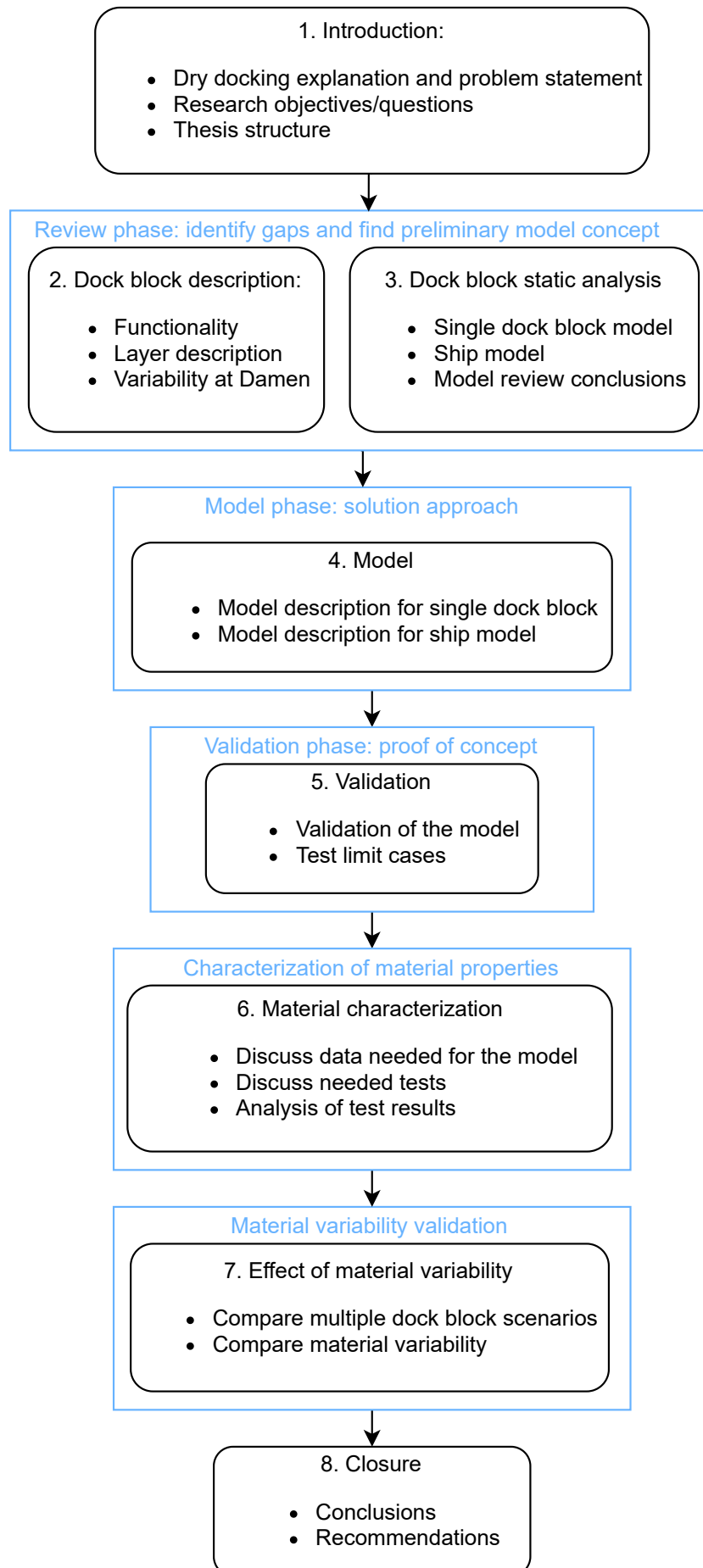


Figure 1.2: Flow diagram of the thesis

2

Review of dock blocks and materials used

This chapter gives an overview of the functionality of a dock block, the different layers, and the variability of dock blocks at Damen.

2.1. Dock type and block overview

One of the oldest and common type of dry docking is the basin or graving dock [26]. These large, fixed basins built into the bottom at water's edge, separated from the water by a dock gate. A graving dock can dock all sizes of vessels and are therefore widely used. Its basic structure consists of a floor, sidewalls, head wall and a dock gate (see Figure 2.1). Because graving dock is a permanent structure, it has many advantages and downsides. One advantage is that a graving dock provides a virtually rigid surface on which to dry dock ships. Another one is that it is usually located at a repair facility, which provides access to shops and factories. A drawback is that a graving dock cannot be relocated to the positioning of upcoming work.



Figure 2.1: Graving dry dock (Damen yard, Schiedam)

Floating dry docks are another commonly used type of dry dock [26]. Floating dry docks are structures with sufficient dimensions, strength, displacement, and stability to lift a vessel from the water using buoyancy. Floating dry docks are usually constructed similar to a rectangular barge with walls on each

side that run the length of the dry dock (see Figure 2.2). Beneath the pontoon deck of a floating dry dock are many ballast tanks, which can be filled in to lower the dry dock below the free surface and vice-versa. This allows the floating dry dock to accommodate an incoming vessel. One major disadvantage of floating dry docks is that there are many maintenance problems, including corrosion.



Figure 2.2: Floating dry dock (Damen yard, Stellendam)

Apart from graving docks and floating docks, ships can also be dry-docked and launched by more alternative docking systems [4]: marine railways, vertical lifts, and marine travel lifts. In this thesis, only graving docks will be discussed because of their ability to provide a nearly rigid surface for the dock blocks to rest on. Besides the rigid surface, this method is mostly used and therefore leading.

The main purpose of the blocks is to ensure the vessel is sufficiently supported for the complete time the vessel is in the dock. Also, each block should be capable of severe overload without failure. The stability of the block is of the identical importance than the strength, the blocks must not have any tendency to maneuver under load. Proper sizing and arrangement of those blocks prevent stability problems and is therefore a very important factor. A properly built blocking system will [25]:

- Support the vertical loads imparted by the vessel in the slightest degree phases of docking without crushing of the timbers or deformation of the hull
- Provide stability to stop the vessel from tipping over in high winds, earthquakes, or shifting of weights on board of the vessel (not a part of this study)
- Provide a cushion to distribute load concentrations caused by hull distortions, or errors in block height, position or contours.
- Leave the maximum amount of room as possible under the vessel free from obstructions to ease cleaning, painting and/or repair of the hull.

Virtually all shipyards which dock ships use the same dock block materials, softwood and hardwood (timbers). Concrete is employed within the base of most of the blocking piers; however, the timber products comprise the upper portion of the blocking system, which is in contact with the ship. The softwood is used in a "soft cap" on top of the hardwood to protect the hull from stress concentrations. The timber provides the elasticity needed in the system to permit for irregularities in the hull or small errors in block height or position without unduly overloading the vessel's hull or the dry dock structure. Typically, the softwood used in drydock blocking systems is a Spruce, and the hardwood an Oak. The capping and hardwood materials that shipyards receive have highly variable properties. Spruce is the principle use for the dock block top layer, this because of its availability, work ability with simple tools, and strength properties [37].

To prevent mistakes with conventions and dimensions figures 2.3, 2.4, 2.5 and 2.6 give an overview of the dock block with respect to the ships orientation. Here the transverse view gives the width (b) of the ship and block and the longitudinal view gives the length (l) of the ship and block. Specific dimensions will be discussed in the next section, there is one point that needs some attention beforehand. The hardwood in figure 2.3 is built of two hardwood layers, both with a specific wedge design to adjust the height when placing the blocks. This typical wedge form is only used at the Amels department of Damen. For modelling purpose the hardwood layer is assumed as one solid layer of a homogeneous material.

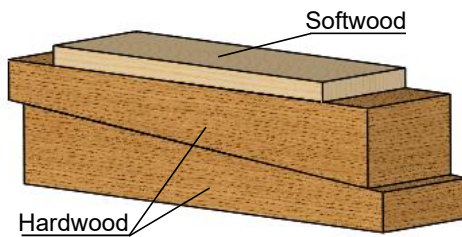


Figure 2.3: Sketch of single dock block (bottom is hardwood and the top is a softwood)

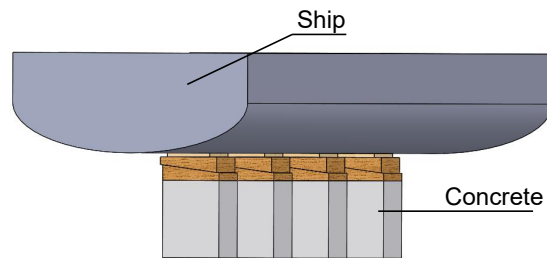


Figure 2.4: Overview of ship on multiple dock blocks, here the concrete is introduced to increase a sufficient height.

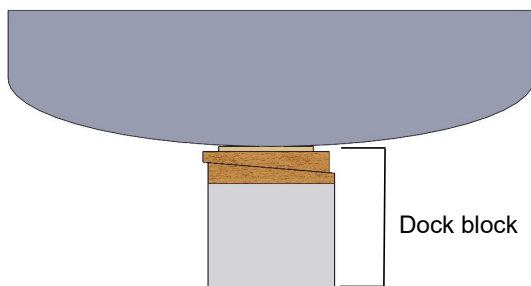


Figure 2.5: Transverse view (or section)

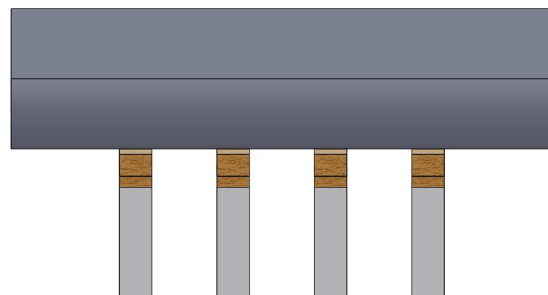


Figure 2.6: Longitudinal view

To prevent localized over-stressed failure of the softwood, a steel plate with another softwood can be placed on top of the block to distribute the load over a larger area and reduce the pressure on the softwood to acceptable values [26]. Just to be consistent, if one has this situation and look from the ground to the keel of the ship one has the following situation: concrete, hardwood, softwood, steel, softwood. So a narrow keel leads to extensive loading, the use of the steel plate gives a higher effective width, which lead to a lower local pressure (see Figure 2.7). The plate must be thick enough (normally the same length and width as the softwood layer) to spread the load over a sufficient area of timber to forestall over-stress without bending the plate, furthermore the softwood layer on top of the steel plate to prevent steel-steel interaction (as this layer is only a few millimeters thick it can be neglected). At DSNS for this stress distribution in steel they use the 45° method. This gives an estimation of the distribution from the contact area of the ship to the new effective width of the timber layers. These values were accepted for simplicity and are appropriate for rough evaluation. Normally the steel plate is thick enough to assume that the complete contact area of the softwood beneath is effective.

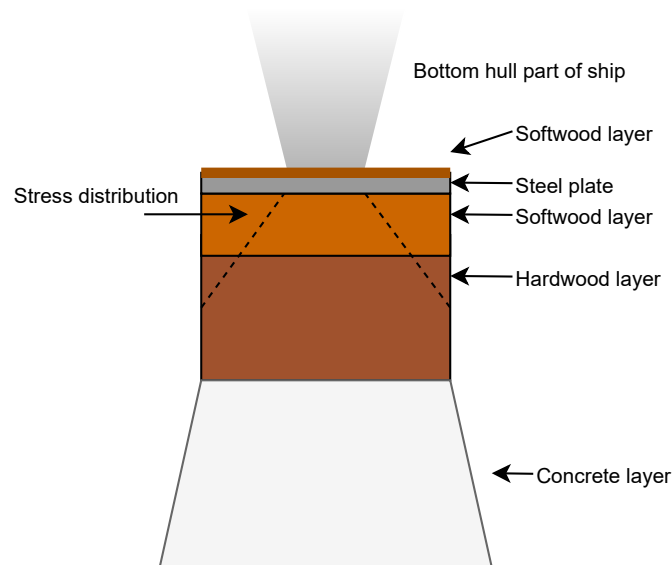


Figure 2.7: Larger effective contact area by placing a steel plate on the dock block. Here the 45° method, used at DSNS, is introduced.

2.2. Variability in dock block configurations

To have an encompassing view on the possible situations within Damen, several yards were visited. Each of the yards have its own approach regarding the docking of the ships, this often in combination with the main focus of the yard. In total 4 yards were investigated; Vlissingen-Oost (or Ritthem), Amels (located in Vlissingen), Schiedam and Stellendam. A sufficient height between the ship and the dock floor is desirable. By supporting the dock blocks with a concrete or steel foundation this is achieved, however, this is assumed as a rigid material layer and therefore not included in the sketches.

2.2.1. Amels

Amels is the yachting department of Damen and located in Vlissingen. Docking of yachts is not of interest in this thesis, however, the materials used can be of interested in the near future if they have promising characteristics. Interviewing the dock master at Amels, the most used materials are known. Figure 2.8 gives an impression of the configuration used at Amels, where figure 2.9 gives the average dimensions of the block. Next to spruce; Amels also makes use of LVL (laminated veneer lumber) as softwood.



Figure 2.8: Amels dock block (photo)

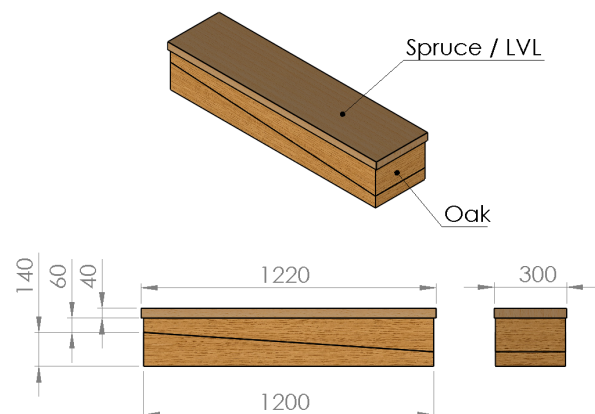


Figure 2.9: Amels dock block (sketch)

2.2.2. Ritthem

Ritthem has one of the larger yards of Damen, where large vessels and marine ships are docked. For this research these ship configurations are the main point of interest. At Ritthem they use 1 layer of hardwood (Azobe) and 2 layers of softwood (Pine and Spruce). Figure 2.10 gives an impression of the configuration used at Ritthem, where figure 2.11 gives the average dimensions of the block. One can clearly see the deformation of the softwood layer in figure 2.10, which isn't likely to happen when docking yachts.

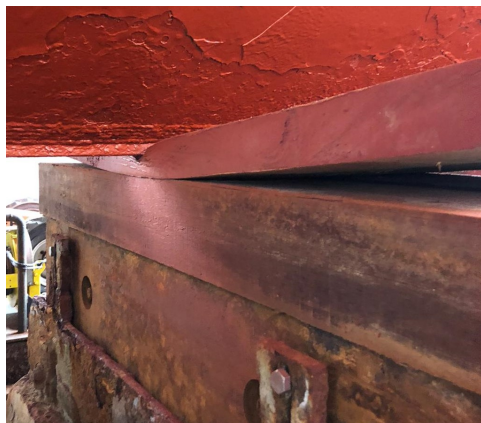


Figure 2.10: Ritthem dock block (photo)

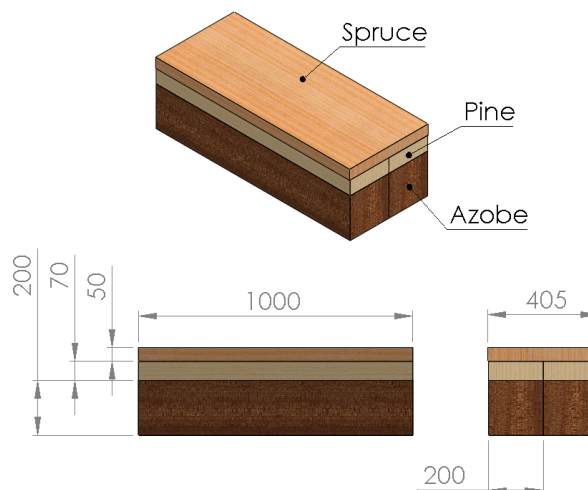


Figure 2.11: Ritthem dock block (sketch)

2.2.3. Schiedam

Just as Ritthem, Schiedam has also one of the larger yards of Damen. The dock at Schiedam is over 300 meters, and often used for large cargo vessels or offshore/dredging vessels. Schiedam makes use of the configuration which is 'well-known' at the DSNS office and therefore standard. The materials are the same as they use at Amels, however the oak layer is just a plane sheet instead of the triangle shape. Figure 2.12 gives an impression of the configuration used at Schiedam, where figure 2.13 gives the average dimensions of the block. This block was a rather old and used one, in case of a new docking the top layer needs to be renewed.



Figure 2.12: Schiedam dock block (photo)

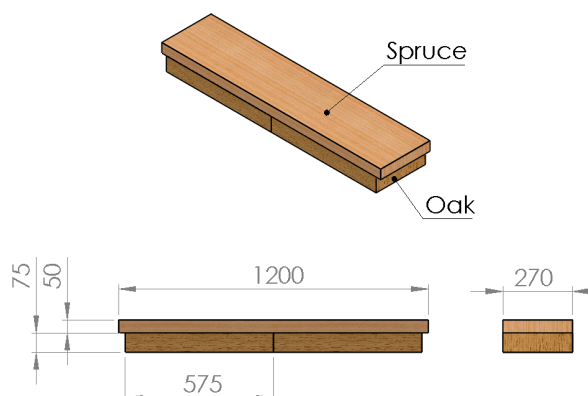


Figure 2.13: Schiedam dock block (sketch)

2.2.4. Stellendam

Stellendam is a small yard where mainly fishery ships are docked. These ships are very strong at their hull (very stiff) compared to marine vessels (preferable as light as possible). Because the ships are so strong, hull damage is unlikely to occur, it is of this reason that they make dock blocks consisting one

layer of hardwood. Figure 2.14 gives an impression of the configuration used at Stellendam. Figure 2.15 shows that due to the load even the concrete foundation is damaged. When there is no hardwood layer the whole block structure is very rigid/stiff, this leads to possible cracking as failure mechanism. Stellendam is out of the scope, and the materials are therefore not used for further evaluation.



Figure 2.14: Stellendam dock block (photo)



Figure 2.15: Stellendam dock block (damage)

2.3. Material characterization

The difference between softwoods (conifers) and hardwoods (deciduous trees) emerge in their growth pattern, different leaf shapes and also the structure of the wood itself. The cellular structure of the timbers won't be discussed, the characteristics are of importance. Clear straight-grained wood is used for determining fundamental mechanical properties; however, because of the natural growth characteristics of trees, wood products vary in density, may contain cross-grain, or may have knots and localized slope of grain (Wood Handbook [32]). Wood is an anisotropic material, which means it demonstrates different properties when stress is applied in different directions. Timber is non-homogeneous based on its growth irregularities and dimensions for load-bearing purposes. The material properties (density, strength modulus of elasticity (MOE) etc.) vary widely, even within a single log cross-section (Bläß and Sandhaas [9]). For this thesis the loading orientation and therefore the direction of the grain are important. The yards and dock blocks are in a marine environment and frequently exposed to rainy conditions and sea water. During the docking phase the graving yard is filled with water, here the blocks are completely flooded. Bearing capacity, compression strength and yield point are strongly influenced by these humidity conditions, therefore the moisture content of the materials is a very important parameter [35]. First the key parameters are discussed and explained, afterwards an evaluation of their influence on the deformation prediction is assessed.

2.3.1. Orthotropic nature of wood

Wood, when used for structural purposes, is almost always stressed parallel to the grain. Docking block timbers are a notable exception: they are loaded and stressed perpendicular to the grain (see Figure 2.16 and Figure 2.17). According to Sandhaas [43] the behaviour in compression perpendicular-to-grain is understood when one recalls that the cells of the wood are honeycombs. If compression occurs the honeycombs will fold. The failure in the radial direction is therefore different than in the tangential direction. Radially, the wood cells are stacked transferring the forces directly over the walls parallel to the force which are failing in buckling. In tangential direction, the cell walls are assembled in a 'stretcher bond' leading to a much smoother passage between the elastic and plastic regions. Here the principal directions which are mentioned by Hepburn [29] and Sandhaas [43] are shown: tangential T, longitudinal L, and radial R. Most studies are based on loading in a parallel direction, only a few results are known for the load in perpendicular (radial) direction.

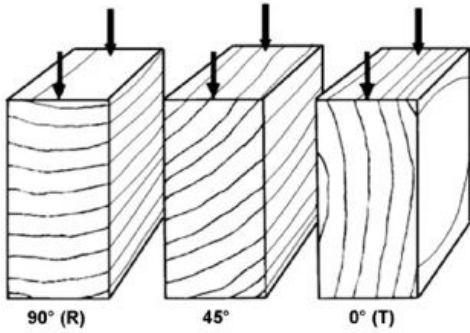


Figure 2.16: Direction of load in relation to direction of annual growth rings: 90° or perpendicular (R), 45°, 0° or parallel (T). [29]

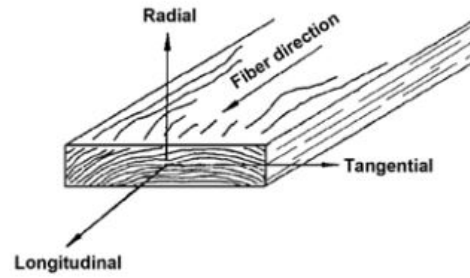


Figure 2.17: Three principal axes of wood with respect to grain direction and growth rings [32]

2.3.2. Elastic properties

Hepburn describes non-linear wood properties as follows:

'The structural anisotropy of wood is a recognized factor that determines its elastic stress-strain relations. Wood has orthotropic symmetry which requires nine elastic constants (3 Young's moduli, 3 shear moduli, and 3 Poisson's ratios) to define its response to generalized stress. In turn, the nine elastic constants for a given wood specimen are functions of time, moisture content, temperature, and stress history' [30]. There are some guidelines regarding the moduli of elasticity in different directions, equation 2.2 from Hepburn [30] gives such a relation. The orthotropic and elastic behaviour can be written in a matrix form according to Hooke's law [10]. It is important to mention that these relationships can be used as verification, but certainly not as a leading formulation. This because the properties beyond the elastic range vary for every specimen, besides, due to size effects larger specimen will experience different relations.

$$\begin{bmatrix} \epsilon_{xx} \\ \epsilon_{yy} \\ \epsilon_{zz} \\ 2\epsilon_{yz} \\ 2\epsilon_{zx} \\ 2\epsilon_{xy} \end{bmatrix} = \begin{bmatrix} \frac{1}{E_x} & -\frac{\nu_{yx}}{E_x} & -\frac{\nu_{zx}}{E_x} & 0 & 0 & 0 \\ -\frac{\nu_{xy}}{E_x} & \frac{1}{E_y} & -\frac{\nu_{zy}}{E_y} & 0 & 0 & 0 \\ -\frac{\nu_{xz}}{E_x} & -\frac{\nu_{yz}}{E_y} & \frac{1}{E_z} & 0 & 0 & 0 \\ 0 & 0 & 0 & G_{yz} & 0 & 0 \\ 0 & 0 & 0 & 0 & G_{zx} & 0 \\ 0 & 0 & 0 & 0 & 0 & G_{xy} \end{bmatrix} \begin{bmatrix} \sigma_{xx} \\ \sigma_{yy} \\ \sigma_{zz} \\ \sigma_{yz} \\ \sigma_{zx} \\ \sigma_{xy} \end{bmatrix} \tag{2.1}$$

Where:

- $E_{i,j}$ = modulus of elasticity in direction i, j [N/mm²]
- ν_{ij} = Poisson's ratio ¹ [-]
- $G_{i,j}$ = Shear modulus in direction j on the 3 plane whose normal is in direction i. [N/mm²]
- $\epsilon_{i,j}$ = strain in direction i, j [mm/mm]
- $\sigma_{i,j}$ = stress in direction i, j [N/mm²]

$$E_L : E_R : E_T \equiv 20 : 1.6 : 1 \tag{2.2}$$

The moduli of elasticity and Poisson's ratios are related by expressions of the form:

$$\frac{\nu_{ij}}{E_i} = \frac{\nu_{ji}}{E_j}, i \neq j, i, j = L, R, T \tag{2.3}$$

When a structure is subjected to a load it material will experience a stress defined to be the ratio of the force (F) to the cross sectional area (A). Correspondingly, the engineering strain (ϵ) would be defined by the original height (h) and the current height ($h - W$). The compressive strength of the material would correspond to figure 2.19. The elastic range refers to the region where material deforms elastically and

¹The first letter refers to the stress applied direction whereas the second subscript refers to the lateral deformation.

returns to its original form when the stress is removed. The elastic region is also referred as the linear region and is terminated by the yield point. After this region plastic deformation occurs where material will not return to its original form once the load is removed. Eventually failure of the material is noticed. Load is acting on the grain in perpendicular direction, hereby the other 2 moduli are ignored from this point. These moduli are obtained by compression tests, however, the literature is almost always based on the modulus in the longitudinal direction.

$$\sigma = \frac{F}{A} \quad (2.4)$$

$$\epsilon = \frac{h - W}{h} \quad (2.5)$$

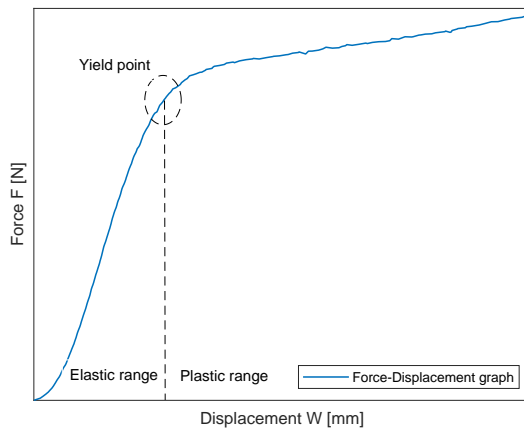


Figure 2.18: Force-Displacement relation where the first region is denoted as elastic behaviour, and the second region to plastic behaviour.

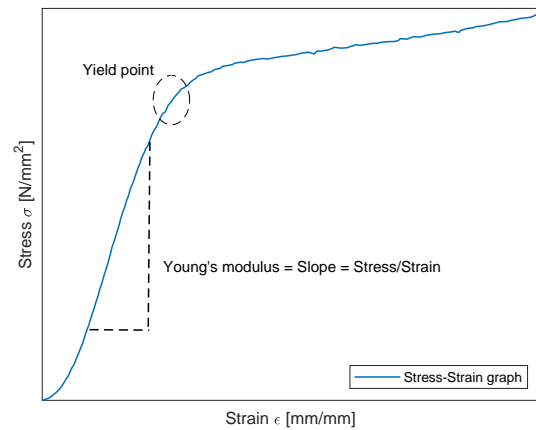


Figure 2.19: Stress-Strain relation where the slope of this curve results in the Young's modulus. Stress and strain are related to the force displacement parameters.

2.3.3. Common Properties

The discussed characteristics are the most important ones when using these types of materials, however there are more involved. According to the 'Wood Handbook' [32] these (strength) properties are often used for basic measurements. The average values are shown in Table 2.1 and explained in Appendix A. The values are obtained by norm EN 338 [12], where the values are given per wood type. From practical point of view the dock masters use literature values, however, they don't exactly know the strength class. Since the exact strength classes are not known, it is wise to evaluate the complete range.

Table 2.1: Characteristic values according to EN 338 [12] and Centrum-hout [51]

Property	Symbol	Softwood C14-C50	Hardwood D18-D70	
Bending strength	f_m	14-50	18-70	$[N/mm^2]$
Mean modulus of elasticity parallel	E_{\parallel}	7-16	9.5-20	$[kN/mm^2]$
Density	ρ	350-550	570-1080	$[kg/m^3]$
Compression strength perpendicular	$f_{c,\perp}$	2.0-3.2	7.5-13.5	$[N/mm^2]$
Young's modulus perpendicular	E_{\perp}	0.23-0.53	0.63-1.33	$[kN/mm^2]$
Mean shear modulus	G_{mean}	0.44-1.00	0.59-1.25	$[kN/mm^2]$

The values from table 2.1 are obtained by using several equations (Annex A of EN 338 [12]). All values refer to mean values, 5th-percentile values can be obtained by equations in these classifications.

2.4. Material characterization analysis

A material characterization is important to narrow down the key parameters of influence in the model to predict the load on the dock blocks. Investigation of all the characteristics would be extremely time consuming and very expensive. Testing material properties is expensive and take long time, therefore this section looks at the importance and influence of the parameters involved. For this thesis it is the goal to have an understanding of the non-linear material behaviour influence on the dock block. The paper written by Hall [24] has some very close related topics regarding this thesis. Although the paper by Hall has nothing to do with dock block loads the configuration of a load acting on a timber perpendicular to the grain is extensively explained. For this reason an in-depth look in Hall's theory and model possibly leads to understanding of the parameters involved. According to the Hall [24], the deformation of a wood specimen under compression is described by 10 parameters:

$$W = f(F, l, h, L, b, E_{\perp}, E_{\parallel}, G, \nu_{\perp\parallel}, \nu_{\parallel\perp}) \quad (2.6)$$

Where:

W	= average deformation	[m]
F	= total applied load	[N]
l	= length of the bearing plate	[m]
h	= depth of the specimen	[m]
l	= length of specimen	[m]
b	= width of the specimen equal to the width of the bearing plate	[m]
E_{\perp}	= Young's modulus perpendicular to grain	[N/m ²]
E_{\parallel}	= Young's modulus parallel to the grain	[N/m ²]
G	= shear modulus	[N/m ²]
$\nu_{\perp\parallel}, \nu_{\parallel\perp}$	= Poisson's ratio	[-]

These parameters need to be known as they are likely to be used in the model to predict the deformation, some of the parameters are already known, others require testing and for a few of them, an assumption will be sufficient. First, the given parameters involved are analyzed and then combinations of parameters that affect the problem are discussed. The dimensionless groups which can be formed with the parameters are:

$$\frac{WblE_{\perp}}{Fh} = f\left(\frac{l}{h}, \frac{h}{L}, \frac{b}{h}, \frac{F}{blE_{\perp}}, \frac{E_{\perp}}{E_{\parallel}}, \frac{E_{\perp}}{G}, \nu_{\perp\parallel}, \nu_{\parallel\perp}\right) \quad (2.7)$$

With a few assumptions and considerations the dimensionless groups can be revised and reduced:

- The material relationship between the Young's modulus and the Poisson's ratio ($E_{\perp} \cdot \nu_{\perp\parallel} = E_{\parallel} \cdot \nu_{\parallel\perp}$) shows a dependence of these four parameters. Therefore one of these four can be removed, Hall removed $\nu_{\parallel\perp}$.
- As an assumption that the problem is similar to a beam on an elastic foundation the consideration that the problem is 2D can be made. This assumption lead to the Poisson's ratio normal to- and out of the plane to be zero. Therefore the term b/a is disregarded.
- For $F/(b \cdot l \cdot E)$ holds that it is an average value in the linear range and therefore also eliminated.
- A new term is introduced as the apparent modulus of elasticity, known as the ratio between 'Mean stress perpendicular to grain' and 'Mean strain perpendicular to grain' and is shown in equation 2.8.

$$E_a = \frac{F/b \cdot l}{\Delta/h} \quad (2.8)$$

The equation shown in 2.8 is also used in the European Standard DIN EN 408 [22].

Then the first term in equation 2.7 can be simplified with some basic calculations to E_{\perp}/E_a , which expresses the ratio of the stiffness of the material loaded over the full cross-sectional area to the apparent stiffness of the material loaded over a part of this area. All these considerations lead to the following

dimensionless groups in expression 2.9, which is an expression dependent on two geometric terms l/h and h/L and three material ratios E_{\perp}/E_{\parallel} , E_{\perp}/G and $\nu_{\perp\parallel}$:

$$\frac{E_{\perp}}{E_{\alpha}} = f\left(\frac{l}{h}, \frac{h}{L}, \frac{E_{\perp}}{E_{\parallel}}, \frac{E_{\perp}}{G}, \nu_{\perp\parallel}\right) \quad (2.9)$$

Hall stated that the deflection response under a load hardly depends on the material ratios, this gives the final form of dimensionless groups:

$$\frac{E_{\perp}}{E_{\alpha}} = f\left(\frac{l}{h}, \frac{h}{L}\right) \quad (2.10)$$

To check the independence of the material ratios, the influence was checked by adjusting these ratios and look at the response. The ratios E_{\perp}/E_{\parallel} , E_{\perp}/G and $\nu_{\perp\parallel}$ were adjusted by 25%, the ratio of E_{\perp}/E_{α} hardly changed after (3%). It is because of this reason that the E_{\perp}/E_{α} ratio is insensitive to changes in the material properties and that it is acceptable to use the selected values of the material for a wide range of specimen. So weakly dependent material properties are: σ_{\parallel} versus ϵ_{\parallel} , τ versus γ and $\nu_{\perp\parallel}$. By this study of Hall [24] one can conclude that for the prediction of the deformation of a timber layer the main parameters involved are the dimensions and the Young's modulus perpendicular to the grain. The Young's modulus is on its turn a relation between the stress and strain.

To give an all-encompassing prediction the work in the plastic range needs also an explanation. An understanding of these material properties is needed to transfer non-linear behaviour to a model. In order to describe the compression perpendicular to grain beyond the elastic range a relationship between stress and strain is known. Where the Hooke's law is well known in the elastic range the material property in the plastic range hasn't been evaluated in most literature. The stress-strain relationship beyond the plastic region should be obtained by physical testing, where this in the elastic region can be obtained from literature.

2.5. Material characteristic values used at DSNS

Predicting timber deformation is dependent of the modulus of elasticity perpendicular to the grain, stress and strain as discussed by the report of Hall [24]. At Damen they make use of these values bases on experience, test results and literature. In this section the values used at Damen is discussed. In 2013 Damen made a report in which it examined the dock block loads with a FE model (ANSYS). For oak the report gives a single value as it is assumed linearly-elastic, $E = 600N/mm^2$. This assumption is important as it is desirable to avoid pressures in the plastic region of the hardwood. The main goal of the thesis is to predict loads on the dock blocks and take non-linear material behaviour in account, however, damage to the hardwood layer should be prevented.

The softwood is a spruce which is tested at compression, the duration for the compression is based on 10 days. The material is assumed to be linear till point 3, at a Young's modulus of $10N/mm^2$. More specification regarding the exact conditions and material type are not known, however these values can be used for validation.

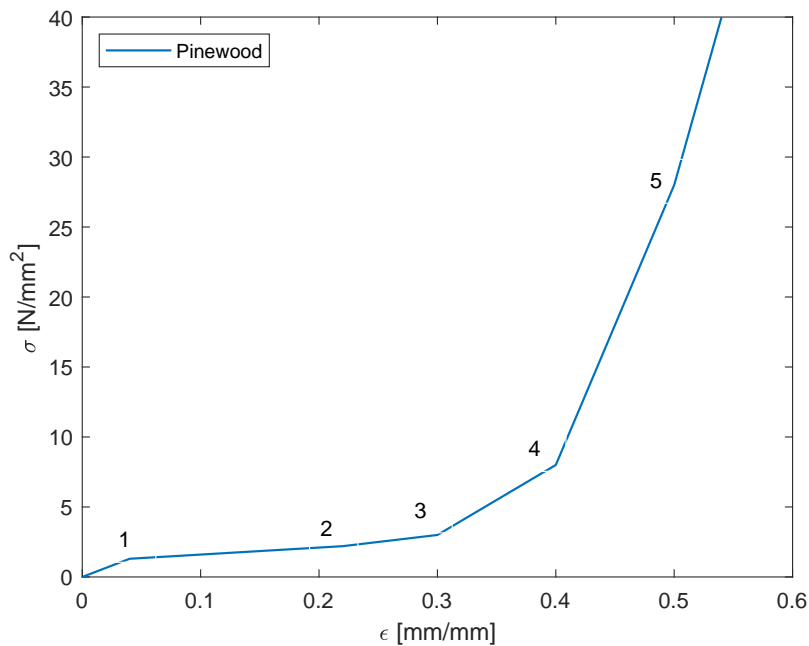


Figure 2.20: Stress-Strain curve pinewood [41]

Table 2.2: Young's modulus pinewood test

	Stress [N/mm^2]	Strain [-]	Young's Modulus [N/mm^2]
Point 1	1.3E6	0.04	32.5
Point 2	2.2E6	0.22	5.00
Point 3	3.0E6	0.30	10.0
Point 4	8.0E6	0.40	50.00
Point 5	28.0E6	0.50	200
Point 6	478E6	2.0	300

The blockload tool from Bedert [7] used at Damen also contains characteristic values, here the modulus of elasticity for the oak is the same. For softwood the tool uses Douglas Fir with $E = 10.3N/mm^2$.

The yachting department of Damen, Amels, has some values for their materials based on experience. The values in table 2.3 are obtained from a thesis commissioned by Amels [16].

Table 2.3: Material properties based on Amels' experience

Material	Young's Modulus [N/mm^2]	Poisson's ratio [-]	Yield strength [N/mm^2]
Hardwood Oak	2005	0.369	3.2
Softwood Spruce	868	0.370	2.2
Azobe Wood	22000	0.372	88
Pitch Pine Wood	41	0.308	7

It is clear that even within Damen a variety of values regarding material characteristics is used. This variability in material properties lead to unreliable results for a dock block model. The gap regarding the material properties can be summarized as wrong use of literature values and incomplete material characterization. Full material characterization will lead to realistic values in order to predict the deformation, and to assess and quantify non-linear influences.

2.6. Conclusion

As Damen Schelde Naval Shipbuilding (DSNS) is designing more and more slender hull forms, the loads produced can cause a nonlinear behaviour of each block, which might lead to an over-stress failure of one or more blocks. The blocks used for dry docking must be optimized to avoid deformation of the hull forms. From the literature study it is concluded that the materials, used for dock blocks in dry docks, are constituted by several layers, normally three or more: concrete foundation, hardwood, and with the top layer usually being a soft material. Using this conclusion it is clear that characterization of the Young's modulus perpendicular to the grain, using the variability of the moisture content, is the key parameter to be investigated by compression tests.

Material properties can be found in literature, however, these refer to a moisture content of 12%. Strength properties perpendicular to the grain with respect to a moisture content higher as a dry (12%) value are hard to find. It is this gap in the literature which needs to be evaluated, this since humidity conditions are very likely in the yards. A research in this field would be valuable for both science and Damen.

Field research at multiple Damen yards pointed out the variety of these hard- and softwood layers, both in material type as in its characteristics. The concrete or steel foundation is assumed rigid, so the thesis is focused on the timber layers. The multiple timber layers of a dock block are loaded perpendicular to the grain, which is an uncommon field of literature values. Classifications and frequently used literature recall rules of thumb or average values for these properties perpendicular to the grain. Multiple studies were investigated to see what the dependency of these parameters are in the prediction of the dock block load. Loading perpendicular to the grain leads to a weak dependency of parameters as; shear stress, shear strain, Poisson's ratio or mean stress parallel to the grain. On the other hand, it is concluded that the high dependency on material deformation comes from the specimen dimensions, moisture content and Young's modulus perpendicular to the grain.

3

Review of dock block static analysis: block loads and non-linear response

The purpose of this chapter is to get an overview of the used calculation methods regarding the static block load. In the past a few different approaches were used, these approaches are critically reviewed in what follows, with particular attention to dock block models and dock block load assessment. First the model approach for a single dock block is discussed, secondly the model for a ship resting on multiple blocks is discussed. For both reviews the empirical, numerical and analytical studies are evaluated.

3.1. Block model methodology: to predict the deformation of the individual material layers

As a ship is docked on multiple blocks the weight of the ship is distributed over the block line. The weight distribution and block positioning lead to load acting on a single dock block. The goal of the block model is to check if the maximum allowable capacity is exceeded as a consequence of this load.

3.1.1. Empirical methods (for single dock block)

Since empirical studies are related on practice experience, it is not advisable to make use of such solution. To capture the physics of compression and represent this in a model it is a risk to make experience based assumptions. Using different material layers, with different properties can lead to a high variability of results. To account for these different parameters, and to use multiple input values an empirical solution has many shortcomings. Validation of empirical results is also an issue as the model can't be rebuilt with mathematical expressions. With the use of an empirical study it is very difficult to capture the non-linear physics involved when compressing a stacked block. This drawback led to the conclusion that an empirical study will not satisfy the objectives.

3.1.2. Numerical studies (for single dock block)

Numerical studies are the types of models which are closest to reality. As they can be modelled as three dimensional models, they are taken into consideration all the possible dimensions. Figure 3.1 is an example of a possible FE analyses for a single dock block with the ANSYS software. Dimensions for this example represent the in-situ used dock block at Damen yards as discussed in chapter 2. The material properties are taken from the ANSYS library, these are to illustrate how the deformation of such a model are likely to occur. Along with the deformation one could possibly look for the equivalent stress at the contact area.

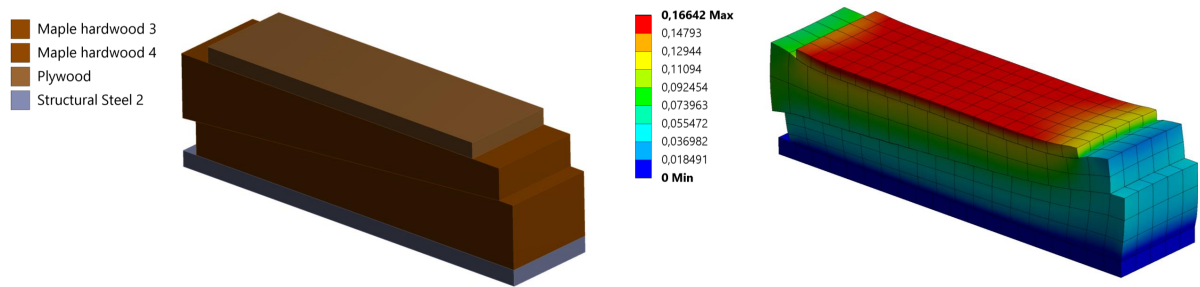


Figure 3.1: Finite Element analysis of single dock block (overview)

Breeveld [11] discussed the differences between the modelling of an 1-D model such as a beam on elastic foundation and the 3-D representation of a FE model. 3D Models take load interaction in multiple direction into account, therefore it is more realistic. With the FE model it is also possible to represent non-linear material properties, which lead to a good accordance of the reality. However, the demerit of this approach is that is time intensive (modelling and calculating), besides not all parameters might be known in the design phase. The results are more difficult to control, and if the situation with respect to materials and load distribution, the model should be rebuilt. As the block line is a sequence of many blocks it would be extremely time consuming to analyse every single position.

3.1.3. Analytical study: Euler-Bernoulli beam theory (for single dock block)

Bending of beams is the most common phenomenon in structural engineering. In nearly every situation one could recognize the beam-shaped form as structural elements. The beam in a bending model can be extremely instrumental for static analysis of structures to predict the deformation. As the dock blocks are represented as stacked rectangular shapes it is a very suitable way to make use of this beam solution procedure. A beam is a bar capable of carrying loads in bending. The loads are applied transverse to its longest dimension. This definition is definitely the case for the loads distributed at the dock block contact area and is therefore a potentially simple method for modelling the deformation of a dock block. Figure 3.2 illustrates the assumption of a dock block modelled as a beam with a transverse load.



Figure 3.2: Dock block modelled as a component that is designed to support transverse loads ($q(x)$), that is, loads that act perpendicular to the longitudinal axis of the beam. The beam supports the load by bending only and lead to a deformation $W(x)$ along this longitudinal axis.

The Euler-Bernoulli beam theory is the most used theory for calculation of a beam deflection. The theory is a simplification of the linear elasticity theory. The Euler-Bernoulli theory is a special case of the more general Timoshenko beam theory, where only small deformation is assumed with no shear. As preliminary concept the Euler-Bernoulli beam theory is the most applicable and effective approach in beam bending problems. By this way the block is modelled as continuous, and therefore it has only one expression per layer (in terms of deflection, slope, moment and shear). However, for the dock blocks the load is not necessary uniform distributed over the complete contact area. For the fore and aft of the ship the width is only partly uniform distributed, and therefore the solution lead to multiple possible approaches. Before discussing the possibilities of the solution, the theory itself is explained. Consider a straight beam undergoing transverse motion, shown in figure 3.3.

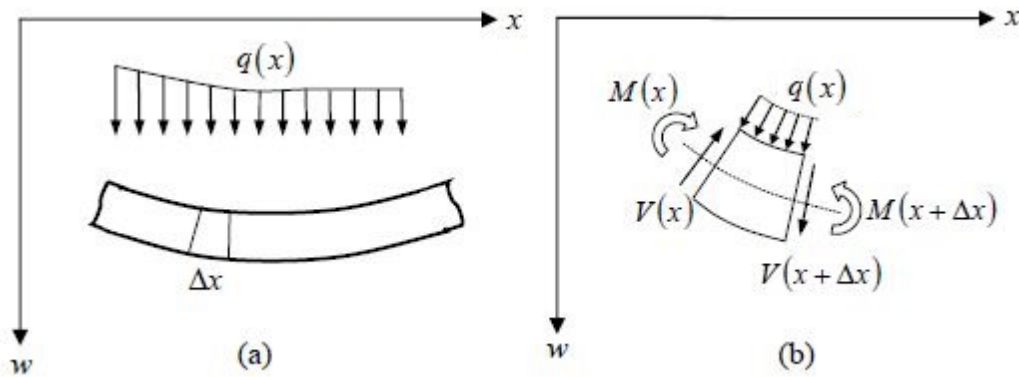


Figure 3.3: (a) Beam undergoing transverse motion and (b) differential element of the beam subject to the shear force, bending moment and external load [36]

One invoke the basic hypothesis of the Euler-Bernoulli theory of beams; namely that the plane cross-sections initially perpendicular to the axis of the beam remain plane and perpendicular to the neutral axis during bending [36]. By this statement it is concluded that the longitudinal strains vary linearly across the beam and that, for elastic behaviour, the neutral axis of the beam passes through the centroid of the cross-section. According to this theory the bending moment and curvature are related as:

$$M = -EI \frac{d^2 w}{dx^2} \quad (3.1)$$

Where:

- $W(x)$ = transverse deflection of the neutral axis
- E = Young's modulus
- I = moment of inertia of the cross-section

In accordance with figure 3.3, the static equation of the beam element, and applying the Taylor expansion and dividing by Δx :

$$V = \frac{dM}{dx} \quad (3.2)$$

Combining equation 3.1 and 3.2 gives a final expression for the transverse deflection W of the beam neutral line:

$$\frac{d^2}{dx^2} (EI \frac{d^2 W}{dx^2}) = q \quad (3.3)$$

Where:

- $q(x)$ = external loading

Because the equation is of the order four with respect to the spatial co-ordinate, each end comes with two boundary conditions. Expression for moment and shear force as they act on the left-end of the beam are represented by equations 3.1 and 3.2. Where the same equations hold on the right-end side, however, they come with a minus. With the appropriate boundary conditions, and possible interface conditions, one can come to the deflection of the beam along the x -axis. However, this theory does not account for the interaction between multiple layers or even so between a layer and the rigid floor. In the next section proposed methodologies for such an interaction are given.

3.1.4. Analytical study: Winkler Foundation (representing floor-block interaction)

The Euler-Bernoulli beam theory as explained above takes no account for interaction when the beam is resting on the rigid floor. In the case of a dock block the hardwood layer is resting on the concrete/steel foundation, which is assumed to be rigid. Elastic foundations allows one to model the stiffness effects of a distributed support without actually modeling the details of the support. If one assume that the reaction force offered by the continuous support is a function of the displacement that of the beam, the support is called as elastic. A beam resting on an elastic support is said to be beam on elastic foundation (figure 3.4) [28] [36]. Introducing of the stiffness effects means also an introduction of the non-linear behaviour of compressing a stacked block. Besides the non-linear material behaviour itself, due to the change from elastic to plastic region, the interaction between layers and foundation is also an non-linear effect.

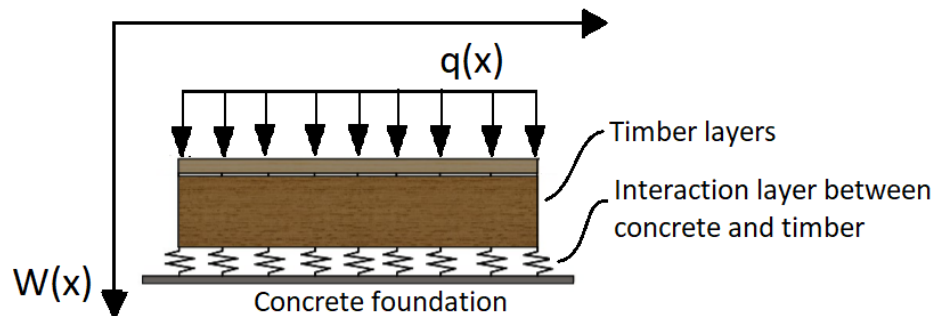


Figure 3.4: Beam on elastic foundation representing the interaction (springs) of the timber layers with the rigid concrete foundation.

There are various ways of approaching a beam on elastic foundation (such as Vlasov [49], Pasternak [52] and Winkler), all with their own advantages. From mathematical and modelling point of view the Winkler foundation is less complex and has the least amount of input parameters. The Winkler model has the assumption of infinitely close linear springs. Hentenyi [28] provided the classical approach for this type of foundation, and for the solution of this fourth order differential equation. The biggest disadvantage for this approach is when discontinuities appear along the beam, in this case the solution is written for every different section for the beam. Consequently, if these parts are n , then the constants of integration to be determined are $4n$ and, the boundary conditions/natural conditions imposed are $4n$ too. From practical point of view, it is mathematical intense to use this classical approach in case of multiple discontinuities. Falsone [19] describes the use of generalized functions in order to solve these discontinuities, this in imitation of Macalulay [34] method. In succession of this paper, Falsone et al. [20] added the elastic foundation to the fourth order solution. This chapter describes the closed form solution for a beam on elastic foundation with multiple discontinuous loads. For the analytical solution of a beam representing the dock block only one discontinuity is expected, the partly uniform distributed load. The Pasternak foundation does take directional spreading into account, however, it is difficult to determine parameters such as shear. The assumption of only one discontinuity lead to the conclusion that the improved continuum model (Pasternak) is not necessary. The interaction parameter (k_d) is normally used as the soil foundation constant in structural analysis. For the application of material interaction is this parameter yet unknown and to be determined by experimental data.

As there is only one discontinuity the classical approach is mathematical and computational not too

demanding and is therefore the first to be discussed. In previous section the Euler-Bernoulli beam theory is explained, now the elastic foundation (representing the interaction between individual layers) is added. For a static response of a beam on elastic foundation the general equilibrium equation is given by equation 3.4. The general solution of this equation can be found by means of superposition of the homogeneous and particular solution.

$$\frac{d^2}{dx^2} \left(EI \frac{d^2 W}{dx^2} \right) = q_1 - k_d W \quad (3.4)$$

Where:

k_d = stiffness per unit length

Full derivation of this classical approach, or the approach where generalized equations are used are not explained as this is just the preliminary concept phase. At this point the use of an elastic foundation is an appropriate mathematical expression for the physical problem. When there is a discontinuity in the beam there are two possibilities, or the beam is divided into segments where the interface conditions are applied to solve by means of the classical approach, or the use of generalized functions are introduced to avoid such segments.

The above approach takes only the interaction between the rigid floor and the timber layers into account. To get a encompassing model another elastic layer is introduced to model the interaction between the individual timber layers. The described approach with 2 elastic layers representing the interaction of individual layers will be referred as a double Winkler foundation model (figure 3.5). This way of approaching the interaction between individual material layers has only been performed a few times in the literature.

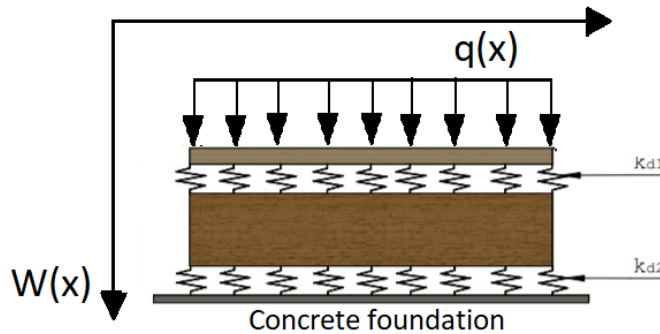


Figure 3.5: Double Winkler foundation: k_{d1} is the interaction between the individual timber layers, k_{d2} is the interaction between the rigid ground and the bottom timber layer.

The consequence of adding the extra elastic layer is that the equation for the deformation is a fourth order coupled differential equation, which becomes mathematically complex. The coupled system as described can be solved by order differential solvers, where superposition of the homogeneous and particular solutions are introduced. Subscript 1 refers to the top layer (softwood), and subscript 2 to the bottom layer (hardwood).

$$\frac{d^2}{dx^2} \left(E_1 I_1 \frac{d^2 W_1}{dx^2} \right) = q - k_{d1} (W_1(x) - W_2(x)) \quad (3.5)$$

$$\frac{d^2}{dx^2} \left(E_2 I_2 \frac{d^2 W_2}{dx^2} \right) = k_{d1} (W_1(x) - W_2(x)) - k_{d2} W_2(x) \quad (3.6)$$

3.2. Ship model methodology: block load response as consequence of docking on multiple blocks

The goal for the ship model is to find the load per dock block location as a consequence of the weight distribution of the ship. Historically, the development of tools for ship docking analysis has lagged far behind the ship design tools. Due to extreme complexity and time-consuming nature the docking plan is nowadays based on only a few parameters; hull form, structure, and weight distribution.

3.2.1. Empirical methods (for ship model)

One of the first to study the block loads was F. Elgar in "The Distribution of Pressure Over the Bottom of a Ship in Drydock and over the Dock Blocks" [18]. In this early stage, the loading of the docking blocks was assumed uniform, the load on one block was just the multiplication of the calculated pressure on the total contact area. It was at this point (1899) that Elgar introduced a trapezoidal pressure distribution to account for a point of gravity that does not coincide with the vertical center of pressure. Before Elgar, the method was only reliable when the ship was relatively stiff, and the load was (uniform) distributed over the total length. A large overhang in the fore and aft of the ship or high local loads results in unreliable results. However the trapezoidal method was more reliable than the first approach, the assumption of a perfectly rigid ship which does not bend at all gave also unreliable results according to Elgar [18] and Jiang and Grubbs [31]. With the same point of view, the first classification to be discussed is the Germanischer Lloyd [44]. As this is a first investigation of the possible modelling methods, a closer look at the calculations and specific equations is not of importance at this stage.

3.2.2. Germanischer Lloyd SE

For large ships or ships with a special design (complex hull form etc.), particularly in the aft, or heavy ships, special docking calculation is required. The method of Germanischer Lloyd assumes uniform weight distribution at the length of the keel. Extensive peak loads close to the transverse bulkheads are corrected with a factor C . This method gives conservative results due to the large safety factor, besides this is the assumption of uniform weight distribution not realistic.

3.2.3. Crandall's trapezoidal method

Both "Best method for predicting dry dock block reactions" [47] as "Accuracy assessment of methods for predicting dry dock block Reactions" [48] summarized Crandall's work from 1964 [13], 1966 [14] and 1986 [15], which describes the most used trapezoidal calculation method. The method described by Crandall is perhaps the simplest to perform and requires the least amount of information regarding the ship's parameters. Unfortunately, Crandall's method, although simple to use, is highly simplified and can be quite inaccurate in some cases. Crandall's Trapezoidal Method for vessels with continuous keel bearing assumes that the ship being docked is very rigid; therefore, the actual weight distribution of the vessel can be transformed into a trapezoidal load distribution, shown in figure 3.6. Along with the assumption that the vessel is rigid, Crandall's method also assumes that the dry docking blocks are rigid.

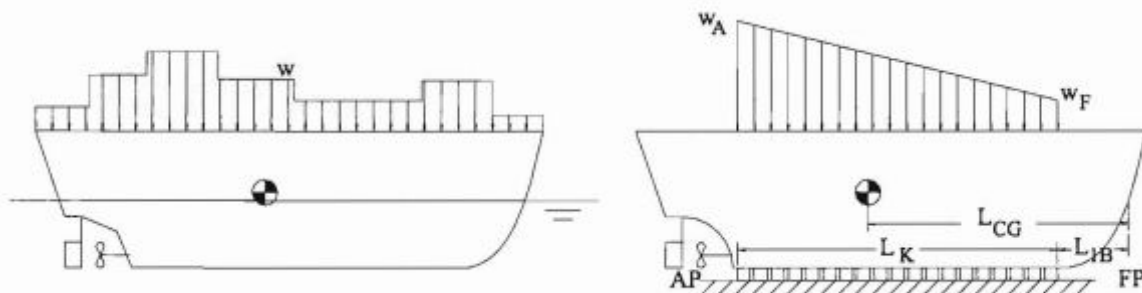


Figure 3.6: Crandall's principle [47]

The work from 1986 presents a method for keel block load prediction in which the bearing length of the vessel and dry docking blocks have a significant gap between keel blocks. These gaps arise when for instance a sonar dome or a discontinuity in the ship's keel is in place. Again, this method is not appropriate when a precise prediction is desired.

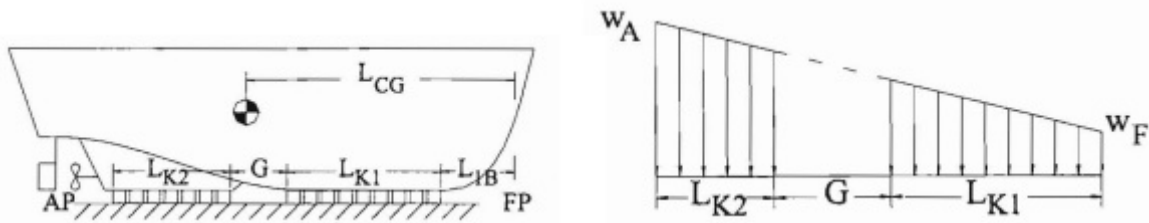


Figure 3.7: Crandall's principle with interrupted keel bearing [47]

The Crandall method delivers a fast prediction of the forces, however, for complex hull forms (large overhang or slender skeg), the estimation is not accurate. The calculations for the gap can easily be expanded to suit with more than one keel bearing gap. Crandall may only be applied for standard short vessels with almost uniform weight distribution.

3.2.4. Lloyd's register

In the classification register of Lloyd [33] a new empirical method is explained. The formulation of Lloyd's Register (LR) is more complex than previous studies, the principal use is shown in figure 3.8. From this figure, the right picture gives the overhang of a ship, here the length of $2L_o$ is the assumption that can be made concerning the increase in load. So, the increased load due to the overhang equals an extended length equal to twice the length of the overhang and is parabolically distributed.

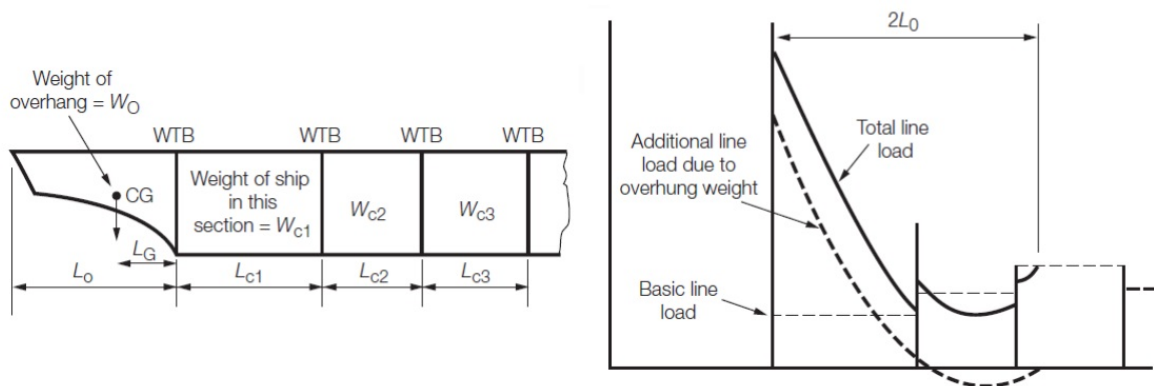


Figure 3.8: Lloyd's register principle [33]

If there is both a fore overhang and aft overhang the possibility could arise that the amidship blocks are fully unloaded. Bedert [7] evaluates the LR method and concludes that if the distribution becomes negative the transverse bulkhead load is consistently underestimated. In contrast to this is the distribution at the overhang overestimated. LR sees the block line as a succession of infinitely rigid support points, which are not bending with the ship. Increased pressure as a result of the overhang is taken into account, but in this method, they are strongly compensated by an underestimation closer to the midship.

3.2.5. Results of empirical studies

The 3 main empirical studies are singled out, all with its advantages and disadvantages. In the thesis of Vanhaesebrouck [16], reactions on dry dock block loads for yachts are investigated. Here a similar approach as the thesis of Bedert [7] is taken, early prediction without non-linear material behaviour considered. Vanhaesebrouck evaluated the empirical studies for a yacht (type YN18801, figure 3.9)

and used a FEM model from Amels (figure 3.10). It is important to note that in this thesis the assumption of a rigid ship is made, therefore, the peak loads at the midship are not part of the research. Yachts are flexible and relatively small ships, this in contrast to cargo or marine vessels.

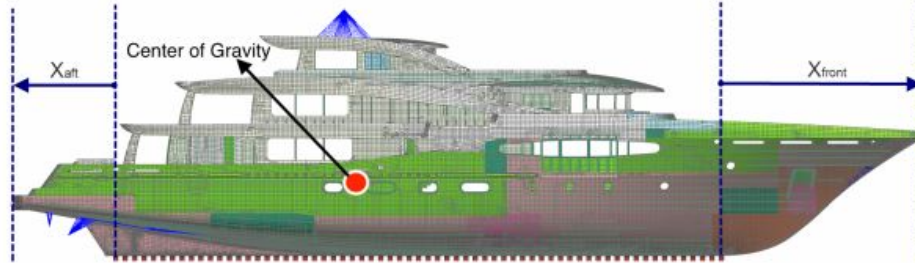


Figure 3.9: YN18801 yacht fully meshed in FEM software (NX9 Siemens) while standing on dock blocks [16]

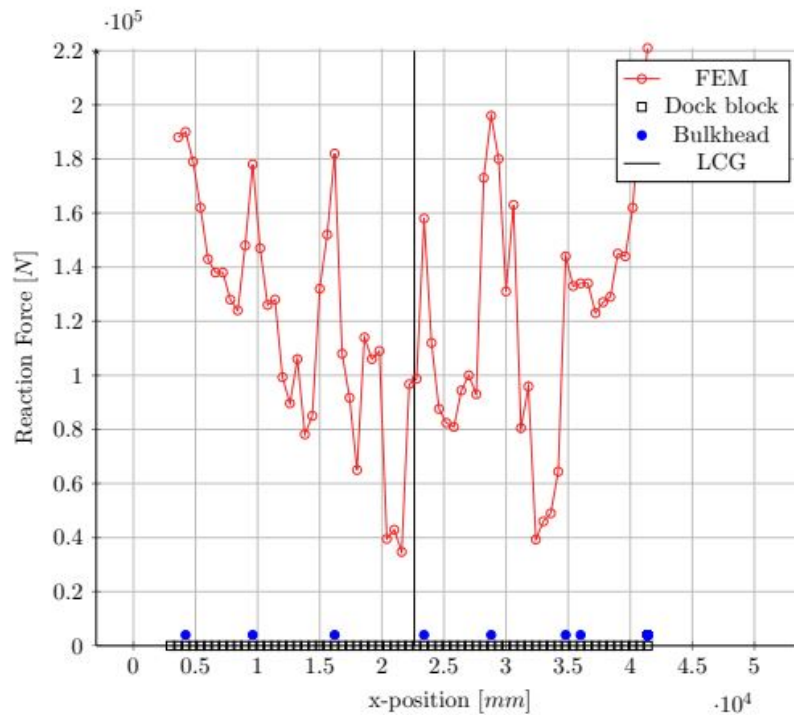


Figure 3.10: Dock block reactions retrieved by FEM for the YN18801 [16]

From figure 3.11 it is clear that this principle is rather conservative and overestimates the load. Due to the assumption of uniform deformation, the peak loads on the individual transverse bulkheads are not resolved. The advantage of Germanischer Lloyd is a fast estimation with only a few input parameters, but the result is not accurate.

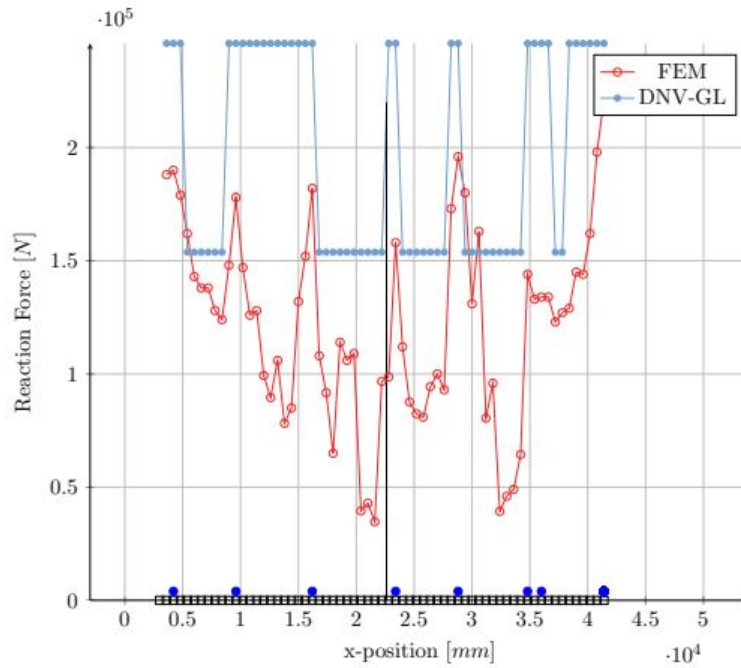


Figure 3.11: Dock block reactions retrieved by FEM for the Germanischer Lloyd principle [16]

The Crandall principle is shown in figure 3.12, obviously, this method is only a simple estimation. Only in case of a short and rigid ship with no overhang, this can be used. In this thesis, when complex hull forms and large overhangs are of importance, this method is of no interest.

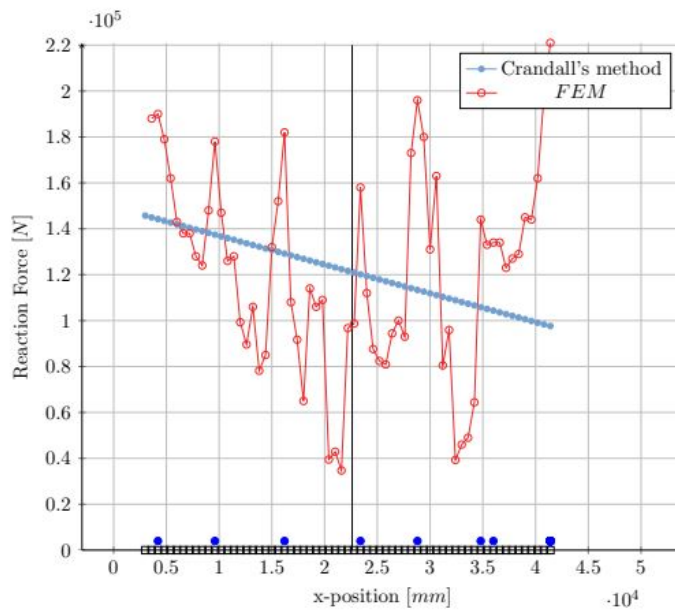


Figure 3.12: Dock block reactions retrieved by FEM for the Crandall principle [16]

In figure 3.13 is the principle of LR depicted, one can clearly notice that especially in the middle section of the vessel the LR closely meets with the FEM analyses. However, not all the individual peaks are covered by the LR it is the most accurate empirical method. At the bow and the aft, LR overestimates the load due to the overhang as mentioned before. It can be concluded that with only a few input parameters the Lloyd's Register is by far the most accurate empirical method.

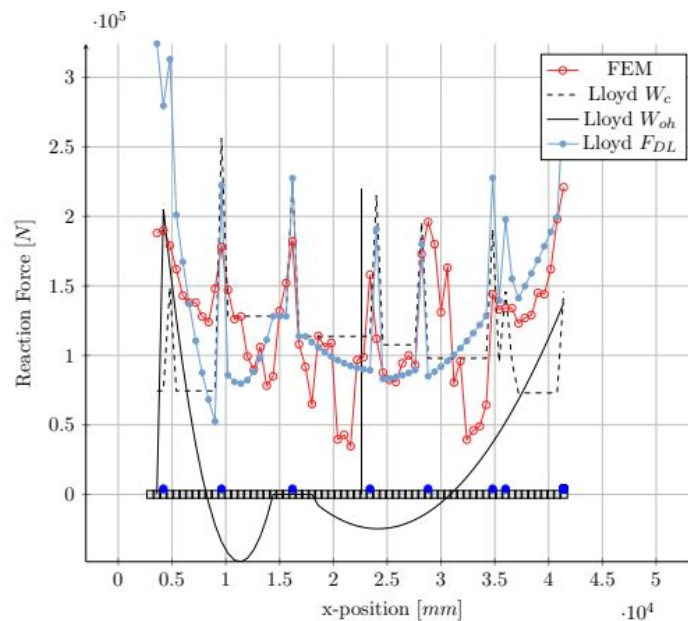


Figure 3.13: Dock block reactions retrieved by FEM for the Lloyds Register principle [16]

A noticeable point for all the empirical methods is that in principle it makes no use of the modulus of elasticity nor of the moment area of inertia. When one accounts for non-linear material behaviour the modulus of elasticity is the key parameter, therefore the LR method is not a good way of predicting dock block loads. To have a precise estimation, but also a solution that suits a wide range of applications an empirical method is not appropriate. Empirical methods are a good way to have a fast estimation, or a specific solution suitable with one typical problem.

3.2.6. Numerical studies (for ship)

Numerical analysis is the study of algorithms that use numerical approximation (as opposed to symbolic manipulations) for the problems of mathematical analysis (as distinguished from discrete mathematics). However, in this thesis one examine finite element studies when numerical analysis is mentioned. Making an own numerical analysis (for the full ship) is not part of the scope, however, if a suitable study is found this can be used. At the DSNS office some FE studies have been developed, one is discussed in this subsection. Other studies such as Hall [24] and Hepburn [29] also discussed FEM results, however, these are rather old and not encompassing to the problem.

DSNS FE specialist P. Pruijssers used the software ANSYS to calculate the pressure on the contact area of the dock blocks. In the model of the ship construction he makes use of plate- (ANSYS, Shell181) and beam-elements (ANSYS, Beam44). Dock blocks are modelled as solid-elements (ANSYS, Solid45). The model is given in figure 3.14.

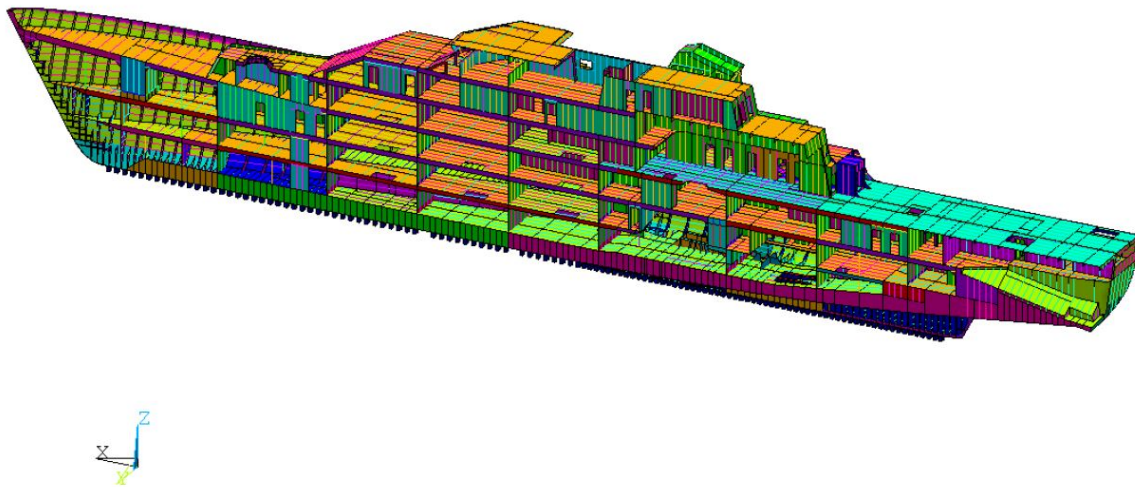


Figure 3.14: Finite Element Model of Damen Patrol Ship

For this calculation the non-linear material behaviour is modeled as bi-linear behaviour for the softwood and linear behaviour for the hardwood. The results for this study can be used in the validation phase, however, using a FE model in every new situation would be time-consuming. If a closed form solution is validated with the FE results this is a faster way of predicting the loads.

3.2.7. Analytical studies (for ship model)

According to Taravella [47, 48], there are a few major analytical studies which cover the problem of determining keel block loads while dry docking a vessel. From an analytical point of view, the problem can be modelled a simple beam on an springs, however, due to the varying weight distribution and section properties, the problem becomes mathematically complex. For this thesis, the key points for the analytical models are of interest before a short historical overview is given. The analytical studies are based on a beam on elastic foundation.

In 1952 Yeh and Ruby presented a method of analysis for the determination of the loads taken by keel block systems as the sole vertical support for vessels resting in graving docks [23].

The main assumptions were:

- The vessel is a monolithic beam (homogeneous, isotropic and elastic)
- The dock floor and the underlying soil, rock, etc., are infinitely rigid
- The reaction forces of keel blocks are proportional at every point to the deflection of the vessel at that point

These assumptions lead the problem to a beam which is free at both ends and on an elastic foundation. The beam experiences bending and is subjected to bending and variable weight distribution. Eventually, this leads to a complicated differential equation which solved by using Ritz's Method¹. In conclusion, the method allows the solution of the problem by a step-by-step routine sequence of operations in one stroke and in a reasonable length of time. The accuracy of the solution may be improved as much as desired by including more terms, the main assumption that the overhang effect of the ship can be neglected gives not the desired result.

¹Ritz's Method consists of assuming a set of functions, each term of which satisfies the boundary conditions of the problem. The unknown multipliers of the functions can be determined from the requirement that the total potential energy of the system has a minimum value in the equilibrium state.

After Yeh and Ruby a similar approach was used by Palermo and Brock [40] (1956), it was felt that a method combining the accuracy of the lengthy Yeh-Ruby method and the simplicity of Elgar's method would be the ideal type of solution for this problem.

The simple solution of a beam on an elastic foundation was used with the following assumptions:

- The ship is long enough that the effect of the weight of stern overhang on the foremost block is negligible
- The moment of inertia of the hull girder is constant forward of the after keel block for an arbitrary distance which will be taken to be equal to the length of the overhang

From the results can be concluded that the general trend of the results of the Yeh-Ruby method is followed. However, the solution of the problem by this method is slightly higher and less time-consuming. Still, the assumption that the effect of the ship overhang (either fore or aft) on the loading of the foremost or aft-most blocks is negligible is chief. The papers from Yeh-Ruby and Palermo are the precursors for what nowadays is used (speaking of beam theory in dock loads).

3.2.8. Beam theory as interaction between ship and dock block

With the same assumptions of Yeh-Ruby and Elgar it can be concluded that the ship, represented as a beam on multiple springs, is a righteous approach of modelling the interaction between the ship and the dock blocks. Figure 3.15 illustrates multiple blocks on which a ship will rest when it is docked, here the red arrows indicate the weight distribution of the ship, where the blue arrow gives the reaction force produced by the blocks (modelled as springs).

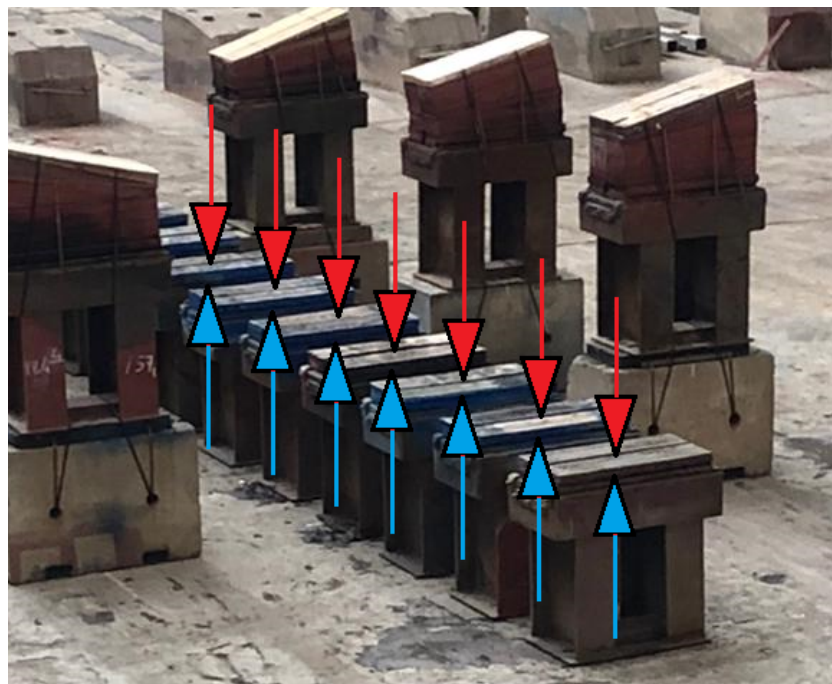


Figure 3.15: Beam theory on multiple spring representing the interaction between the dock blocks and the ship

The weight distribution can be presented by either point loads or uniform distributed loads. The ship support is represented by springs, figure 3.16 shows a sketch of this situation, here the bold numbers below the beam are indicating the nodes and the other numbers are the element numbers. The nodes are the location where a dock block is presented, and the elements are the segments as a distance between two nodes. As the ship is in static equilibrium the weight results in reaction forces per dock block (modelled as springs). This reaction force is equal to the force acting on this particular block

location. By this relation one could find all the loads per location, where this load is used for the model of a single dock block [47, 48], Bedert [7] and Vanhaesebrouck [16].

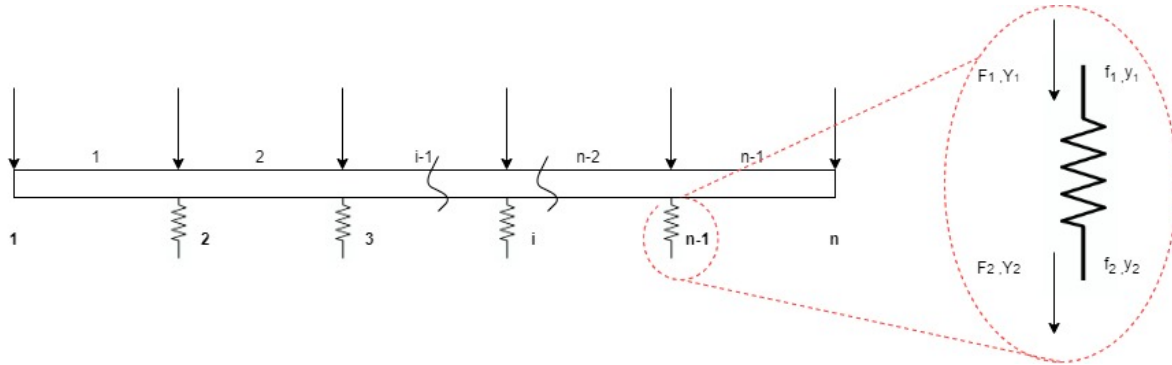


Figure 3.16: Principle of beam theory

The beam in figure 3.16 can be divided in multiple segments where the classical beam theory equations can be used to find the forces at the interaction points where a block is located. By introducing the interface and boundary conditions the equations can be written in matrix form and solved by computational software. If one decouple one element of the beam its principle configuration is shown in the red circle (figure 3.16). The local quantities for this spring are depicted with lowercase letters whereas the global quantities are uppercase letters which are applied to the whole model. Here the spring stiffness is calculated according to Hooke's law [50]. Knowing the weight distribution matrix, the displacement matrix and the stiffness matrix, one can easily calculate the pressure (P) on each block by using the effective block area.

In the past several beam theories are developed based on various assumptions, and lead to different levels of accuracy. One of the most useful of these theories was first described by Euler-Bernoulli (Bauchau and Craig [6]). With respect to the empirical studies discussed before this method requires more information and is much more complex. Input parameters are the weight distribution and the inertia distribution, both known for the vessel. For the Euler-Bernoulli theory one can recall the relations as explained in the study for a single dock block.

Looking at the FEM analysis done by Vanhaesebrouck [16] it is clear that this analytical method is too simple to get realistic results. From this result one can conclude that the loads are smoothed, this because in reality the individual beam elements are higher w.r.t. their length. So the elements can not have the assumption to be slim and thin, this leads to the result shown in figure 3.17. It should be mentioned that this analysis is on a yacht, which has noticeable different properties as a marine vessel. As the stiffness of marine vessels is relatively high compared to luxury yachts it can possibly give different results, therefore the beam on elastic foundation according to the Euler-Bernoulli beam is a good preliminary concept for the ship model.

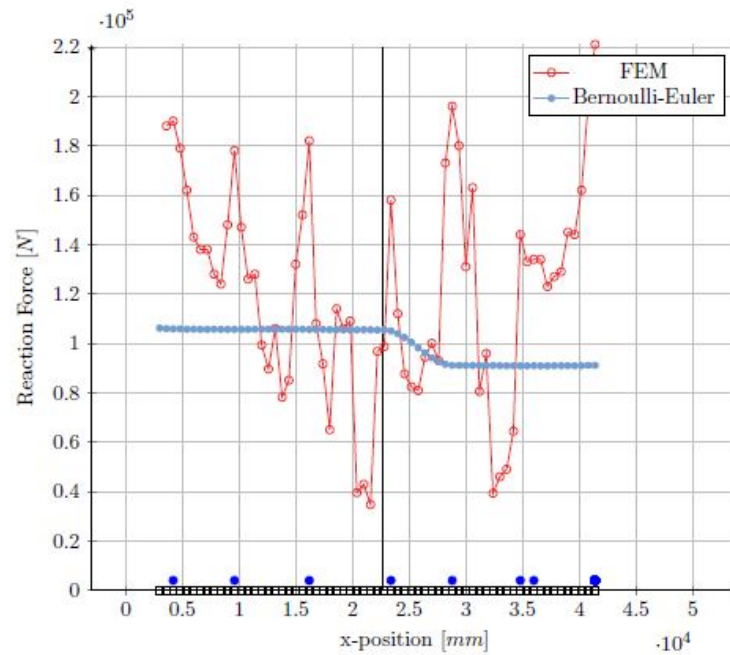


Figure 3.17: Dock block reactions retrieved by FEM for the Euler-Bernoulli principle [16]

Similar to the Euler-Bernoulli beam theory there is the Timoshenko beam theory [21], with some similar assumptions as well. The Timoshenko beam theory is an extension of the Euler-Bernoulli beam theory that includes first-order transverse shear effect [46]. The plane cross-sections remain plane but not necessarily perpendicular to the neutral axis after bending, which generates an improved theory which needs to be checked. However, Timoshenko requires the shear area distribution as necessary input, with this the shear deflection is not neglected. From figure 3.18 one can conclude that the Timoshenko theory is an already more accurate approach as seen in previous sections. There are some over- and underestimations but the physics are captured in a reliable manner.

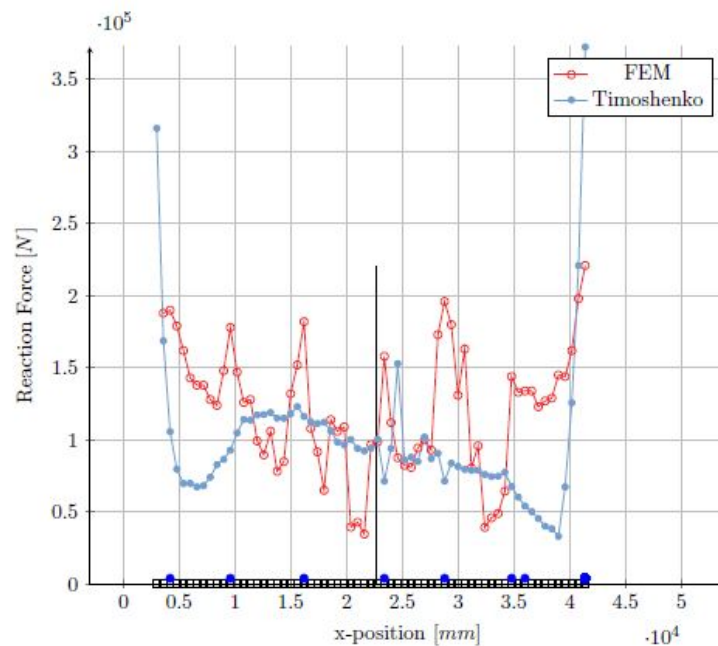


Figure 3.18: Dock block reactions retrieved by FEM for the Timoshenko principle [16]

3.3. Conclusions

3.3.1. Block model methodology

The objective to predict deformation of the individual material layers for one single dock block is a coherence of changing parameters and time wise optimal modelling. With the change of parameters, one could recall the use of different material specimens or a varying distributed load. With a time wise optimal model it is desired to have a fast prediction in a closed form solution, by this way adjustments does not lead to an increase in prediction time. The model should consider the interaction between materials and should be able to yield correct, fast (computational and modelling time) and use-able results for the designer. So, unless the fact that the Winkler model not account for directional load spreading it is still a fast and reliable way of predicting the deformation. By using the double Winkler foundation it is possible to capture both the non-linear material effects as also the non-linear material interaction. Other analytical models can become mathematically complex and lead to parameters which are hard to determine.

3.3.2. Ship model methodology

The problem of the ship on multiple blocks and the fact that failure of one block needs to be avoided leads to an analytical way of solving. Considering the load variation, and therefore the consequent response variation is the most important problem which needs to be solved. As discussed before, a finite element method is too demanding and only applicable to one situation. Finite element methods can be used to validate the obtained model; however, this method is not suitable in order to solve various problems with general basics. The difference between the empirical and analytical method, is the assumptions made. When using an empirical method to solve a problem the assumptions are based on experiences from practice, where in analytical methods the problem is solved by a mathematical expression. In order to find the optimized dock block configuration, the model needs to solve an encompassing problem which can be described by mathematical expressions. By using the beam on elastic foundation as starting point the model can be developed by adding complexity, doing so the assumptions made can be clarified. The model used for this thesis is described in chapter 4. The preliminary concept is the standard Euler-Bernoulli beam theory, which can be expanded too the Timoshenko theory when needed.

Modelling of dock block and ship behaviour

In this chapter, the modelling of a single dock block and the ship behaviour are introduced.

4.1. Modelling of single dock block

The preliminary concept of the model of a single dock block is a double Winkler beam as described in the review of a dock block static analysis, this with the assumption that the shear strains are approximately zero. This assumption is justifiable if the influence of this shear effect is evaluated.

4.1.1. Classical beam theory and introduction of the interaction parameter

The classical beam theory is also known as the Euler-Bernoulli theory and the leading theory for the double Winkler as described in chapter 3 lead to the equation for the shear, moment, slope and deflection. Figure 4.1 gives the sign convention in order to prevent mistakes.

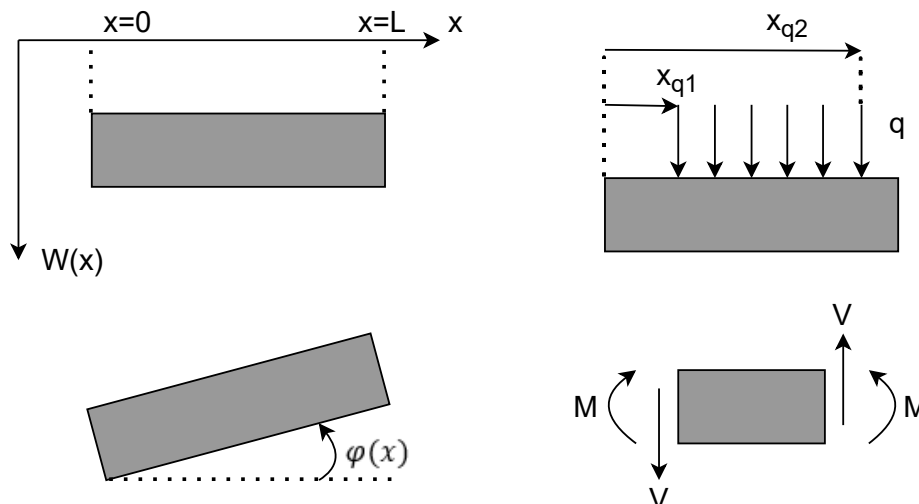


Figure 4.1: Sign convention for: Displacements, applied loads and internal forces when using beam theories

The double Winkler foundation is the model of 2 beams elastically connected to each other and to the rigid ground. To get understanding of the elastic layer and the according interaction parameter a parametric study is obtained by using a beam on elastic foundation. This situation would describe an occasion where only one timber layer is presented. The differential equation of equilibrium of an

infinitely small element, with deflection $W(x)$, of a homogeneous elastic bending beam with constant bending stiffness resting on a Winkler foundation and subjected to a load $q(x)$ can be written as:

$$\frac{d^2}{dx^2} \left(EI \frac{d^2 W}{dx^2} \right) = q - k_d W \quad (4.1)$$

Where:

W	= Material deformation	$[mm]$
E	= Material Young's modulus	$[N/mm^2]$
I	= Material inertia term ($= \frac{bh^3}{12}$)	$[mm^4]$
q	= Uniform distributed load	$[N/mm]$
k_d	= Interaction parameter	$[N/mm^2]$

The solution of equation 4.1 is the sum of the homogeneous solution $W_h(x)$ and the particular solution $W_p(x)$. Under the assumption that EI (flexural rigidity) is constant along the beam. In order to solve the general expression, the homogeneous part needs to be solved by using the characteristic equation of the differential equation. The full derivation for the beam on elastic foundation with a uniform load is described in appendix B. To complete the superposition the particular solution should be added to the solution of the homogeneous equation. The total solution is given in equation 4.2, where C_1, C_2, C_3 and C_4 are the integration constants.

$$W(x) = C_1 \exp\left(\frac{(-k_d E^3 I^3)^{1/4} x}{EI}\right) + C_2 \exp\left(-\frac{(-k_d E^3 I^3)^{1/4} x}{EI}\right) + C_3 \exp\left(i \frac{(-k_d E^3 I^3)^{1/4} x}{EI}\right) + C_4 \exp\left(-i \frac{(-k_d E^3 I^3)^{1/4} x}{EI}\right) + \frac{q}{k_d} \quad (4.2)$$

Every structure has a finite length and is fixed or attached to another structure at its ends. To predict the mechanical behaviour of a structure, one have to describe mathematically the conditions at the ends of the structure. This is done with the help of the boundary conditions. The equation of the static beam is described by a fourth order differential equation, therefore, at each end in the beam, two boundary conditions have to be formulated. For the dock block multiple boundary condition situation could arise, where the individual layers could be pinned, clamped or no fixation (free) at all.

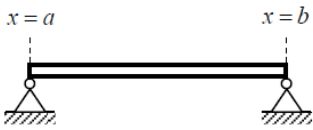
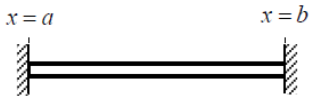
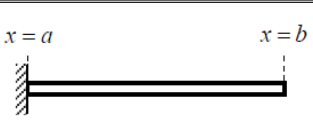
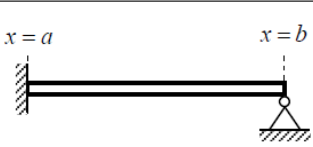
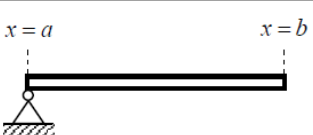
Type of fixation	Schematization	Boundary Conditions
Pinned-Pinned		$x = a: w = d^2w/dx^2 = 0$ $x = b: w = d^2w/dx^2 = 0$
Clamped-Clamped		$x = a: w = dw/dx = 0$ $x = b: w = dw/dx = 0$
Clamped-Free		$x = a: w = dw/dx = 0$ $x = b: d^2w/dx^2 = d^3w/dx^3 = 0$
Clamped-Pinned		$x = a: w = dw/dx = 0$ $x = b: w = d^2w/dx^2 = 0$
Pinned-Free		$x = a: w = d^2w/dx^2 = 0$ $x = b: d^2w/dx^2 = d^3w/dx^3 = 0$

Figure 4.2: Euler-Bernoulli boundary conditions (W=deflection, ϕ =slope, M=moment and V=shear) [36]

The mechanical characteristics of a structure, such as the cross sectional area or an elasticity modulus, can change abruptly along the structure. The cross-section at which this happens is called an interface. At the interface, the equations of motion are not valid and the interface conditions have to be formulated. This situation could arise where not the complete area of the dockblock is loaded, as shown in figure 4.3. One could easily divide the beam in 3 segments where equation 4.2 and its derivatives are used for every segment. The boundary conditions are still valid at $x = 0$ and $x = L$, however, the interface conditions need to be introduced at $x = x_{q1}$ and $x = x_{q2}$. For the situation of a pinned-pinned beam with partly uniform distributed load between abscissa x_{q1} and x_{q2} the following boundary and interface conditions need to be substituted (table 4.1):

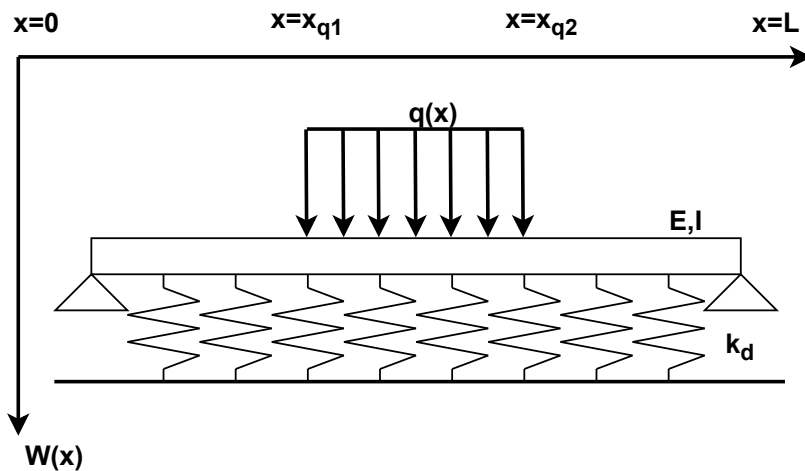


Figure 4.3: Euler-Bernoulli boundary and interface conditions for a partly uniform distributed load (load is located between abscissa x_{q1} and x_{q1})

Table 4.1: Boundary and interface conditions for Euler-Bernoulli beam (Pinned-Pinned)

Condition	Location	$V_i(x)$	$M_i(x)$	$\phi_i(x)$	$w_i(x)$
BC_1	$x = 0$	-	$M_1(0) = 0$	-	$W_1(0) = 0$
IC_{1-4}	$x = x_{q1}$	$V_1(x_{q1}) = V_2(x_{q1})$	$M_1(x_{q1}) = M_2(x_{q1})$	$\phi_1(x_{q1}) = \phi_2(x_{q1})$	$W_1(x_{q1}) = W_2(x_{q1})$
IC_{5-8}	$x = x_{q2}$	$V_2(x_{q2}) = V_3(x_{q2})$	$M_2(x_{q2}) = M_3(x_{q2})$	$\phi_2(x_{q2}) = \phi_3(x_{q2})$	$W_2(x_{q2}) = W_3(x_{q2})$
BC_2	$x = L$	-	$M_3(L) = 0$	-	$W_3(L) = 0$

After substitution of the conditions one can find the integration constants C_1 , C_2 , C_3 and C_4 . In case the beam is divided into 3 segments to solve for the discontinuous load there are 3 times 4 constants (12 in total). Applying the appropriate conditions gives the final solution, dependent of the interaction parameter (k_d). In order to demonstrate the influence of this parameter a numerical example is used, where flexural rigidity (EI) is known by practical values. For this example the boundary conditions are set to be pinned-pinned and the load is completely uniform over the length. Figure 4.4 illustrates the influence of the interaction parameter. There are two limit cases: if $k_d \rightarrow 0$ the beam acts as a simply supported beam with no interaction between ground and beam, if $k_d \rightarrow \infty$ the interaction between the beam and the ground is assumed to be infinitely rigid.

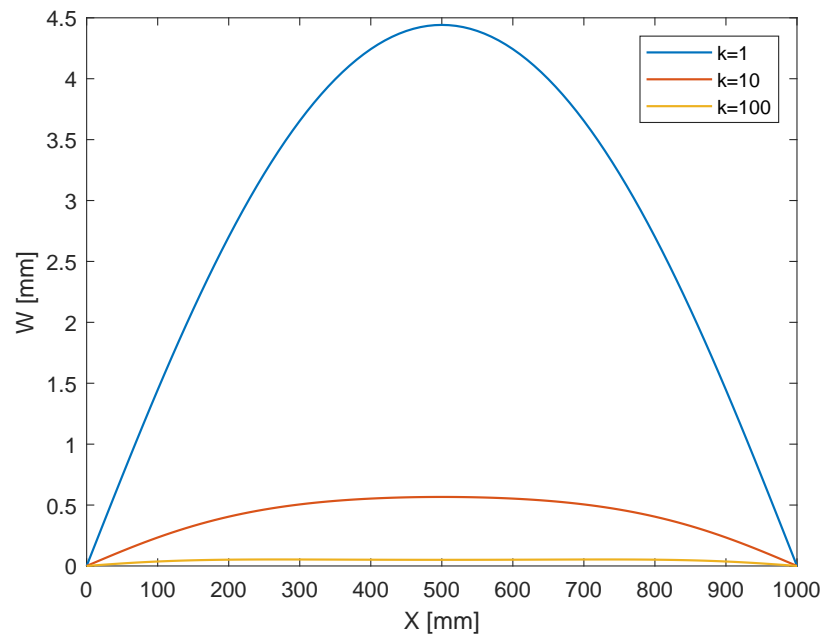
Figure 4.4: Characterization of interaction parameter k_d for the deflection diagram of a pinned-pinned boundary condition

Table 4.2 give the results for the interaction parameter between the rigid floor and the single dock block material layer. In practice it is assumed that the concrete or steel foundation is very stiff compared to the timber layer placed on top of it, therefore it is safe to say that the value for the interaction between these two layers will tend to a high value. For a stacked block the deformation will mainly occur at the softwood on top, this because the stiffness is lower for the softwood (compared to the hardwood).

Table 4.2: Characterization of interaction parameter k_d

Value for k_d	Deflection [mm]
$k_d = 1$	4.4418
$k_d = 10$	0.5666
$k_d = 100$	0.0533

4.1.2. Solution approach for a single dock block: double Winkler method

Finally, after understanding the physics of the elastic layer and knowing the governing equations for a Euler-Bernoulli beam the final model approach can be discussed. The assumptions for this thesis lead to a dock block of two layers, top layer is softwood, and second layer is hardwood. Figure 4.5 illustrates the model of a single dock block, which can be described by a system of coupled differential equations:

$$\frac{d^2}{dx^2} \left(E_1 I_1 \frac{d^2 W_1}{dx^2} \right) = q - k_{d1} (W_1(x) - W_2(x)) \quad (4.3)$$

$$\frac{d^2}{dx^2} \left(E_2 I_2 \frac{d^2 W_2}{dx^2} \right) = k_{d1} (W_1(x) - W_2(x)) - k_{d2} W_2(x) \quad (4.4)$$

Where subscript 1 is devoted to the softwood layer and subscript 2 to the hardwood layer:

$W_{1,2}$	= Deformation	[mm]
$E_{1,2}$	= Young's modulus	[N/mm ²]
$I_{1,2}$	= Material inertia term	[mm ⁴]
k_{d1}	= Interaction parameter between hardwood and softwood	[N/mm ²]
k_{d2}	= Interaction parameter between hardwood and floor	[N/mm ²]
q	= Uniform distributed load	[N/mm]

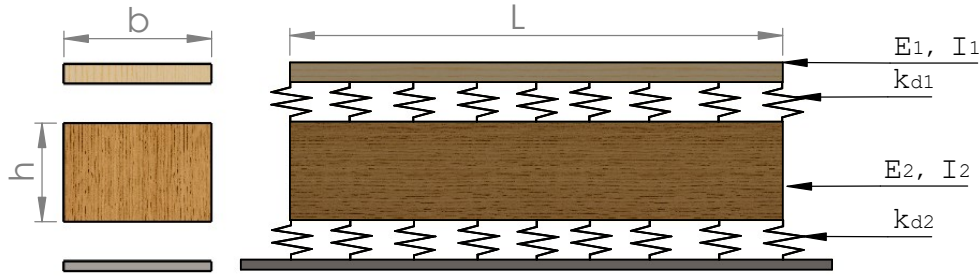


Figure 4.5: Illustration of the model representing two material layers with a double elastic foundation connecting them

Solving such a coupled system of differential equations is less straightforward as for a single uncoupled case. The coupling term lead to long mathematical expressions which need to be solved by means of computational solvers. In both MAPLE and Matlab the ODE-solve function (solve function for order differential equations) can be used. The same approach of splitting the solution in a homogeneous and particular solution is used.

So, the homogeneous solution for the deflection of the top layer holds:

$$\begin{aligned} W_{1h}(x) = & C_1 \exp \left(\frac{1}{EI_2 EI_1} \left(-\frac{i}{2} x (-8EI_2^3 EI_1^3 (A_2 + A_1))^{1/4} \right) \right) + C_2 \exp \left(\frac{1}{EI_2 EI_1} \left(\frac{i}{2} x (-8EI_2^3 EI_1^3 (A_2 + A_1))^{1/4} \right) \right) \\ & + C_3 \exp \left(\frac{1}{EI_2 EI_1} \left(-\frac{i}{2} x (-8EI_2^3 EI_1^3 (A_2 - A_1))^{1/4} \right) \right) + C_4 \exp \left(\frac{1}{EI_2 EI_1} \left(\frac{i}{2} x (-8EI_2^3 EI_1^3 (A_2 - A_1))^{1/4} \right) \right) \\ & + C_5 \exp \left(-\frac{1}{2EI_2 EI_1} \left(x (-8EI_2^3 EI_1^3 (A_2 + A_1))^{1/4} \right) \right) + C_6 \exp \left(\frac{1}{2EI_2 EI_1} \left(x (-8EI_2^3 EI_1^3 (A_2 + A_1))^{1/4} \right) \right) \\ & + C_7 \exp \left(-\frac{1}{2EI_2 EI_1} \left(x (-8EI_2^3 EI_1^3 (A_2 - A_1))^{1/4} \right) \right) + C_8 \exp \left(\frac{1}{2EI_2 EI_1} \left(x (-8EI_2^3 EI_1^3 (A_2 - A_1))^{1/4} \right) \right) \end{aligned} \quad (4.5)$$

Where :

$$\begin{aligned} A_1 &= \sqrt{EI_1^2 k_{d1}^2 + 2EI_1^2 k_{d1} k_{d2} + EI_1^2 k_{d2}^2 + 2EI_1 EI_2 k_{d1}^2 - 2EI_2 EI_1 k_{d1} k_{d2} + EI_2^2 k_{d1}^2} \\ A_2 &= EI_1 k_{d1} + EI_1 k_{d2} + EI_2 k_{d1} \end{aligned}$$

For the second layer the following expression for the homogeneous solution is found:

$$\begin{aligned}
W_{2h}(x) = & \frac{1}{2EI_2k_{d1}}(-C_1(A_2 + A_1) \exp\left(\frac{1}{EI_1EI_2}\left(-\frac{i}{2}2^{3/4}(-EI_2^3EI_1^3(A_2 + A_1))^{1/4}x\right)\right) \\
& -C_2(A_2 + A_1) \exp\left(\frac{1}{EI_1EI_2}\left(\frac{i}{2}2^{3/4}(-EI_2^3EI_1^3(A_2 + A_1))^{1/4}x\right)\right) \\
& -C_3(A_2 - A_1) \exp\left(\frac{1}{EI_1EI_2}\left(-\frac{i}{2}2^{3/4}(-EI_2^3EI_1^3(A_2 - A_1))^{1/4}x\right)\right) \\
& -C_4(A_2 - A_1) \exp\left(\frac{1}{EI_1EI_2}\left(\frac{i}{2}2^{3/4}(-EI_2^3EI_1^3(A_2 - A_1))^{1/4}x\right)\right) \\
& -C_5(A_2 + A_1) \exp\left(-\frac{1}{2EI_1EI_2}\left(2^{3/4}(-EI_2^3EI_1^3(A_2 + A_1))^{1/4}x\right)\right) \\
& -C_6(A_2 + A_1) \exp\left(\frac{1}{2EI_1EI_2}\left(2^{3/4}(-EI_2^3EI_1^3(A_2 + A_1))^{1/4}x\right)\right) \\
& -C_7(A_2 - A_1) \exp\left(-\frac{1}{2EI_1EI_2}\left(2^{3/4}(-EI_2^3EI_1^3(A_2 - A_1))^{1/4}x\right)\right) \\
& -C_8(A_2 - A_1) \exp\left(\frac{1}{2EI_1EI_2}\left(2^{3/4}(-EI_2^3EI_1^3(A_2 - A_1))^{1/4}x\right)\right) \\
& +2k_{d1}(C_1 \exp\left(\frac{1}{EI_1EI_2}\left(-\frac{i}{2}2^{3/4}(-EI_2^3EI_1^3(A_2 + A_1))^{1/4}x\right)\right) \\
& +C_2 \exp\left(\frac{1}{EI_1EI_2}\left(\frac{i}{2}2^{3/4}(-EI_2^3EI_1^3(A_2 + A_1))^{1/4}x\right)\right) \\
& +C_3 \exp\left(\frac{1}{EI_1EI_2}\left(-\frac{i}{2}2^{3/4}(-EI_2^3EI_1^3(A_2 - A_1))^{1/4}x\right)\right) \\
& +C_4 \exp\left(\frac{1}{EI_1EI_2}\left(\frac{i}{2}2^{3/4}(-EI_2^3EI_1^3(A_2 - A_1))^{1/4}x\right)\right) \\
& +C_5 \exp\left(-\frac{1}{2EI_1EI_2}\left(2^{3/4}(-EI_2^3EI_1^3(A_2 + A_1))^{1/4}x\right)\right) \\
& +C_6 \exp\left(\frac{1}{2EI_1EI_2}\left(2^{3/4}(-EI_2^3EI_1^3(A_2 + A_1))^{1/4}x\right)\right) \\
& +C_7 \exp\left(-\frac{1}{2EI_1EI_2}\left(2^{3/4}(-EI_2^3EI_1^3(A_2 - A_1))^{1/4}x\right)\right) \\
& +C_8 \exp\left(\frac{1}{2EI_1EI_2}\left(2^{3/4}(-EI_2^3EI_1^3(A_2 - A_1))^{1/4}x\right)\right))EI_2)
\end{aligned} \tag{4.6}$$

The particular solution for the toplayer is easily found by the following equation:

$$W_{1p}(x) = \frac{q(k_{d1} + k_{d2})}{k_{d1}k_{d2}} \tag{4.7}$$

Where the particular solution for the second layer is recalled by:

$$W_{2p}(x) = \frac{q}{k_{d2}} \tag{4.8}$$

Solution procedure for the double elastic foundation model is the same as for a single elastic foundation. First determine what boundary conditions should be applied, afterwards substitute these in the equivalent equations for the shear, moment, slope and deflection. The model represents two beams, and therefore there are 2 times 4 boundary conditions. Since there is a coupled system of 2 differential

equations of the order 4, one must find 8 integration constants. For this solution the only unknown values at this point are the interaction parameters k_{d1} and k_{d2} , which are discussed by means of a parametric study in the next subsection.

4.1.3. Parametric study for interaction foundation modulus

The most standard dock block configuration is the one with a hardwood at the bottom and with a spruce on top, here the difference in Young's modulus is significant. Besides the Young's modulus, is the inertia term for the hardwood in almost every situation larger, this because the height is larger (respectively $\approx 50 \text{ mm}$ and $\approx 200 \text{ mm}$). Since the elastic foundation incorporates the elasticity of the individual layers of the specimens, the foundation modulus may be found by comparative study with test data. For engineering purpose, it is desired to have a specific value of k_d for every specimen (according their flexural stiffness). Solution procedure is to use the width (b), height (h) and Young's modulus (E) to find the interaction modulus. Where Shokrieh [45] uses a Winkler foundation to represent the delamination interaction in a cantilever beam it is now used for similar purpose.

$$k_d = E \frac{b}{h} \quad (4.9)$$

One is interested in the maximum allowable pressure at the contact area, therefore the interaction parameters are determined by this limit. It is also possible to correct the Young's modulus to an average value for the complete elastic range, or even with the non-linear range, but this will lead to underestimation of the deformation in the end. Interaction parameter one is therefore a trade-off between the softwood Young's modulus and its dimensions, where the hardwood interaction layer is the same trade-off for the hardwood properties. Exceeding of the hardwood yield point should be avoided, but for the softwood it is not the case. Using the secant modulus for the softwood layer it is possible to capture the non-linear material range. The secant modulus is the slope of the line between the origin and a point of the non-linear range. For this parametric study it is desired to have a full spectrum of material information, having the Young's modulus and the graphs for force-displacement and stress-strain relation would lead to insight in the non-linear interaction of the material layers. Using these results it is possible to assess the interaction parameters for every block configuration.

4.1.4. Final dock block deformation evaluation

The solution approach for the deformation and resulting pressures are calculated by the Euler-Bernoulli theory. To account for the rigid interaction between the ground and the hardwood layer, and to account for the interaction of the hard- and softwood an elastic layer is introduced. The elastic layer is introduced as the Winkler foundation which represents the mathematical expression of the physics observed by compression a stacked block. Where the EI term represents the flexural rigidity, are the k_{d1} and k_{d2} terms represented as the interaction parameters. The steps taken to estimate if an individual material layer exceeds the maximum allowable capacity is found as:

- Step 1: Calculate the deformation (W) with the equation for a double Winkler system.
- Step 2: Express the deformation as a strain per material layer with the strain relation: $\epsilon = W/h$, where h is the original height of the layer.
- Step 3: Recall the stress-strain relation to find the pressure of the individual material layer: $\sigma = E\epsilon$. Or check if the hardwood strain has exceeded the yield point, which lead to plastic deformation.

For these steps, the Young's modulus, and according force-displacement and stress-strain relation need to be determined. An accurate and realistic value for these parameters lead to a better prediction of the deformation. An experimental campaign will be carried out to find these values for the specimens used at Damen. Doing compression tests on both individual materials, and combination of materials, lead to a physical representation of the configuration at the yards. With this data the interaction parameter can be evaluated and the non-linear behaviour is introduced. The Matlab script for the model of a single dock block is provided in appendix B by figures B.1-B.4.

4.2. Modelling of ship behaviour

From the literature review in chapter 3 it is clear that for a close form solution with multiple changing variables the beam theory (on multiple springs) is a suitable way of representing the physical problem with mathematical expressions. The objective of this model is to find the spring reaction forces, which will be used as load input value for the single dock block analysis.

The known input parameters for the ship model are:

W_s	= Ship's weight distribution (per section)	[ton/m]
E_s	= Ship's Young's modulus	[N/m ²]
I_s	= Ship's inertia (per section)	[m ⁴]
x_f	= Ship's frame location	[m]
x_s	= Ship's section location	[m]
x_b	= Keel block location	[m]
K	= Keel block spring stiffness	[N/m ²]
A_{eff}	= Keel block contact area	[m ²]
l_{hw}, b_{hw}, h_{hw}	= Hardwood dimensions	[mm]
l_{sw}, b_{sw}, h_{sw}	= Softwood dimensions	[mm]

With these input parameters it is obtained to find the spring reaction forces. The ship is divided in multiple segments, a segment is the distance between two dock blocks (figure 4.6). Normally the keel blocks are placed on the locations where a transverse bulkhead is located, however, this can differ due to ship restrictions. When the block is not exactly located at the bulkhead, the distributed load is percentage wise calculated. In the parts of the ship where no block is located one can just use the weight distribution as given, when the frame spacing and block spacing are equal, the weight distribution between two blocks is directly used. If the spacing between two blocks is not equal to the frame spacing, the weight distribution between two blocks is calculated as:

$$W_s = W_s(i) \frac{x_f(i) - x_b(i)}{x_b(i+1) - x_b(i)} + W_s(i+1) \frac{x_b(i+1) - x_f(i)}{x_b(i+1) - x_b(i)} \quad (4.10)$$

Secondly the weight distribution is calculated to a distributed load (N/m) per segment with:

$$q(x) = W_s \cdot 1000 \cdot g \quad (4.11)$$

The only unknown for this model is the spring stiffness (N/mm) representing the dock block. To model the ship and dock block interaction, the blocks can be modelled as just one solid material with an equivalent modulus of elasticity (equation 4.12). So for a dock block consisting of a softwood and hardwood (as the concrete or steel foundations are assumed rigid), the following calculations can be made:

$$E_{eq} = \frac{h_{sw} + h_{hw}}{\frac{h_{sw}}{E_{sw}} + \frac{h_{hw}}{E_{hw}}} \quad (4.12)$$

The spring stiffness (K) is required for the interface conditions where a block is located.

$$K = \frac{E_{eq} A_{eff}}{h_{sw} + h_{hw}} \quad (4.13)$$

4.2.1. Euler-Bernoulli model approach for ship

The preliminary approach is the classical Euler-Bernoulli beam, with the assumption that the shear strains are approximately zero. For every segment in figure 4.6 the input is known, now the Euler Bernoulli beam equations and the corresponding conditions can be implemented. Integrating the governing equation for the Euler-Bernoulli beam as described in chapter 3 lead to the equations for the shear, moment, slope and deformation, all with the integration constants C_1, C_2, C_3 and C_4 .

$$V(x) = -EI \left(\frac{qx}{EI} + C_1 \right) \quad (4.14)$$

$$M(x) = -EI \left(\frac{qx^2}{2EI} + C_1x + C_2 \right) \tag{4.15}$$

$$\phi(x) = \frac{1}{EI} \left(\frac{qx^3}{6} + \frac{C_1x^2}{2} + C_2x + C_3 \right) \tag{4.16}$$

$$W(x) = \frac{1}{EI} \left(\frac{qx^4}{24} + \frac{C_1x^3}{6} + \frac{C_2x^2}{2} + C_3x + C_4 \right) \tag{4.17}$$

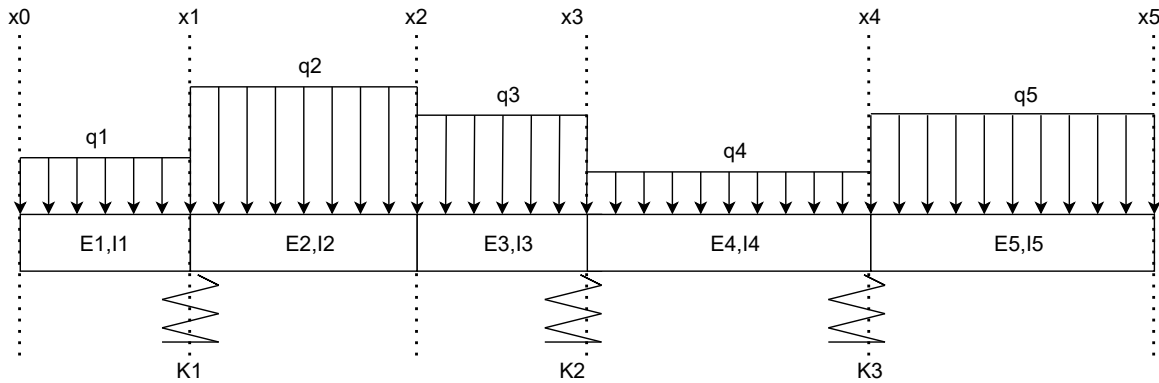


Figure 4.6: Segmentation view of ship model with 3 springs representing the dock blocks located at x_1, x_3 and x_4

One uses the boundary and interface conditions to find the integration constants, for a ship on dock blocks the very first and last segments are always without a block, and therefore modelled as free-free ends. The interface conditions describes the conditions between two segments, when there is no block present at this location (for example at x_2), it is predefined that the deformation, slope, moment and shear at this point should be equal for both segments. In case there is a dock block at the interface it is defined by a shift in the shear force, which leads to the condition where the shear difference of two segments needs to be equal to the spring reaction force. For the illustration of figure 4.6 the boundary and interface conditions are given in table 4.3.

Table 4.3: Boundary and interface conditions

Condition	Location	$V_i(x)$	$M_i(x)$	$\phi_i(x)$	$w_i(x)$
BC_1, BC_2	$x = 0$	$V_1(0) = 0$	$M_1(0) = 0$	-	-
$IC_{1,1} - IC_{1,4}$	$x = x_1$	$V_2(x_1) - V_1(x_1) = K_1 \cdot w_2$	$M_1(x_1) = M_2(x_1)$	$\phi_1(x_1) = \phi_2(x_1)$	$w_1(x_1) = w_2(x_1)$
$IC_{2,1} - IC_{2,4}$	$x = x_2$	$V_2(x_2) = V_3(x_2)$	$M_2(x_2) = M_3(x_2)$	$\phi_2(x_2) = \phi_3(x_2)$	$w_2(x_2) = w_3(x_2)$
$IC_{3,1} - IC_{3,4}$	$x = x_3$	$V_4(x_3) - V_3(x_3) = K_2 \cdot w_4$	$M_3(x_3) = M_4(x_3)$	$\phi_3(x_3) = \phi_4(x_3)$	$w_3(x_3) = w_4(x_3)$
$IC_{4,1} - IC_{4,4}$	$x = x_4$	$V_5(x_4) - V_4(x_4) = K_3 \cdot w_5$	$M_4(x_4) = M_5(x_4)$	$\phi_4(x_4) = \phi_5(x_4)$	$w_4(x_4) = w_5(x_4)$
$BC_3 BC_4$	$x = L$	$V_1(L) = 0$	$M_1(L) = 0$	-	-

Substitution of the conditions in the equivalent equations for the shear, moment, slope and deformation gives for this situation 20 equations with 20 unknowns. So n segments give $4n$ conditions (2 boundary conditions and $4(n - 1)$ interface conditions), $4n$ equations (4.14-4.17) and $4n$ unknowns (A_i, B_i, C_i, D_i). The equations and unknowns will give a linear set of equations which can be solved by means of matrix equations. Equation 4.18 gives the matrix for the example of a ship with 5 segments. When the boundary and interface conditions are substituted one gets equations containing a homogeneous and a particular part. The homogeneous parts will be located in the rectangular matrix on the left, where the particular parts represent the force vector on the right. Multiplying the homogeneous matrix with the vector containing the constants equals the force vector. This expression can easily be expanded in case of more segments, however, the location of the boundary conditions remain the same.

$$\begin{bmatrix}
H - BC_1(A_1) & H - BC_1(A_2) & \dots & H - BC_1(D_3) & H - BC_1(D_4) \\
H - BC_2(A_1) & H - BC_2(A_2) & \dots & H - BC_2(D_3) & H - BC_2(D_4) \\
H - IC_{1,1}(A_1) & H - IC_{1,1}(A_2) & \dots & H - IC_{1,1}(D_3) & H - IC_{1,1}(D_4) \\
H - IC_{1,2}(A_1) & H - IC_{1,2}(A_2) & \dots & H - IC_{1,2}(D_3) & H - IC_{1,2}(D_4) \\
\vdots & \vdots & \dots & \vdots & \vdots \\
H - IC_{4,3}(A_1) & H - IC_{4,3}(A_2) & \dots & H - IC_{4,3}(D_3) & H - IC_{4,3}(D_4) \\
H - IC_{4,4}(A_1) & H - IC_{4,4}(A_2) & \dots & H - IC_{4,4}(D_3) & H - IC_{4,4}(D_4) \\
H - BC_3(A_1) & H - BC_3(A_2) & \dots & H - BC_3(D_3) & H - BC_3(D_4) \\
H - BC_4(A_1) & H - BC_4(A_2) & \dots & H - BC_4(D_3) & H - BC_4(D_4)
\end{bmatrix}
\begin{bmatrix}
A_1 \\
B_1 \\
C_1 \\
D_1 \\
\vdots \\
A_4 \\
B_4 \\
C_4 \\
D_4
\end{bmatrix}
=
\begin{bmatrix}
P - BC_1 \\
P - BC_2 \\
P - IC_{1,1} \\
P - IC_{1,2} \\
\vdots \\
P - IC_{4,3} \\
P - IC_{4,4} \\
P - BC_3 \\
P - BC_4
\end{bmatrix} \quad (4.18)$$

With symbolic computational software (MAPLE, Matlab) one could make the matrix as discussed above. The matrix will be a $4n \times 4n$ squared matrix and the vector a $4n \times 1$, which lead to very large matrices for the whole ship as a system of segments. With a linear solve function one can find the unknown coefficients, which can be substituted back in the governing equations to have a full expression for the deformation. Knowing the deformation one can recall the following relation to obtain the reaction force:

$$F_r(x_i) = K_i W_n(x_i) \quad (4.19)$$

Where:

$$\begin{aligned}
F_r(x_i) &= \text{Dock block reaction force at location } i & [N] \\
K_i &= \text{Dock block stiffness at location } i & [N/mm^2] \\
W_i &= \text{Deformation of segment } n \text{ at location } i & [mm]
\end{aligned}$$

The spring reaction force (F_r) is a point load which needs to be converted to a distributed load to use as an input parameter in the single dock block model. The point load is divided by the length (L_{sw}) of the contact area which results in the uniform distributed load (q).

$$q = F_r/L_{sw} \quad (4.20)$$

4.3. Conclusion

For both models it is desired to have realistic input values. An experimental campaign will be carried out to assess the material properties (including also for the moisture content) of the different layers by considering larger specimens (to avoid size effects) and multiple samples. The values for the Young's modulus, yield point and equivalent stress-strain relation are the goal in this study. Evaluating the measured data will also give an insight in the interaction parameters for both the floor-material, as material-material interaction.

4.3.1. Single dock block model

The double Winkler foundation represents the two material layers with the flexural rigidity. The connection between the bottom layer and the rigid support may be found as: $k_{d2} = E_{hw}b_{hw}/h_{hw}$. The interaction parameter between the softwood and hardwood layer can be found as: $k_{d1} = E_{sw}b_{sw}/h_{sw}$. In case the keel width is smaller than the block width a partly uniform distributed load is the consequence. Measured data will give an yield point which will be used to evaluate the maximum capacity of the block. From the single dock block model one can recall the strain on an individual material layer, which can be evaluated with respect to it's yield point.

4.3.2. Ship model

The model with multiple blocks and the ship represented as a beam on top is known by the Euler-Bernoulli theory. Here the ship is divided into multiple segments representing the the parts between two dock blocks, or two frames. Boundary and interface conditions in combination with the governing equations for the Euler-Bernoulli beam theory lead to a linear set of equations. By means of a matrix solution the integration constants are found and substituted back in the equations for the deflection per segment. With the deformation of the segment one can find the reaction force on the interface location where a dock block is present. This reaction force is the input value for the single dock block model.

5

Validation of single dock block model and ship model

In this chapter the model for the single dock block deformation and the reaction force by a ship model is validated.

5.1. Validation of single dock block model

In this thesis it is the objective to predict the block deformation, accounting the non-linear effects. With the model for a single dock block it is obtained to reproduce the material interaction and reproduce the physical effect of compression by mathematical expressions. The assumptions and choices made in chapter 4 are here discussed.

5.1.1. Validation of neglecting the Timoshenko shear effect for the single dock block model

The model for a single dock block makes use of the fundamentals of the Euler-Bernoulli theory. In this section it is validated if the assumption of neglecting the Timoshenko shear effect is justifiable. The validation is done with a simply supported homogeneous beam subjected to a uniform distributed load. Integrating the governing Euler-Bernoulli equation (eq. 5.1) lead to the equation for the shear (V), moment (M), slope (ϕ) and deformation (W), all with unknown integration constants C_1 , C_2 , C_3 and C_4 .

Governing equation for the static analysis Euler-Bernoulli theory:

$$\frac{d^2}{dx^2} \left(EI \frac{d^2 W}{dx^2} \right) = q \quad (5.1)$$

$$W(x) = \frac{1}{EI} \left(\frac{qx^4}{24} + \frac{C_1 x^3}{6} + \frac{C_2 x^2}{2} + C_3 x + C_4 \right) \quad (4.17 \text{ revisited})$$

The analytical solution of the Timoshenko theory is constituted by the superposition of the related bending effect (equal to the Euler-Bernoulli theory), and the related shear effect. The governing equations are the following coupled system of ordinary differential equations:

$$\frac{d^2}{dx^2} \left(EI \frac{d\phi}{dx} \right) = q \quad (5.2)$$

$$\frac{dW}{dx} = \phi - \frac{1}{\kappa AG} \frac{d}{dx} \left(EI \frac{d\phi}{dx} \right) \quad (5.3)$$

Where:

- κ = Timoshenko shear coefficient (= $5/6$ for rectangular section) [-]
- G = Shear modulus [N/mm^2]
- A = Cross section area [mm^2]

By integration and substitution one can get an expression for the deflection of the Timoshenko beam. Just as for the Euler-Bernoulli theory there are some relations for the bending moment and the shear force, which relate to the displacement and the rotation. Integration of equation 5.2 and substitution in equation 5.3 lead to a final expression of the deflection for a Timoshenko beam with integration constants C_1 , C_2 , C_3 and C_4 .

$$M = -EI \frac{d\phi}{dx} \quad (5.4)$$

$$V = \kappa AG \left(-\phi + \frac{dW}{dx} \right) \quad (5.5)$$

$$W(x) = \frac{1}{EI} \left(\frac{qx^4}{24} + \frac{C_1x^3}{6} + \frac{C_2x^2}{2} + C_3x + C_4 \right) - \frac{1}{\kappa AG} \left(\frac{qx^2}{2} + C_1x + C_2 \right) \quad (5.6)$$

In order to check the influence of the shear deflection on the total deflection a numerical example is carried out. The example deals with a timber beam (Oak) of $L = 1000 \text{ mm}$, $E_{\perp} = 404 \text{ N/mm}^2$ and is $\nu = 0.3$ (Poisson's ratio). The cross-section is a rectangular one, with height $h = 40 \text{ mm}$ and width $b = 300 \text{ mm}$. The load is uniformly distributed along the length with a value of $q = 5 \text{ N/mm}$. All the numerical values represent practical numbers. The deformation as function of its location x is illustrated for the pinned-pinned (figure 5.1) configuration.

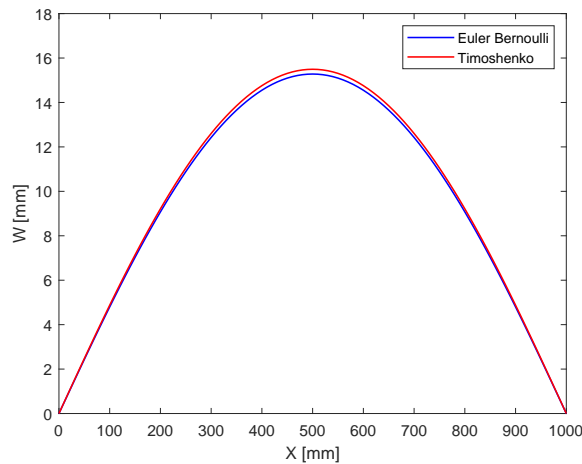


Figure 5.1: Deflection graph to check the influence of the Timoshenko shear deflection for a pinned-pinned boundary condition

The results for the scenario described in the numerical application is shown in table 5.1. On average the approximation of neglecting the Timoshenko shear part can be made when the following rule of thumb holds:

$$\frac{EI}{\kappa GAL^2} \ll 1 \quad (5.7)$$

Table 5.1: Difference between deflection of Euler-Bernoulli theory and Timoshenko theory for numerical application

Theory	Boundary Condition	Deflection [mm]	Difference [%]
Euler-Bernoulli	Pinned-Pinned	15.279	1.39
Timoshenko	Pinned-Pinned	15.494	

The Euler-Bernoulli beam is recovered when the practical limit case is reached. The shear beam and the flexural stiffness (EI) need to be in precise accordance to recover this classical beam. When $GA \rightarrow \infty$ there is no shear, which implies that the derivative of the deflection is the slope and $M \rightarrow -EI \frac{d^2W}{dx^2}$. The other way around is also a limit case, however, not very likely to occur: $EI \rightarrow \infty$ results in no bending and the shear beam is recovered. Consequently to this limit case one obtains $q = -EI \frac{dV}{dx} \rightarrow -GA \frac{d^2W}{dx^2}$.

The rule of thumb for this example has a value of 0.0015, which is definitely lower than 1, and therefore the shear effect can be neglected. As the numerical example is based on practical values it is safe to assume this situation for future engineering as well. The approximation of the shear modulus (or the Poisson's ratio) is difficult in practice, which lead to another reason to neglect the Timoshenko effect for the model of a single dock block.

5.1.2. Validation of limit case scenarios for the single dock block model

Using the elastic foundation as an representation of the ground-block interaction and material-material interaction lead to 4 possible limit case scenarios. The 4 limit cases for the model with 2 elastic beams with identical flexural rigidity are evaluated with a pinned-pinned support and subjected to a uniformly load at the complete contact area (top layer). However it is very unlikely that one of the limit cases occur in practice, it is still a good representation of the physics involved, and a validation of the work-ability of the model. For these examples once again the yard representative values were used: $E_1 = E_2 = 404 \text{ N/mm}^2$, $b_1 = b_2 = 300 \text{ mm}$, $h_1 = h_2 = 75 \text{ mm}$, $L_1 = L_2 = 1000 \text{ mm}$ and $q = 5 \text{ N/mm}$. To avoid misunderstanding it is good to mention that for all parameters and plots the subscript 1 is according the top layer (softwood) and subscript 2 is according the bottom layer (hardwood).

- Case 1: $k_{d1} \rightarrow 0 \quad k_{d2} \rightarrow 0 \quad (k_{d1} = k_{d2})$
Case 2: $k_{d1} \rightarrow \infty \quad k_{d2} \rightarrow \infty \quad (k_{d1} = k_{d2})$
Case 3: $k_{d1} \rightarrow \infty \quad k_{d2} \rightarrow 0 \quad (k_{d1} \gg k_{d2})$
Case 4: $k_{d1} \rightarrow 0 \quad k_{d2} \rightarrow \infty \quad (k_{d1} \ll k_{d2})$

Case 1 (figure 5.2): $k_{d1} \rightarrow 0 \quad k_{d2} \rightarrow 0 \quad (k_{d1} = k_{d2})$

If both the interaction parameters go to zero the deformation of the top layer returns to the original pinned-pinned Euler-Bernoulli deflection (without elastic foundation). As the value for k_{d1} is very low it results in a physical phenomenon where the second beam doesn't 'feel' any pressure and therefore doesn't deform. From this point the value for k_{d2} has no influence on the deformation of both beams.

Case 2 (figure 5.3): $k_{d1} \rightarrow \infty \quad k_{d2} \rightarrow \infty \quad (k_{d1} = k_{d2})$

When both interaction parameters go to infinity the interaction parameters are so stiff that the individual layers have no possibility to deform. The bump in the middle of the beam is a model issue which does not represent the actual material behaviour, the interaction between two individual layer, or between the rigid floor and a layer cannot cause a reaction force higher than the acting load. The deformation of the second beam is half the deformation of the top beam, this because the value for k_{d1} causes the acting load to be toned down. The model issue with respect to the boundary condition of a pinned-pinned support will be discussed later in this chapter

Case 3 (figure 5.4): $k_{d1} \rightarrow \infty \quad k_{d2} \rightarrow 0 \quad (k_{d1} \gg k_{d2})$

The influence of the interaction parameter between the rigid floor and bottom layer is already discussed in the situation where only one layer is modelled. If the value for k_{d2} goes to zero, the system does not interact with the rigid floor. When this parameter is in combination with a very stiff interaction parameter between the two individual layers, the two layers can be seen as one solid movement.

Case 4 (figure 5.5): $k_{d1} \rightarrow 0 \quad k_{d2} \rightarrow \infty \quad (k_{d1} \ll k_{d2})$

The last limit case is like the first one, since the interaction between the two individual layers is close to zero there is no deformation of the bottom beam.

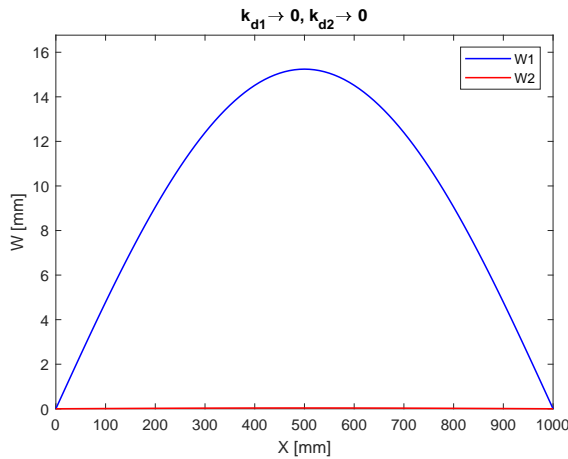


Figure 5.2: Limit case 1 for double elastic foundation beam deflection and pinned-pinned boundary conditions

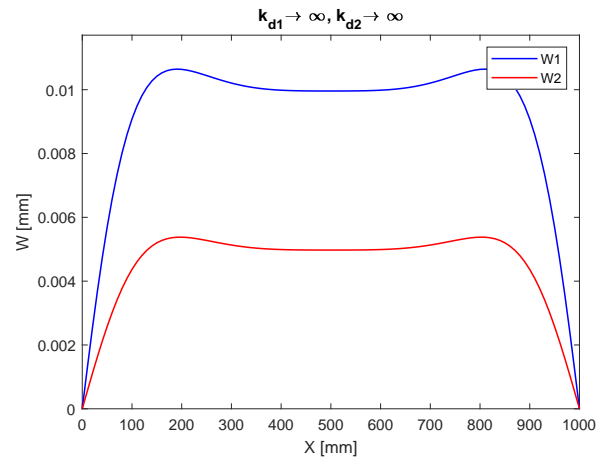


Figure 5.3: Limit case 2 for double elastic foundation beam deflection and pinned-pinned boundary conditions

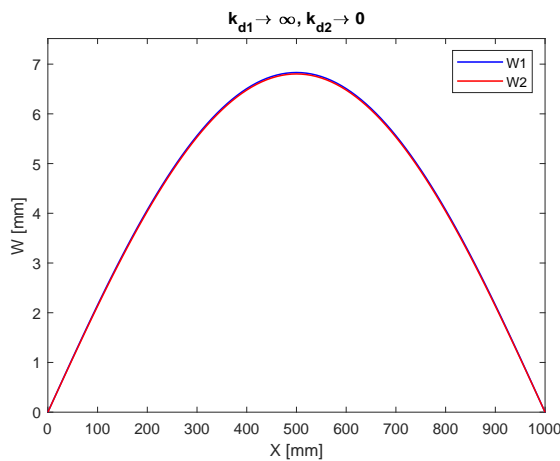


Figure 5.4: Limit case 3 for double elastic foundation beam deflection and pinned-pinned boundary conditions

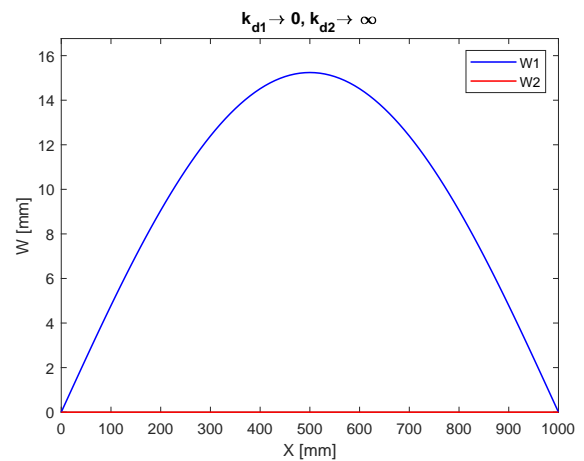


Figure 5.5: Limit case 4 for double elastic foundation beam deflection and pinned-pinned boundary conditions

5.1.3. Validation of the boundary conditions for the single dock block model

Validation with respect to the boundary conditions gives the appropriate support at the finite ends of the beam. In practice two possibilities are very likely to occur: free-free movement without any fixation or pinned-pinned constraints where no deflection is allowed at the boundaries. The Matlab script with the input parameters is shown in appendix B figures B.1 - B.4. Figure 5.6 gives the deformation of the two layers for free-free boundary conditions as a function of its position along the blocks length. Figure 5.7 gives the deformation for the pinned-pinned boundary condition.

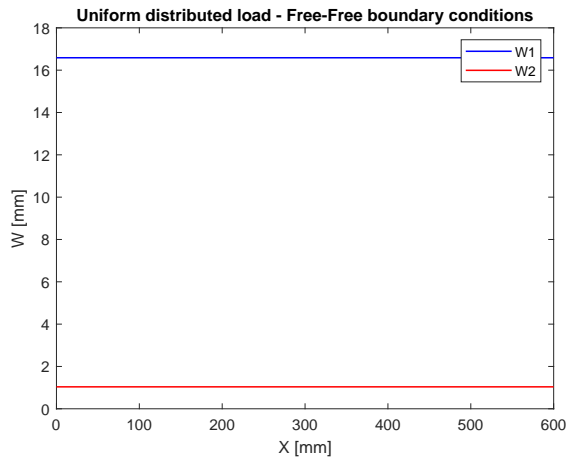


Figure 5.6: Deformation graph for Free-Free boundary conditions with two elastic layers

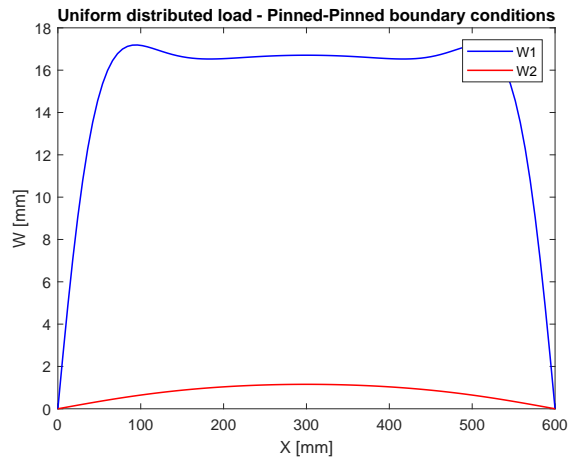


Figure 5.7: Deformation graph for Pinned-Pinned boundary conditions with two elastic layers

Result of both boundary scenarios are shown in table 5.2 (location at $x = 300$). Where the pinned-pinned boundary conditions gives a better understanding in the course of the deformation, it has some model constraints. Due to the elastic connection and the limitations of no deformation at the boundaries a non-physical situation could occur. At some locations the springs act in the opposite direction what results in negative values for deformation. One is interested in the maximum deformation, which is located at the midpoint of the block (in practice). Assuming free-free conditions for the calculation of the deformation is safe as this represents this value at the midpoint, here negative or non-physical results due to boundary restrictions does not result in local negative values. From table 5.2 it is clear that the deformations of the free-free and pinned-pinned conditions are almost exactly the same. This difference is fully dependent on the pinned-pinned block length, and the flexural rigidity of the material. If the material is stiff and short the beam has not enough 'space' to fully bend and has therefore a lower deformation. These restriction due to boundary conditions are not likely to occur in practice and a risk for the output. Assuming that the connection of the individual layers is free-free lead to a safe prediction of the deformation.

Table 5.2: Results for boundary condition scenarios

Boundary conditions	Result	Softwood	Hardwood	Units
Free-Free	Displacement	16.587	1.0367	[mm]
Pinned-Pinned	Displacement	16.706	1.1554	[mm]

5.1.4. Validation of the uniform distributed load for the single dock block load

Where in previous sections it is assumed that the complete area is effective it is now checked what happens if the top layer is not completely loaded. The area where the load is active is still the same as in previous example (600mm), however the layer itself is now larger (800mm and 1200mm). For the model this means that the layers are divided in 3 segments as discussed before, here the interface conditions are introduced. The script becomes 3 times larger what gives a longer computation time, for this reason it is important to check what the accuracy is for the assumption of complete contact area versus partly uniform contact area. So, in order to check the influence of the partly uniformly load with respect to a full uniform distributed load the deformation on the scenarios is evaluated.

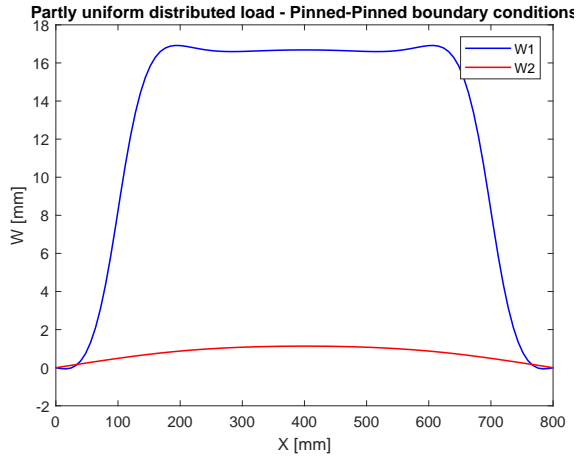


Figure 5.8: Pinned-Pinned boundary conditions - partly uniform distributed load between $x_{q1} = 100$ and $x_{q2} = 700$ with total block length of 800

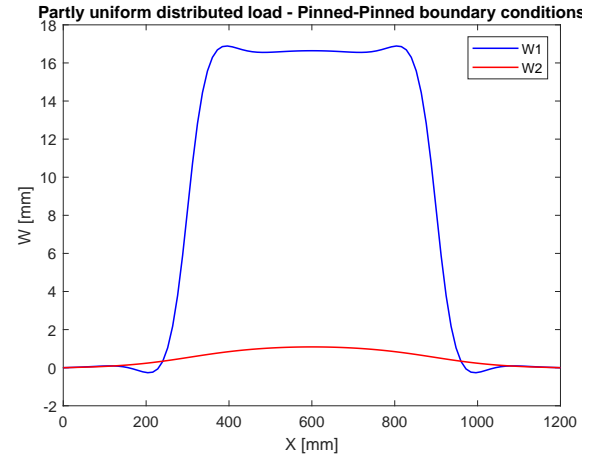


Figure 5.9: Pinned-Pinned boundary conditions - partly uniform distributed load between $x_{q1} = 300$ and $x_{q2} = 900$ with total block length of 1200

The results from table 5.3 gives values which are close to the results obtained for a complete effective contact area. The negative displacement indicates the movement at the boundaries. The larger the distance between the pinned boundary and the distributed load, the closer a free-free condition is recalled. In figure 5.8 is the distance smaller than in figure 5.9, consequently the deformation of both the soft- and hardwood are closer to the free-free situation obtained in figure 5.6. On average one can conclude that the accuracy of the 2 situations are close, taking computation time into account, it is advisable to use the simplest approach to calculate the deformation. For the final model it is safe to use the dimensions as the effective area dimensions, this with free-free boundary conditions.

Table 5.3: Results for boundary condition scenarios - partly uniform distributed load

Boundary conditions	Result	Softwood	Hardwood	Units
Free-Free	Displacement	16.6826	1.1320	[mm]
Pinned-Pinned	Displacement	16.6412	1.0907	[mm]

5.1.5. Validation of single dock block with FE model

To see if there are no mistakes made in the calculations for the single dock block model itself, it is desired to validate with a numerical study. For the numerical study the finite element software FEMAP is used. Here the exact same configuration is made, which must lead to complete accordance of both results. In the numerical solution one needs to discretize the infinitely close springs. The beams are represented as 2D bars with the dimensions representing the material layer dimensions. The top layer represents the softwood (deformation is the largest and displayed by the red color), the second layer is the hardwood (deformation is shown in purple), the pink layer is the rigid fixed ground where no deformation could occur. Interaction parameters are calculated for this situation according to equation 4.9.

Input parameters:

$$\begin{array}{llll}
 b_1 & = & 300 & [mm] \\
 h_1 & = & 50 & [mm] \\
 l_1 & = & 1000 & [mm] \\
 E_1 & = & 10 & [N/mm^2] \\
 k_{d1} & = & 60 & [N/mm^2] \\
 q & = & 559.8 & [N/mm] \\
 b_2 & = & 300 & [mm] \\
 h_2 & = & 200 & [mm] \\
 l_2 & = & 1000 & [mm] \\
 E_2 & = & 600 & [N/mm^2] \\
 k_{d2} & = & 900 & [N/mm^2]
 \end{array}$$

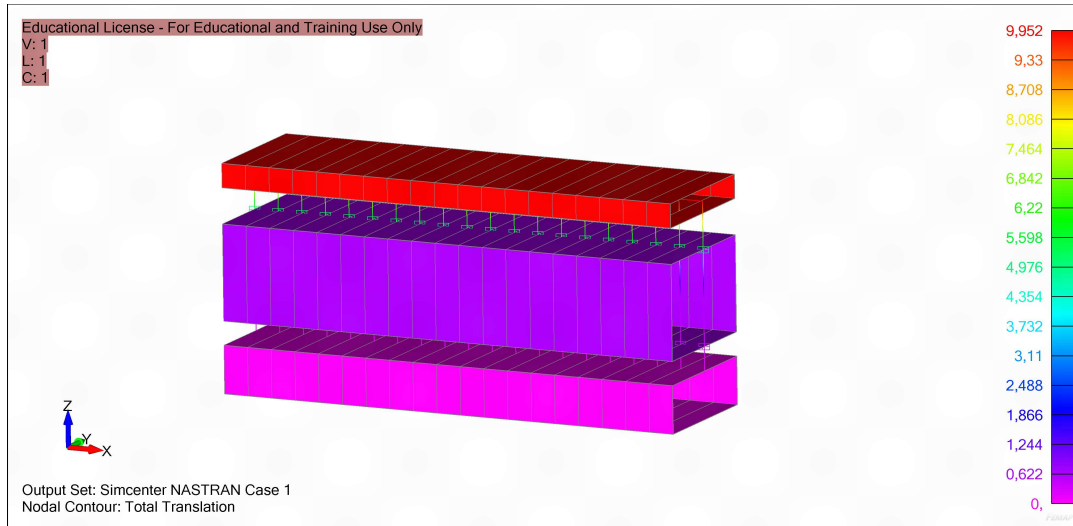


Figure 5.10: Validation of the deformation of a stacked block with FE software (FEMAP) for a practical configuration

Using the model for a single dock block as described in chapter 4 with the input parameters above give the same results as obtained from the FE analysis. With this validation it is concluded that there are no mathematical mistakes in predicting the deformation on individual material layers for a single dock block.

Table 5.4: Validation results for FE analysis compared to the single dock block model

Material layer	Deformation	Units
Softwood	9.952	[mm]
Hardwood	0.622	[mm]

5.1.6. Validation of single dock block model with case study results

Now the Matlab model is validated with a FE model it is valuable to check the results with a case study. By reproducing the configuration used in a particular situation it is checked if the results are comparable. The mathematical model predicts the deformation of the individual layers of the dock block, from this deformation the strain can be recalled. To validate the deformation of the individual material layers the already existing tool at Damen is used as validation material. This model evaluates the deformation of the dock block by means of the equivalent Young's modulus, what means that it treats the block as one solid. For this case the load is taken from the weight distribution and identical in both cases, therefore the validation is only on the blocks itself. The block spacing is 600mm according to the dockplan in figure C.1, so 1 frame has a length of 600mm . Interaction parameters are calculated by equation 4.9 as: $k_{d1} = 60\text{N/mm}^2$ and $k_{d2} = 900\text{N/mm}^2$.

Input parameters for deformation calculation (values can be found in appendix C table C.3):

Block frame number	= Location where the blocks are located	[–]
l_{sw}	= block length of the softwood	[mm]
l_{hw}	= block length of the hardwood	[mm]
b_{sw}	= block width of the softwood	[mm]
b_{hw}	= block width of the hardwood	[mm]
h_{sw}	= block height of the softwood	[mm]
h_{hw}	= block height of the hardwood	[mm]
A_{eff}	= effective contact area	[mm ²]
E_{sw}	= Young's modulus softwood	[N/mm ²]
E_{hw}	= Young's modulus hardwood	[N/mm ²]

As the procedure for each block is the same it is not necessary to evaluate every single block in this validation. The first 10 blocks are checked for the new model as for the already existing tool. The loads on the first blocks are the highest, and therefore the most interesting ones to evaluate. Table 5.5 gives the results for the two approaches. The difference column represents the difference of the softwood deformation with respect to the total block deformation of the existing tool.

Table 5.5: Material deformation for both the existing tool as the new tool

Frame	Softwood displacement	Hardwood displacement	Blocktool displacement	Difference
[–]	[mm]	[mm]	[mm]	[–]
24.5	16.587	1.037	16.615	0.00171
25.5	16.032	1.002	16.059	0.00168
26.5	15.520	0.970	15.543	0.00148
27.5	15.040	0.940	15.063	0.00153
28.5	14.592	0.912	14.618	0.00178
29.5	14.181	0.886	14.205	0.00167
30.5	13.803	0.863	13.823	0.00147
31.5	13.451	0.841	13.470	0.00144
32.5	13.120	0.820	13.143	0.00175
33.5	12.816	0.801	12.838	0.00171
34.5	12.533	0.783	12.556	0.00181

The displacements of both the models are very close and therefore it may be assumed that the new model has at least the same accuracy as the already existing one. The benefit is that one can evaluate the hardwood layer by means of strain. Since one is not interested in the softwood layer a total deformation is not the most suitable way of presenting the maximum capacity. At Damen the maximum allowable pressure for softwood is 2 N/mm^2 , and for hardwood 3 N/mm^2 . Using a hardwood Young's modulus of 600 N/mm^2 , and a softwood Young's modulus of 10 N/mm^2 gives the maximum strain per timber as: hardwood 0.005, softwood 0.0427 (for softwood the equivalent Young's modulus should be used as it is a stacked layer). In table 5.6 the maximum allowable strain is evaluated. Where for the blockload tool used at Damen it is difficult to see when the hardwood strain is exceeded it is clear for the new tool. The first two blocks need a new configuration if one wants to avoid the exceedance of the hardwood capacity.

Table 5.6: Evaluating the maximum allowable strain for the softwood, hardwood and blockload tool

Frame	Softwood ϵ	Exceeds	Blockload tool ϵ	Exceeds	Hardwood ϵ	Exceeds
[–]	[mm/mm]	[%]	[mm/mm]	[%]	[mm/mm]	[%]
24.5	0.0663	55.49	0.0665	55.76	0.0052	3.6667
25.5	0.0641	50.29	0.0642	50.55	0.0050	0.2000
26.5	0.0621	45.49	0.0622	45.71	0.0049	0
27.5	0.0602	40.99	0.0603	41.21	0.0047	0
28.5	0.0584	36.79	0.0585	37.04	0.0046	0
29.5	0.0567	32.94	0.0568	33.17	0.0044	0
30.5	0.0552	29.39	0.0553	29.58	0.0043	0
31.5	0.0538	26.09	0.0539	26.28	0.0042	0
32.5	0.0525	22.99	0.0526	23.21	0.0041	0
33.5	0.0513	20.14	0.0514	20.35	0.0040	0
34.5	0.0501	17.49	0.0502	17.71	0.0039	0

So, if the load on the blocks and the dimensions are known one can predict the deformation, strain and stress very accurately. The single dock block is therefore a reliable and realistic way of predicting the

load. The effect of the non-linear interaction behaviour is displayed in table 5.5, where the differences between the linear approach and the non-linear approach are hardly visible.

5.2. Validation of ship model with case study on a patrol ship (PS)

5.2.1. Validation of the ship model by using the Euler-Bernoulli theory

Since the single dock block model is validated, the ship model and reaction force as output must also be validated. The load is predicted by the ship model as a consequence of the ship resting on multiple blocks. The case study is on a patrol ship (PS) built at Damen, this portrays the event of docking as it exists in reality. The weight distribution, block positions, block dimensions, block spacing (where 1 frame spacing is equal to 600mm) and Young's moduli are known and shown in tables C.1, C.2 and C.3. Figure 5.11 gives the weight distribution for the ship, which is calculated to a uniform distributed load per segments as explained in the model for a ship in chapter 4 (equation 4.11).

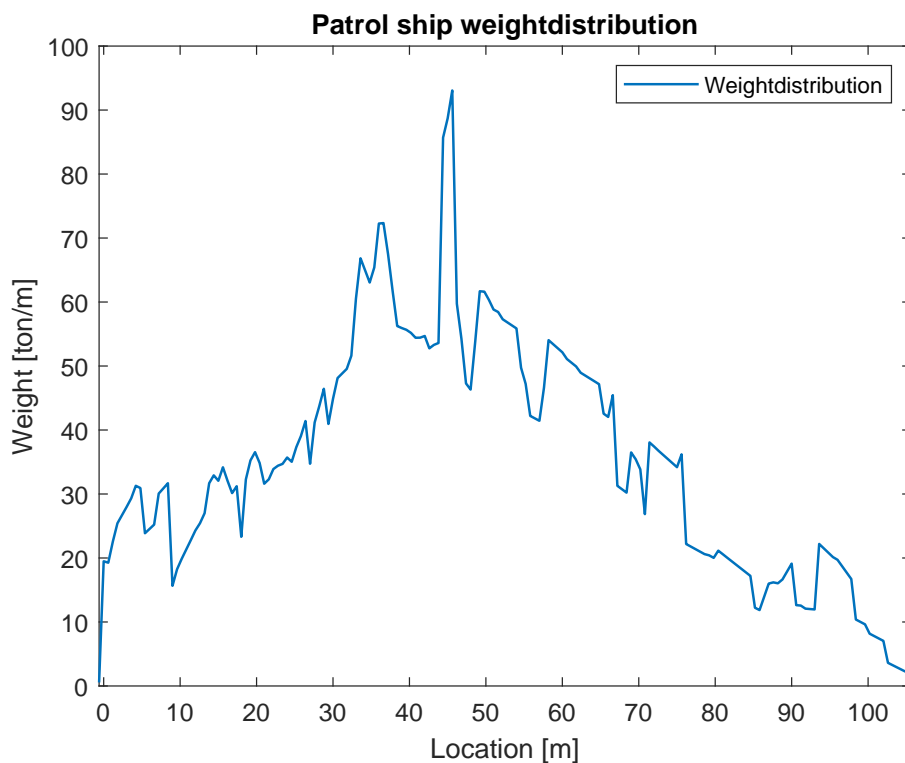


Figure 5.11: Patrol ship weight distribution

From figure 5.12 it is clear that the analytical approach of the Euler-Bernoulli theory for the ship as a model under- and overestimates the loads. Where the load is relatively accurate predicted in the midship (Frame 80 - 140) it is not accurate at the fore and aft. The fore of the ship (located around frame 160-180) is placed on steel plates as the keel width is very small. The loads around frame 60 are not predicted well, this due to the fact that the ship has a transverse bulkhead located here. The transverse bulkhead causes the ship to have a local increase of stiffness, this is very hard to predict by means of an analytical study. On average it is concluded that the complete load curve is flattened, which is possibly caused by neglecting the Timoshenko deflection term. The average difference between the FE model, and the ship model is 16.2%.

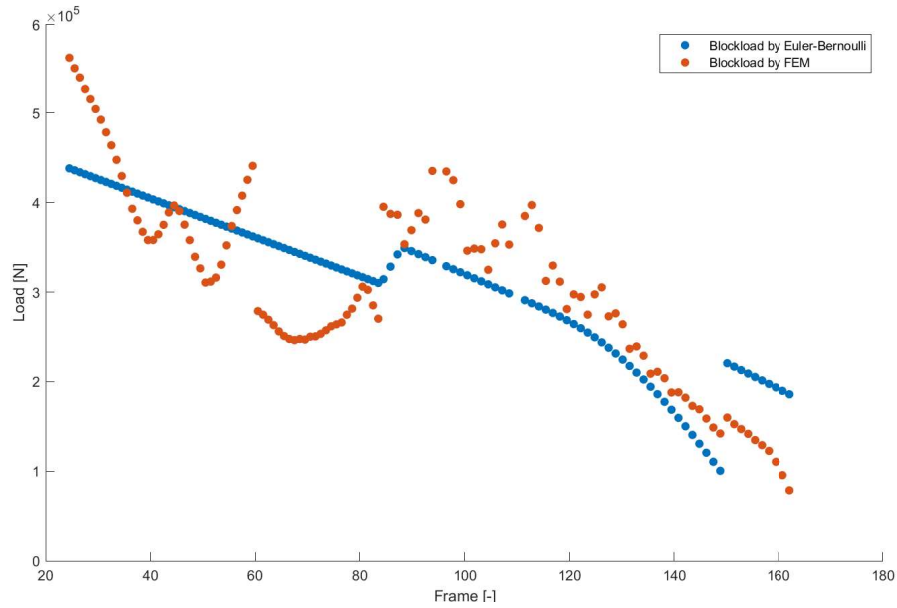


Figure 5.12: Validation of the ship model reaction force with the Euler-Bernoulli theory

5.2.2. Validation of the Timoshenko shear effect in the ship model

The validation for the ship model with the Euler-Bernoulli theory lead to an underestimation of the load in the aft of the ship. In this section the influence of the Timoshenko theory is evaluated and validated. Equations regarding the Timoshenko theory can be recalled in the first section of this chapter. The deflection can be found by:

$$W(x) = \frac{1}{EI} \left(\frac{qx^4}{24} + \frac{C_1x^3}{6} + \frac{C_2x^2}{2} + C_3x + C_4 \right) - \frac{1}{\kappa AG} \left(\frac{qx^2}{2} + C_1x + C_2 \right) \quad (5.6 \text{ revisited})$$

Beforehand the check for the Timoshenko shear effect can be done with the rule of thumb. For this relation the exact values can change per ship, however, the order of magnitude will be the same. Using the values below one can find that the Timoshenko shear effect is definitely not something to neglect, as the value is 150.

$$\frac{EI}{\kappa GAL^2} \ll 1$$

Where:

E	$= 2 \cdot 10^5$ (for steel as main construction material of the ship)	$[N/mm^2]$
I	$= 1 \cdot 10^{13}$	$[mm^2]$
κ	$= 5/6$ (rectangular section)	$[-]$
G	$= 8 \cdot 10^4$ (for steel as main construction material of the ship)	$[N/mm^2]$
A	$= 2 \cdot 10^5$	$[mm^2]$
L	$= 1 \cdot 10^3$	$[mm]$

As the effect of the Timoshenko theory is clearly expected it is also illustrated for the example with 5 segments as showed in figure 4.6. Here the limit case (if the term above goes to zero) for the Timoshenko theory is also illustrated, the Euler-Bernoulli theory is recovered in this case. Only the shear modulus (G) is changed in this scenario analysis, this to demonstrate the influence of the Timoshenko part. In the limit case where the factor for the Timoshenko shear is very low (figure 5.16) the Euler-Bernoulli deflection is recovered. Table 5.7 gives the spring reaction force for the 3 springs located at x_1 , x_2 and x_4 . Even with a factor of 0.64, which is just below 1, what indicates to a safe assumption of shear term neglecting, the reaction force is almost 40% higher. In contrast to the single dock block model is the Timoshenko effect necessary for the ship model. The dotted vertical lines are the location of the interface conditions, and consequently the segment borders.

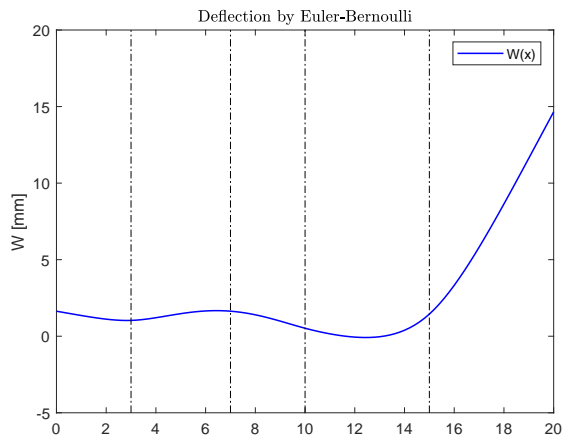


Figure 5.13: Deflection curve for the 5 segments with Euler-Bernoulli

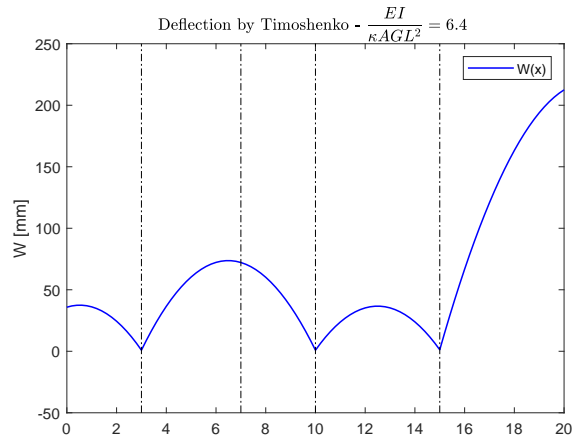


Figure 5.14: Deflection curve for the 5 segments with Timoshenko ($G=0.1$)

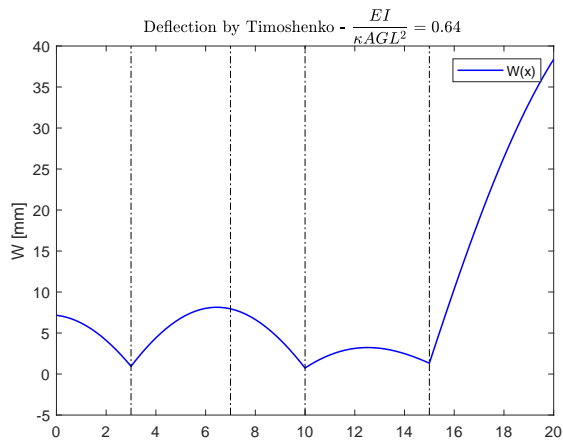


Figure 5.15: Deflection curve for the 5 segments with Timoshenko ($G=1$)

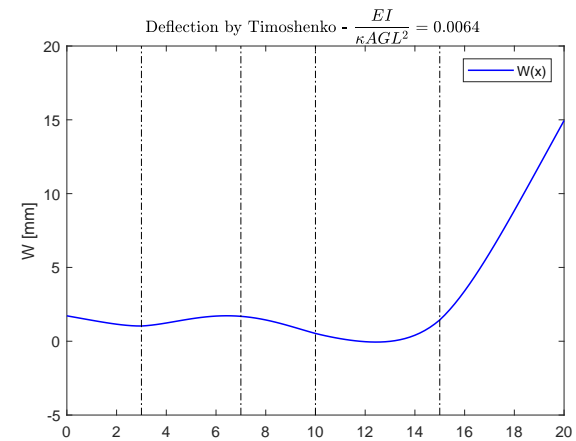


Figure 5.16: Deflection curve for the 5 segments with Timoshenko ($G=100$)

Table 5.7: Spring reaction forces for model with 5 segments

Theory	$EI/\kappa AGL^2$	F_{r1} [N]	F_{r2} [N]	F_{r3} [N]
Euler-Bernoulli	-	20.65	10.44	28.91
Timoshenko	6.4	17.73	17.44	24.82
Timoshenko	0.64	18.89	14.65	26.45
Timoshenko	0.0064	20.61	10.53	28.86

5.2.3. Validation of the ship model by using the Timoshenko theory

Since the Timoshenko shear effect can not be neglected for the ship model a new evaluation of the case study is done. There are more input values for the Timoshenko validation compared to the Euler-Bernoulli theory. Now the shear area and shear modulus of the beam (ship) are introduced. The report from Bedert [7] describes an average gradient of these two parameters along the length of the ship. There is no information in the parameters used for the FE model, which makes the comparison for some parameters difficult. The main construction material of the ship is steel with an Young's modulus of 206000 N/mm^2 and a shear modulus (G) of 79230 N/mm^2 .

Table 5.8: Shear area for a patrol ship according to [7]

Frame number	Shear area [mm^2]
45	202978.77
60	193691.46
75	212004.11
81	216485.9
96	230572.46
111	243814.47
126	231672.29
144	228347.88

Figure 5.17 displays the individual block loads along the keel line. The Timoshenko theory is more accurate at the aft of the ship. On average the difference between the Timoshenko approach and the FE model is 15.5%, which is slightly better as the Euler approach. For the same reason as discussed in the Euler-Bernoulli validation, is the peak located at frame 60 not covered by the model.

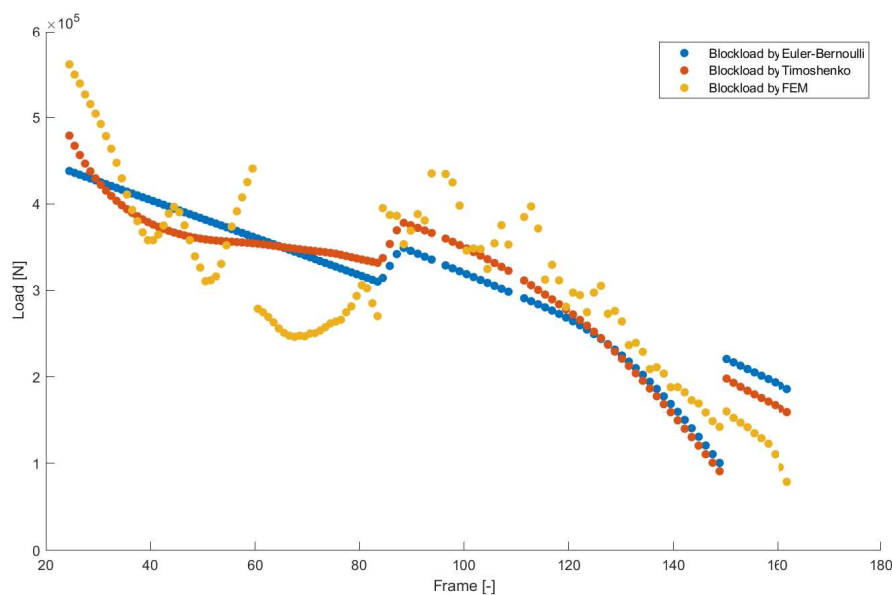


Figure 5.17: Validation of the ship model reaction force with the Timoshenko theory

5.2.4. Validation the Timoshenko theory with the existing tool from Bedert

The Timoshenko theory is the obtained solution approach for the reaction force prediction, and is therefore compared to the already existing tool of Bedert. The existing tool makes use of the same approach of a beam on multiple springs. The difference with this approach is the number of segments, where in the new tool the segments are defined by the frame spacing, divides the Bedert approach the beam in many more segments to represents the weight distribution as a large amount of point loads. Figure 5.18 gives the individual dock block reaction forces for the FE model, the Bedert approach, and the new approach with the Timoshenko theory.

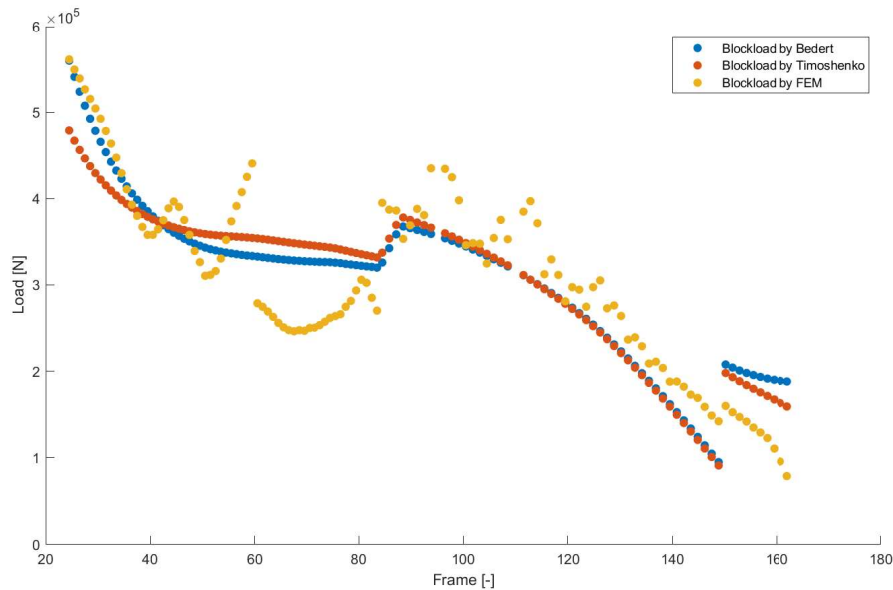


Figure 5.18: Validation of the ship model reaction force with the Bedert report

From the figure 5.18 it is clear that the prediction in the aft of the ship is more accurate for the Bedert approach. The prediction at the locations where a steel plate is placed is more accurate for the new approach. The midship prediction is comparable for both approaches, both has an underestimation in the increase of local stiffness due to transverse bulkheads. On average the approach by Bedert has a under- and overestimation of 13.1%, which is 1.4% more accurate as the new approach with the Timoshenko theory.

5.2.5. Timoshenko theory with optimized input parameters

From the validation of the Timoshenko theory with the Bedert's tool it is clear that the theory is promising, however, still underestimated in the aft of the ship. For the case study of a patrol ship the input parameters are known by the report of Bedert [7], where the weight distribution is displayed in tables C.1, C.2. As initial guess it was assumed that the inertia and shear can be averaged between the frames displayed in table 5.9. This means that from frame 45 till frame 60, the inertia is used as a constant value of 9.422 m^4 , and the shear a value of 202978.77 mm^2 . After a parametric study it is concluded that the influence of these values is significant, this means that it is not safe to use averaged values. In the validation with optimized values the values for the inertia and shear are evaluated by using interpolation between two points, hereby every single frame has an according value for the shear and inertia.

Table 5.9: Inertia and shear area for a patrol ship according to [7]

Frame [-]	$I_{ship} [\text{m}^4]$	Frame [-]	$A_{shear} [\text{mm}^2]$
45	9.422	45	202978.77
60	11.844	60	193691.46
75	10.173	75	212004.11
81	9.933	81	216485.9
96	14.032	96	230572.46
111	13.447	111	243814.47
126	9.496	126	231672.29
144	5.503	144	228347.88

Using the same input values with respect to the Young's moduli as discussed before a final validation is displayed by figure 5.19, where the accuracy is slightly higher as the Bedert tool. The tool developed in this thesis, Jacobse tool, has a accuracy of 12.9 % which is 0.2 % higher as the already known tool.

The validation is only done on 1 case study, which could lead to wrong conclusions with respect to accuracy. More FE results should be developed, which can be used as validation for the new obtained tool.

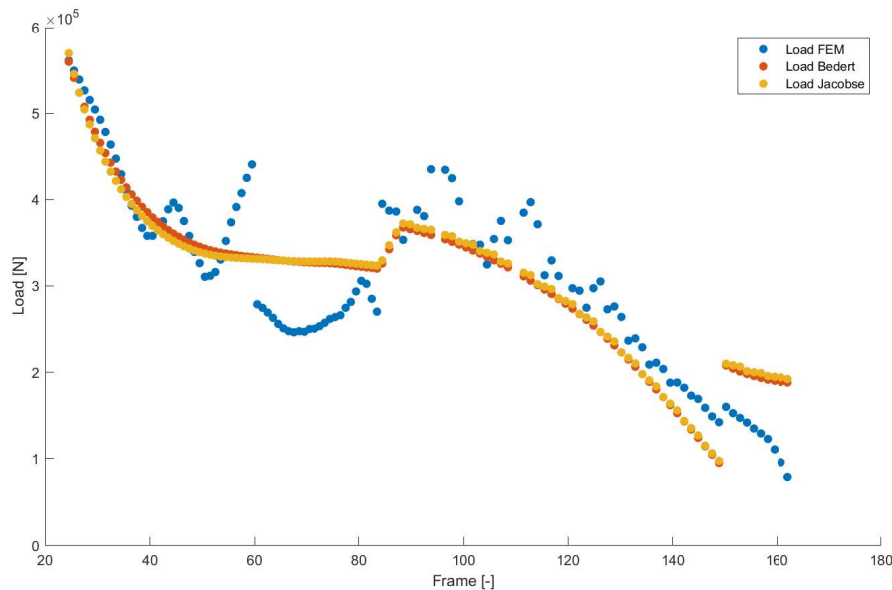


Figure 5.19: Validation of the ship model reaction force, Bedert vs Jacobse

5.3. Conclusions

5.3.1. Conclusion for the model of a single dock block

The model of a single dock block is very accurate compared to the FE results from Damen. There is no need for the Timoshenko shear effect, as this does not influence the maximum deformation. The contact area can be modelled as a complete effective area, with free-free boundary conditions, which lead to simple and fast approximation of the deformation of the individual layers. Using the stress-strain relation and the calculated deformation it is very easy to check the maximum allowable capacity. Input parameters need to be as realistic as possible to have an accurate results, therefore a test campaign is carried out. Comparing the influence of the non-linear material interaction effect with the linear approach, it can be concluded that this effect is hardly noticeable. Using equivalent Young's moduli satisfies the physical effect of a compressed multilayered block, however, the behaviour of the hardwood layer is easier to evaluate with the double Winkler method.

5.3.2. Conclusion for the ship model

From the validation chapter it is clear that predicting the load with an analytical study is a good and fast approach. The benefits are the fast modelling time, the changing parameters as input and the work-ability for a large range of cases. The accuracy is $\approx 13\%$ lower as the FEM analyses. Over- and underestimations are neither results that an engineer wants, nevertheless is an overestimation less catastrophic. Using the input parameters as described in the optimized validation section it can be concluded that the new obtained tool has a high accuracy in the aft of the ship. The local increased stiffness as result of a transverse bulkhead is not covered in any of the evaluated analytical solutions, which is a shortcoming of the beam on spring support theory.

Complete Matlab script can be found in the appendix B where all the necessary files for the complete load and strain prediction can be found.

6

Characterization of the material properties of the dock block layers

6.1. Why testing?

Predicting the deformation on the dock block layers is approached by the model of a single dock block as described in chapter 4. For this model the necessary input values are the Young's modulus perpendicular to the grain, and the yield point. Besides the input values is the interaction between the timber layers, and the interaction between the ground and dock block a key parameter in the deformation prediction. A test campaign gives realistic results with a clear impression in the compression behaviour of a stacked block. Key parameters regarding the material properties are discussed in chapter 2. Hereby chapter 2 also mentioned the large natural variability of the mechanical properties of wood. A too sophisticated approach is not valuable in case the parameters are hard to determine or estimated as best guess. However, material properties such as stiffness and strength can be derived from test and can be used in the mathematical models afterwards, these are the parameters of interest in the material characterization. The average values from the Wood Handbook are also obtained by testing, however these tests are done on clear wood specimen with small dimensions and can be different from practical use. Nor are Young's modulus values in compression perpendicular to the grain available elsewhere in the literature. Norm NEN-EN 338 gives average values for the test results of a load perpendicular to the grain, however this is on small and clear specimen and therefore not the same. So, the main reason to do the testing, is to obtain material characterization to be used in the model. Here the material conditions met the in-situ yard conditions to get a realistic result. Eurocode 5 describes the linear relation between stresses and strains by Hooke's law. However, Eurocode 5 does not account for the non-linear behaviour, which is one of the fundamental parts of this research.

6.1.1. Importance of testing

A test plan is needed to describe the test strategy, objectives, schedule, estimation, deliverables, and resources. Several closely related norms are used as guidance; however, these situations are different from the situation described in this thesis and therefore this test phase is desirable. This detailed document also contains previous studies like desired results, hereby identifying key characteristics such as test method, specimen sizes, and test quantities are identified. The importance for this thesis is to have a realistic and precise input value for the model, this to get a high value product.

Almost all the required parameters for a mathematical model can be derived from empirical relationships, as shown in chapter 2. However, it would be rather difficult to find all the relevant values (Young's modulus, modulus of rupture, shear strength etc.) in one test, it is possible to obtain those via the correlation between them. From this point of view, testing would be useless, however these test values always come from small test specimen with clear structure. Due to this reason it is highly advisable to find some of the parameters by testing, besides, most literature only represent values up to a certain level of deformation. As mentioned before for this thesis the deformation depends on a several

parameters of which the compression needs to be tested. For this reason, tensile strength tests and shear strength tests are not part of the project. Besides it is stated in the report from Sandhaas [43] that the shear strength has low importance, because no tension forces could develop as the load is acting perpendicular to the grain. The correlation between moisture content and strength properties is also an important part of the test phase, this because the variability in moisture content at the yards can be high.

6.2. Studies on compression tests perpendicular to the grain

From previous section it is clear that a test phase is desirable to get a Young's modulus perpendicular to the grain and to find the yield point in order to distinguish the elastic and plastic region. In this section multiple studies are investigated, all with similar approaches as the one which is most likely to use in this thesis. This literature study on testing perpendicular to the grain gives an insight on the ways of testing, the parameters which are worth of varying and to see what the gap is in this field. This gap can be covered with the test plan and with the test itself.

A compression test according to EN 408 [22] gives a smaller deflection at any stress level than would be obtained with the full surface loaded. The configurations found in practice are substantially different from that of the norms. The behaviour of the same specimen depends on the geometry, this can be explained by the following: different load distribution and cell configuration. When only part of the surface is loaded, the longitudinal cells are acting as beams. The more the cells are acting as beams the more the load carrying capacity increases and at the same time the more the deformation reduces. Besides, the beam shear strength is not constant, it decreases with an increase in the shear span to depth ratio, and is therefore rather difficult to use in a mathematical model. It is hard to decide which results are reliable. There are only limited efforts of tests to deal with keel block properties and problems. Due to this gap several studies with respect to material behaviour are used, these papers carry out test perpendicular to the grain.

The thesis of Hall [24] attempted to develop a more encompassing method for determination of wood's capacity to withstand loads acting perpendicular to grain. Testing was done on a Baldwin testing machine, this is a hydraulic compression machine, where the deflections were measured with dial gauges. The test specimens were from timber pieces, respectively Amabilis Fir and Grand Fir. To find the Young's modulus E_{\perp} and the yield point the specimen was tested with 100% of its cross-sectional area loaded. The curve from this typical load deflection plot starts with an upward curvature, but straightens to the mentioned linear relationship (Stress-Strain). The upward curvature is due to material imperfections such as small height differences in the surface area. After some time an uniform pressure distribution is found and the line straightens out. It is this curve that is the objective during the test phase, for both linear as non-linear range.

Nobel [39] describes in his paper the load perpendicular to the grain on a Spruce. The dimensions of the test specimens are $70 \times 45 \times 90$ [mm] ($l \times b \times h$), both dry and wet condition. The procedure he describes is in accordance with EN 408.

Table 6.1: Results from Nobel [39]

Dimensions	Number of tests	ω	$f_{c,\perp,mean}$	$f_{c,\perp,k}$	$E_{\perp,mean}$
$70 \times 45 \times 90$ [mm]	[-]	[%]	[N/mm ²]	[N/mm ²]	[N/mm ²]
Spruce (dry)	14	12.9	3.41	1.34	163
Spruce (wet)	14	45.3	1.50	1.00	71.0

Dolganov [17] describes in his paper the load perpendicular to the grain, here the height of each specimen is changing. The paper don't mention anything regarding the moisture content, therefore it is assumed that this is in perfect accordance with the EN 408 norm. The spruce in the paper has a density of 460 kg/m^3 , which indicates to the C30 strength class. The paper concludes that the height has hardly any influence on the perpendicular compression strength.

Table 6.2: Results from Dolganov [17]

Dimensions ($l \times b \times h$) [mm]	Number of tests [-]	$f_{c,\perp,mean}$ [N/mm ²]
70 × 45 × 115	5	3.3
70 × 45 × 90	5	4.0
70 × 45 × 65	5	3.3
70 × 45 × 40	5	3.1

Ali et al. [5] describes compression perpendicular to grain in timber, and compares different calculation models for bearing strength. All calculations in this paper are according several obtained codes (EU-5 before and after amendment, Italian code, German code, Swedish BKR 2003 code and Swedish old code).

Table 6.3: Results from Ali et al. [5]

Dimensions ($l \times b \times h$) [mm]	Number of tests [-]	ω [%]	Mean density [kg/m ³]	$E_{c,\perp,mean}$ [N/mm ²]	$E_{0,mean}$ [N/mm ²]	$F_{c,\perp,max}$ [kN]
500 × 45 × 95	11	12.1	412	363	11822	21.81
500 × 90 × 95	11	12.1	412	363	11822	36.52

Ali et al. [5] concludes that the Eurocode shows the closest results, compared to experimental results. Furthermore the paper concludes that in all cases the experimental results were lower than the capacity calculated according to the code.

The investigation of similar studies lead to several conclusion, which will be used in the test campaign. A first conclusion is given by Hall: even when the cross-section area of the specimens is tested at 100% of their area the same stress-strain relation can be used. Classification rules can be used to calculate the pressure, even when the dimensions are different as mentioned in the rules. For the linear Young's modulus (perpendicular to the grain) one can use the stress-strain slope. The evaluation of the non-linear (bi-linear) Young's modulus is not identified in these previous studies and need to be evaluated by the results of the tests. From Nobel's research the high moisture dependency on compression strength perpendicular to the grain is visible. As there is hardly any height dependency, it is not permitted to vary this dimension during the compression tests. The last study discussed pointed out that the Eurocode classification is the most applicable and most precise one for a regular compression test. None of the studies has tested a combination of materials to investigate the equivalent modulus of elasticity. In the test campaign these gaps will be covered, and a conclusion will lead to a more encompassing view.

6.3. Test requirements, limitations and preparation

For the method and mechanical properties, the prescribed standard EN 408 are followed, however, at some point this standard was not suitable for the test (dimensions are different in this test). The previously mentioned hydraulic testing machine is available at the Delft University of Technology. The test bank has a capacity of 3000kN with dimensions $l \times b \times h = 300 \times 500 \times 600mm$. In order to prevent mistakes with respect to dimensions and the notation of it, figure 6.1 gives the symbols for the dimensions.

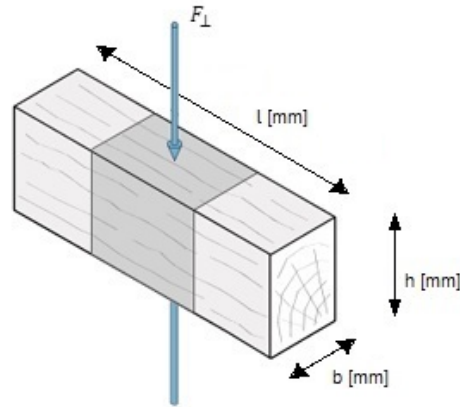


Figure 6.1: Block dimensions with respect to the load perpendicular to the grain

6.3.1. Test dimensions and size effects

EN 408 gives test piece dimensions of structural timber, shown in table 6.4. However the test in this thesis is similar to the one described in this norm it is not exactly the same, the specimen in this test have different dimensions.

Table 6.4: Dimensions of structural timber according to norm EN 408

Material	l [mm]	b [mm]	h [mm]
Structural timber	70	45	90

To test the timber parts the influence of size effects have to be ruled out. These size effects can have their influence mainly in the height and width of the specimens. In the length direction less size effect is expected, because the timber acts a continuous support over the length, with only a small possibility for load distribution at the edges. Therefore a length of 200 mm is proposed to be used for the testing. The width of the specimen is also 200 mm. Size effects were described by Weibull (1939) for homogeneous brittle materials. The theory of Weibull assumes that a system is as strong as the weakest link, and therefore the strength will reduce as the dimensions increases. From this theory the following relation can be used (equation 6.1):

$$\frac{f_{m,2}}{f_{m,1}} = \left(\frac{h_1}{h_2}\right)^k \quad (6.1)$$

Where:

$f_{m,1}$	= strength at a chosen reference height h_1	[N/mm ²]
$f_{m,2}$	= strength at a chosen reference height h_2	[N/mm ²]
k	= strength factor	[-]

The above relation is obtained from Eurocode 5, there is no note for the width and length size effects, nevertheless it is applicable. In the thesis from Ravenshorst [42] the size effect is also mentioned. From this thesis the conclusion is made that the size effect for Young's moduli are only expected if the density changes over the height. As the dimensions in this report are larger with respect to the norms it is advisable to take size effects into account. Larger dimension could possibly lead to a change in density over the height.

In table 6.5 the dimensions from the materials as used in practice as also the test sample dimensions are listed. The test materials are taken from the Damen yards as explained in chapter 2. The abbreviations represents the yard where the material is used, the material itself and the age status. These abbreviations will be used throughout the report and are shown in table 6.6 ¹.

¹Spruce 1 and 2 for different strength classes as it turned out in the test phase that the materials are not exactly the same

Table 6.5: Test sample dimensions

Name	Full scale dimensions			Test sample dimensions		
	l [mm]	b [mm]	h [mm]	l [mm]	b [mm]	h [mm]
AOO	1200	290	200	200	200	200
ALN	1220	350	40	200	200	40
ALO	1220	300	40	200	200	40
RPN	1000	200	70	200	200	70
RSN	1000	405	50	200	200	50
RAN	1000	200	200	200	200	200
SSN 1	1200	270	50	200	200	50
SSN 2	1200	270	50	200	200	50
SON	575	270	75	200	200	75

Table 6.6: Material labels

Name	DAMEN yard	Material	Material status
AOO	Amels	Oak	Old
ALN	Amels	LVL	New
ALO	Amels	LVL	Old
RPN	Ritthem	Pine	New
RSN	Ritthem	Spruce	New
RAN	Ritthem	Azobe	New
SSN	Schiedam	Spruce	New
SON	Schiedam	Oak	New

6.3.2. Dimension check

Previous subsection showed the dimensions of all the samples and test dimensions. The hydraulic test press machine has a maximum load capacity of $3000kN$. In order to make an estimation of the maximum area which can be used for the samples a simple check is done (equation 6.2 from Blass and Görlacher [8] and Hek [27]), this equation holds because in this case one speak of the ultimate limit state.

$$A_{max} = \frac{F_{max}}{f_{c,\perp}} \quad (6.2)$$

Where:

A_{max}	= maximum area	[mm ²]
$F_{cap,max}$	= test machine capacity	[N]
$f_{c,\perp}$	= maximum compression perpendicular to grain (mentioned in table 2.1)	[N/mm ²]

Table 6.7: Maximum sample dimensions

Material	$f_{c,\perp}$ [N/mm ²]	$F_{cap,max}$ [N]	A_{max} [mm ²]
Softwood	2.0 - 3.2	3×10^6	$937.5 \times 10^3 - 1500 \times 10^3$
Hardwood	7.5 - 13.5	3×10^6	$222 \times 10^3 - 400 \times 10^3$

From table 6.7 it is safe to use the chosen dimensions.

6.3.3. Moisture content

To determine the material properties, the tests are carried out using material of different moisture content. By doing so the influence of the moisture content can be recognized. In order to get the moisture content, the oven dry testing method is used. From every specimen a small sample (20 mm thick) in the middle is taken.

$$\omega = \frac{m_1 - m_0}{m_1} \times 100\% \quad (6.3)$$

In practice the moisture content can have a large range, this because of the different conditions per yard. Taking this parameter into account during testing provides insight in the variability. In practice it is not possible to guarantee a specific value for the moisture content, therefore it is important to have insight in the effects. However, in drydock use, where timbers are close-packed in storage and re-wetted frequently, most timbers can be considered to be above the fiber saturation point ².

From Madsen [35] table 6.8 is used to verify the test results. The values from this table are obtained by testing 600 specimens: half of them wet and half of them dry (12 % moisture content). The test configuration is according to the ASTM (American Society for Testing and Materials) standard where the complete contact area is loaded, compression is perpendicular to the grain. Dimensions of these specimens are small compared to the dimensions used in this test research, therefore, some deviations are expected.

Table 6.8: Ratios of wet to dry bearing stresses [35]

Species	Wet/Dry Stress	Wet/Dry M.O.E.
Douglas Fir	0.48	0.67
Hem-Fir	0.49	0.50
S-P-F	0.39	0.36

6.3.4. Density

The density can be important to make an assumption of the strength class if this is unknown. To determine the density, all samples will have to be weighed according to the norm. The density can then be determined with equation 6.4:

$$\rho = \frac{m_{specimen}}{b \times h \times l} \quad (6.4)$$

According to EN 408, should the density of a sample been tested with a clear section of this material. The section must be free from visual damage and knots. The minimum length of the section is 25 mm. In this research the method of EN 408 is used and the results are shown in table 6.9. The values in this table are average values, for all the individual moisture contents and densities the table in appendix D is added (Table D.1).

Table 6.9: Moisture content and density

Name	Moisture content [%]	Density [kg/m^3]	Density at 12% [kg/m^3]
AOO	20.03	742.41	682.81
ALN	13.92	516.08	506.19
ALO	50.13	924.71	572.09
RPN	25.76	691.70	596.53
RSN	25.57	476.10	411.50
RAN	22.22	1152.41	1034.63
SSN 1	15.04	639.90	620.44
SSN 2	16.94	398.98	379.25
SON	38.42	944.05	694.66

6.3.5. Expected failure mechanism during compression of a stacked dock block

The mentioned moisture content is also of importance to prevent cracking. An appropriate moisture content helps to avoid swelling and shrinking movements of the wood, which results in cracking [8]. In this tests the materials are loaded perpendicular to the grain, which results in squeezing of the

²The fiber saturation point is the point at which, as wood dries, there is no more moisture in cell cavities and moisture starts to be lost from cell walls, causing shrinkage

fibres. If only part of the contact area is exposed to a load, the stiffness value will be higher. This is because the load is distributed to the parts which are not loaded, for this thesis the complete contact area is loaded. Testing with old materials with moisture contents above 12% can lead to a failure mechanism other than the expected compression. In practice (at Damen yards), some cracking failure mechanisms are visible (figure 6.2). Nevertheless, most of the failure mechanisms are over-stress failure by compression (figure 6.3).



Figure 6.2: Cracking failure mechanism



Figure 6.3: Compression failure mechanism

6.3.6. Specimen status

With the moisture content known, the age of the material could possibly influence the result. To examine if the age of the materials has significant influence both old as new materials would be used in the test. From the Wood Handbook [32] the characteristics of wood knots are known. Knots are remnants of branches in the tree appearing in a board. Knots refer to the continuity, or lack thereof. Usually, wood of this quality cannot be obtained in larger pieces, particularly in those sizes used for dry-docking timbers [38]. The incidence of knots, splits, sloping grain and decay all may detract from strength.

6.3.7. Statistical terms

In statistics it is well known to use the standard deviation (σ_s) as a value for the spread of a variable. The standard deviation is used to give a scatter; the extent to which the values differ from each other. To see what the accuracy of the test results is one can use the coefficient of variation (CV), this is a measure of dispersion. The coefficient of variation is often expressed as a percentage and is calculated by the mean and standard deviation. In this subsection the formulas for these variables are discussed, they will be used in every parameter discussing to check whether the results are reliable and of usage.

The mean of a sample is the sum of the sampled values divided by the number of tests (N):

$$\bar{x} = \frac{x_1 + x_2 + \dots + x_N}{N} \quad (6.5)$$

The variance is calculated with the mean:

$$\sigma_s^2 = \frac{\sum (x_i - \bar{x})^2}{N - 1} \quad (6.6)$$

Directly from the variance the standard deviation follows as:

$$\sigma_s = \sqrt{\frac{1}{N} \sum_{i=1}^N (x_i - \bar{x})^2} \quad (6.7)$$

Finally one can express the coefficient of variation as the standard deviation divided by the mean:

$$CV = \frac{\sigma_s}{\bar{x}} \quad (6.8)$$

6.4. Compression test procedure

The first test procedure is to identify parameters belonging to the linear and non-linear range. Both procedures are compared with the analytical results explained in chapter 2. First tests are on individual timbers, second series are on the combinations of soft- and hardwood. For the combination of a softwood and a hardwood one is interested in two things, the interaction of the two individual materials, and the devoted deformation per layer. There are multiple samples taken from each specimen, all with the same dimensions mentioned in 6.5. By doing so the variation within one and the same sample is given, and multiple tests are done to reduce possible errors. By testing the materials individually the material properties are obtained for this specific type. However, a combination of materials gives a understanding of the combined compression interaction. By testing the compositions it is checked if this equivalent modulus of elasticity is similar in practical situations. Testing goes beyond the yield point, this in both the individual as in the combination tests. So the deformation controlled compression tests consists of:

- Characterization of softwood material properties by individual compression tests
- Characterization of hardwood material properties by individual compression test
- Characterization of combined compression properties, representing configuration as used in practice

6.4.1. Creep test on material combinations

Creep occurs when a structure is loaded over a long period, which is certainly the case for dock blocks. If a ship is in the dock for maintenance the dock blocks are loaded for a period up to several months. The duration of the test will be 1 or 5 days, depending on the time-deformation time. For this test series each configuration consist of multiple tests, each at different load levels. So, different levels of load, different duration of tests and different combinations are carried out in the creep tests.

6.4.2. Test overview and flowchart

In appendix D is an overview given of the steps which need to be taken to get the desired test results (figure D.1). Besides a flowchart there are also overview per test scenario, here the dimensions, names and test numbers are given. The scenarios are the ones described in this chapter: individual material compression tests (figure D.2), material combination compression tests (figure D.3), and creep deformation tests (figure D.4).

6.5. Individual material test results

In the next sections the results per test series are discussed, this will be done with an illustration of one test specimen (SON), here the statistics and parameters are discussed. Average values for all the tests will be discussed after each subsection. For the oak from Schiedam (SON) is only one individual compression test done, this due to material availability purpose. The variance for the SON is therefore not applicable and represented in the tables with the abbreviation n/a.

6.5.1. Young's Modulus in linear range (individual material test)

From EN 408 one can use the relation to estimate the Young's modulus perpendicular to the grain (equation 6.11). During the compression tests the computer records the load according to the controlled deformation. Besides the approach mentioned in the norm there are 2 more approaches used. As mentioned before, the compression tests are deformation controlled, so that the displacement steps (Δ) are an input value. The resultant output value is the needed force (F_{\perp}) to compress the specimen this amount of displacement. From these forces and displacements, the total force displacement graph is made (figure 6.4). The Young's modulus perpendicular to the grain (E_{\perp}) is calculated by the equivalent slope of the stress-strain relation. The stress and strain values are calculated by the data from the force and displacement by (graph is shown in figure 6.5):

$$\sigma = \frac{F_{\perp}}{A_{eff}} \quad (6.9)$$

$$\epsilon = \frac{\Delta}{h} \quad (6.10)$$

Where:

- σ = yield stress [N/mm²]
- F_{\perp} = applied force perpendicular to the grain [N]
- A_{eff} = loaded contact area [mm²]
- ϵ = Strain [mm/mm]
- Δ = displacement [mm]
- h = original specimen height [mm]

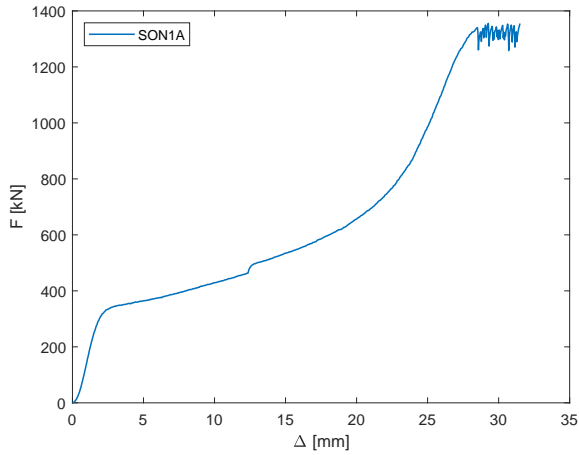


Figure 6.4: Total force displacement - SON

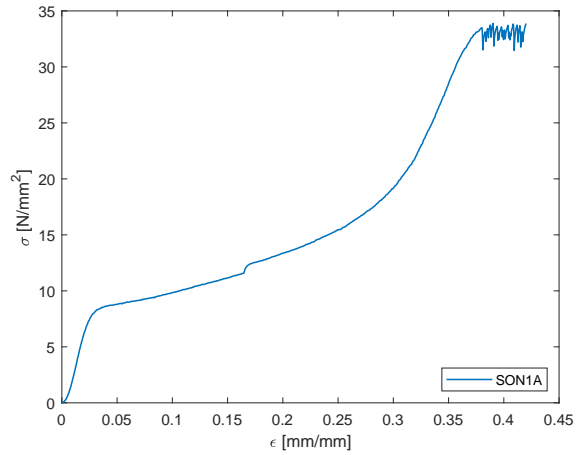


Figure 6.5: Total stress strain - SON

First approach is the one mentioned in the norm. Here an assumption for the maximum force lead to the 0.1 and 0.4 values, which are used in the iterative process to calculate the Young's Modulus.

$$E_{\perp} = \frac{(F_{40} - F_{10})h}{(w_{40} - w_{10})A_{eff}} \tag{6.11}$$

Where:

- $F_{40} - F_{10}$ = increment of load on the straight line portion of the load-deformation curve. [N]
- F_{10} shall be 10% and F_{40} shall be 40% of $F_{\perp,max}$
- $w_{40} - w_{10}$ = increment of deformation corresponding to $F_{40} - F_{10}$ [mm]

Second approach is the one which makes use of the raw data from the compression test. Since at every displacement step the force, stress and strain are known one can easily calculate the according Young's modulus. For this approach the difference between two consecutive recordings is taken, and at the end the average of the linear range is taken. Figure 6.6 shows the force displacement graph in the linear range, here the assumption is made that the displacement from 0 to 0.5 is due to material imperfections and referred as settling time. The range between the two red dotted lines is referred as the pure linear range.

$$E_{\perp} = \frac{\sigma_{i+1} - \sigma_i}{\epsilon_{i+1} - \epsilon_i} \tag{6.12}$$

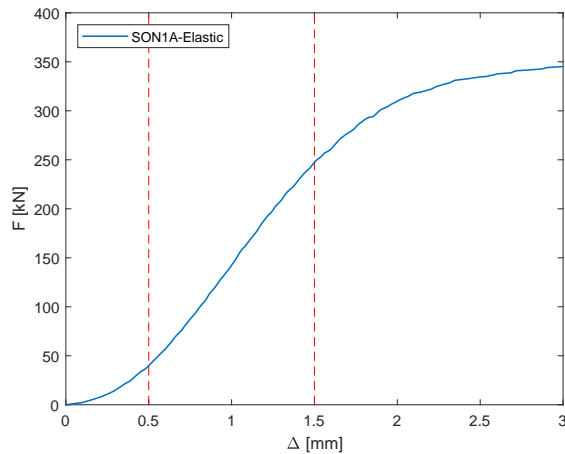


Figure 6.6: Linear force displacement range - SON

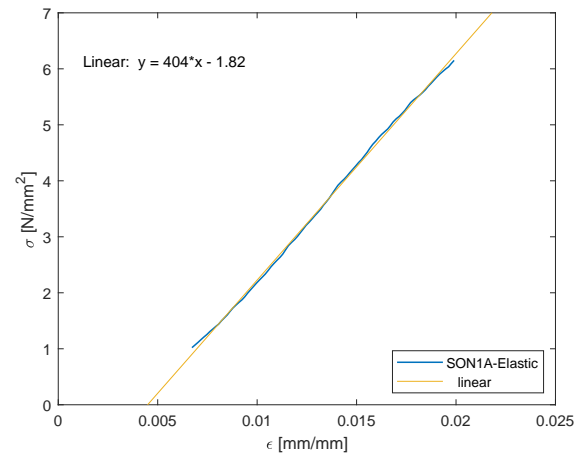


Figure 6.7: Linear stress strain range - SON

Third approach is based on the norm, however, now the range is based on the largest 'visible' linear range. Instead of assuming for the largest force in the linear range it is now assumed as the largest range of linear behaviour. From this linear range the trendline represents the slope between the stress and the strain, which is directly related to the Young's Modulus. Figure 6.7 gives the linear range and the trendline for the oak from Schiedam. From the plot one can use the slope equation, here the E_{\perp} is 404MPa .

Evaluating all three approaches lead to the conclusion that the second approach is very sensitive to errors and therefore definitely not the best one. The errors could occur when there are imperfections in the positioning of the specimen or possibly due to small bumps in the measured data (due to surround effects or software issues). Results from approach 1 and 3 are very similar, where the average results from the last approach are a bit more conservative. As the last approach uses a large range of variables to plot the trendline it has a lower risk with respect to measurement errors, the smallest imperfections are flattened by the trendline. For this reason, the values obtained by the 'trendline' method are the most realistic ones.

Table 6.10 give the average results for every specimen Young's modulus (E_{\perp}), here the number of tests is given, the moisture content (MC) and the coefficient of variance (CV).

Table 6.10: Young's Modulus (E_{\perp}) perpendicular to the grain in the linear range

Material	Name	Tests	MC[%]	E_{\perp} [MPa]	CV[%]
Azobe	RAN	3	23.3	930.5	29.3
Oak	AOO	4	20.7	228.5	5.4
Oak	SON	1	36.9	404.4	n/a
Pine	RPN	5	25.9	244.9	23.6
LVL	ALN	8	14.2	349.9	6.8
LVL	ALO	6	50.4	147.3	65.6
Spruce	RSN	5	25.7	67.6	11.8
Spruce	SSN 1	3	15.2	242.3	1.7
Spruce	SSN 2	3	17.2	90.4	19.6

First conclusion from this table is that the moisture content strongly affects the Young's modulus; the higher the moisture content the lower the Young's modulus (w.r.t. its original value). The influence of the moisture content was already mentioned in the literature phase and is therefore taken into account for the evaluation of the test results. In figure 6.8 the influence of the moisture content is clearly visible, here the blue lines represent the linear stress strain curves of the LVL specimens with a very low moisture content, where the red lines represent the high moisture content. Besides a lower Young's

modulus, the curves are hard to predict and the behaviour is therefore less reliable. Figure 6.9 gives the relation between the moisture content and the variance of the Young's modulus in the linear range. Moisture content below 30% display less variability of the linear behaviour.

Second point to be noticed is that the values of SSN1 and SSN2 are very different (as already mentioned), SSN1 tends to be a stronger softwood, where SSN2 is the expected specimen type.

Finally, one can conclude that the results for the individual compression test are significantly lower as the expected values based on literature information. From the literature one would expect the softwoods to be in the range of $230 - 530\text{MPa}$ and the hardwoods $630 - 1330\text{MPa}$, however this is clearly not the case. Only the Azobe and the LVL (new) are within these values. Using literature values for engineering purpose is an overestimation of the block capacity and can lead to failure. Relations of the Young's modulus with respect to the moisture content as introduced in table 6.8 are not applicable after evaluating the results of the individual tests. It is not possible to give a relation for the moisture content and the Young's modulus for this wide range of moisture contents. To recognize a trend one should test a large amount of similar specimens (with different moisture content). Comparing test values with literature values is not completely correct, where the moisture content in the literature is always 12%, which is significantly lower as the test specimens. In both cases the mean values are used to compare, this because for the 5th – percentile values more data is needed.

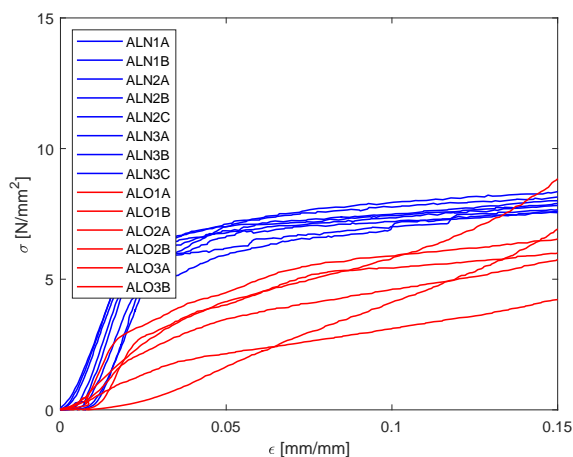


Figure 6.8: Stress-Strain for ALN and ALO - linear range

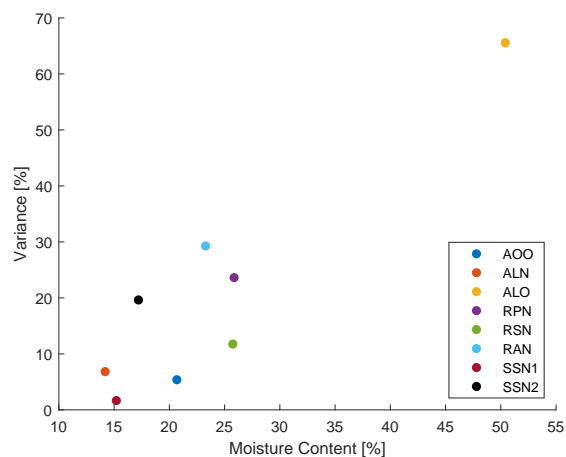


Figure 6.9: CV vs MC for E-modulus in the linear range

In appendix D all the individual test results are shown, here figures D.5-D.36 represent all the graphs (force-displacement and stress-strain graphs for total range, linear range as also non-linear range). Table D.1 give all the results with respect to the Young's modulus in the linear and non-linear range for individual test results. Young's modulus values in the non-linear range is described in the next section.

6.5.2. Young's Modulus in non-linear range (individual material test)

In the classifications there is no approach mentioned for the Young's modulus in the non-linear range. Figure 6.10 displays the force displacement graph for the non-linear range. The range from 0 to 5 is the part where linear deformation occurs, and an initial start at the non-linear deformation. The range from 15 to 25 can be identified as pure compression, which is unlikely to occur in large specimens (cracking due to over-stress will occur at some point). The range between the two red dotted lines is account as pure non-linear deformation, the same approach as for the linear range is used ('trendline method').

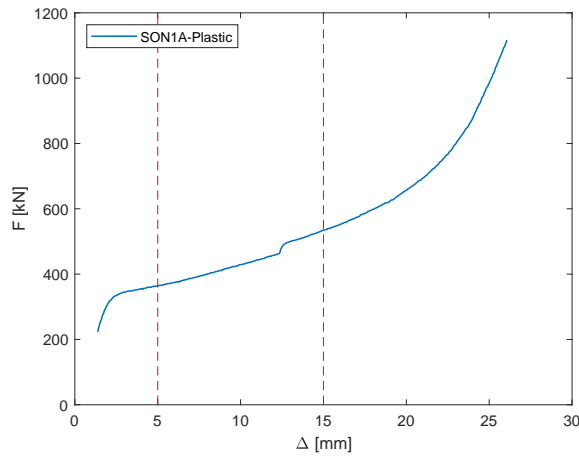


Figure 6.10: Non-linear force displacement range - SON

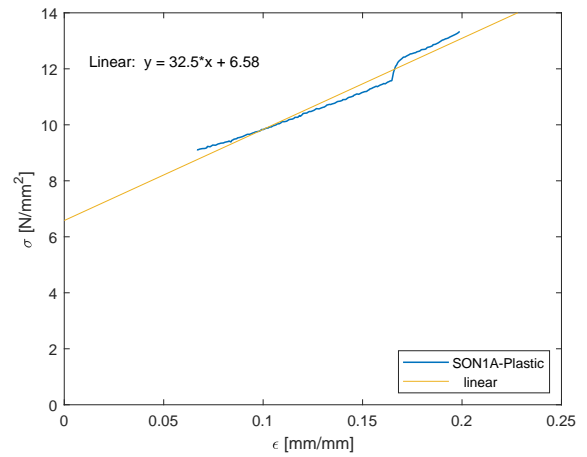


Figure 6.11: Non-linear stress strain range - SON

So for every specimen the trendline method is applied and afterwards once again per specimen the average value is given in table 6.11.

Table 6.11: Young's Modulus (E_{\perp}) perpendicular to the grain in the non-linear range

Material	Name	Tests	MC[%]	E_{\perp} [MPa]	CV[%]
Azobe	RAN	3	23.3	128.1	40.1
Oak	AOO	4	20.7	21.5	54.8
Oak	SON	1	36.9	13.2	n/a
Pine	RPN	5	25.9	13.9	29.2
LVL	ALN	8	14.2	15.0	6.9
LVL	ALO	6	50.4	33.1	39.2
Spruce	RSN	5	25.7	3.8	20.6
Spruce	SSN 1	3	15.2	9.4	51.1
Spruce	SSN 2	3	17.2	4.8	37.4

From table 6.11 one can conclude that in the values for the Young's modulus are way lower with respect to the linear range, nevertheless, for example the Azobe specimen has still a relatively high capacity to carry the load. The variance in the non-linear range is higher and therefore the material behaviour is less predictable, this is also shown by the scatter plot in figure 6.13. Where for the linear range almost all the specimens have a comparable variance, it is certainly not the case in the non-linear range.

Figure 6.12 displays the difference in stress strain curves for the non-linear range of ALN and ALO. Even for the linear range, the predictability is lower if the moisture content is very high. The difference with the linear range is that it is very difficult to make an assumption for the range of values which represent this non-linear curve. It can be concluded that it is impossible to take non-linear material behaviour into account when the moisture content is so high. There is no clear yield point, material hardly behaves like an elastic material at very low applied force, which lead to high risks in engineering application.

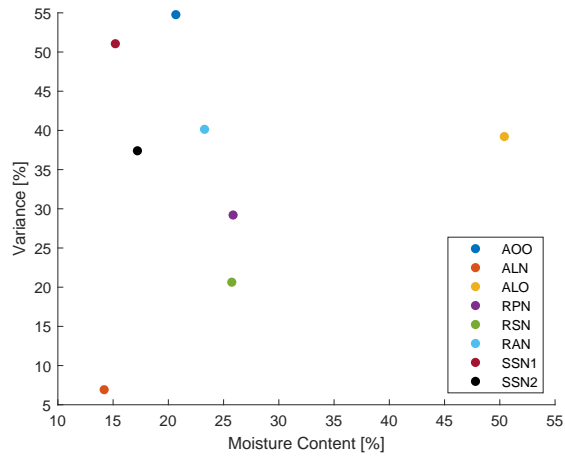
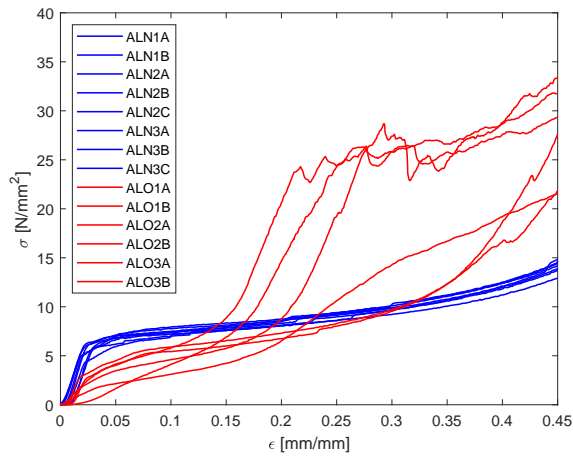


Figure 6.12: Stress-Strain for ALN and ALO - non-linear range Figure 6.13: CV vs MC for E-modulus in the non-linear range

6.5.3. Yield point (individual material test)

For materials without a 'sharp' yield point phenomenon there is a method called the 0.2% offset method. The 0.2% offset yield is the stress where the material has plastic deformation behaviour, or in other words, the elongation is irreversible. From previous sections one can recall the Young's modulus of the elastic range, parallel to this line the offset line is drawn. So steps taken to find the yield point ($R_{p0.2}$) are: first use the stress strain curve to find the Young's modulus (E_{\perp}) in the elastic range, then draw a trendline according to this modulus, and at last use this trendline as a reference to the offset line. The point of intersection between the offset line and the trendline (representing the modulus of elasticity) is the yield point. The procedure for the yield point is displayed in figure 6.14. The horizontal distance is referred as the yield strain (ϵ_y), where the vertical distance is the yield stress (σ_y). Same procedure holds when one is interested in the yield force (F_y) or yield deflection (Δ_y), both from the force deflection curve.

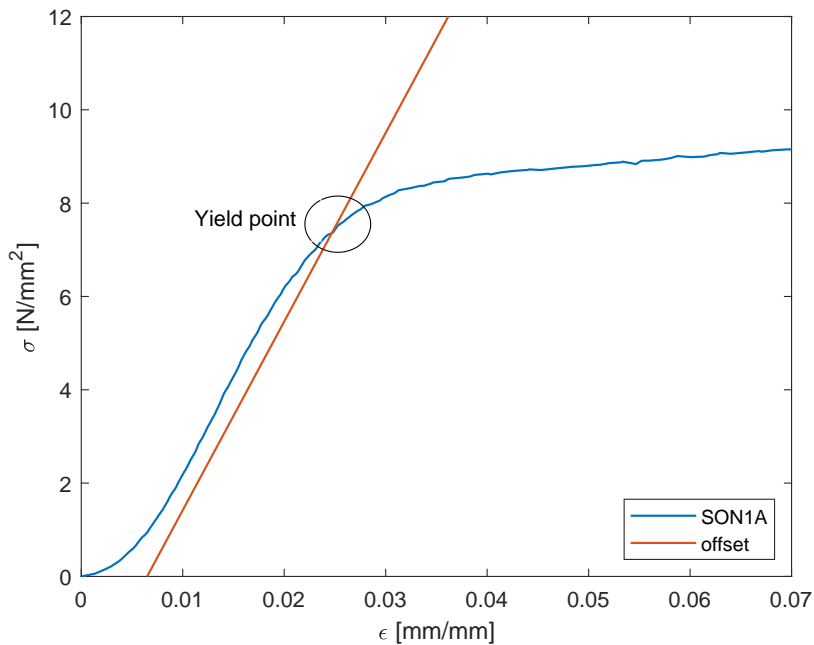


Figure 6.14: SON yield point

Just as for the Young's modulus the yield points for all the specimens are averaged and given in table 6.12. The yield point is important for model usages as it displays the limit of the linear range. Just as the Young's modulus also the yield point is largely affected by the moisture content.

Table 6.12: Yield point and CV for material specimen on individual compression tests

Material	Name	Tests	σ_y [MPa]	CV[%]	ϵ_y [-]	CV[%]
Azobe	RAN	3	15.54	25.6	0.02	1.8
Oak	AOO	4	3.52	18.9	0.02	17.7
Oak	SON	1	6.92	n/a	0.02	n/a
Pine	RPN	5	3.59	8.0	0.02	23.6
LVL	ALN	8	4.51	12.5	0.02	14.3
LVL	ALO	6	2.47	19.8	0.03	61.1
Spruce	RSN	5	1.82	19.2	0.06	30.1
Spruce	SSN 1	3	4.66	14.8	0.03	25.6
Spruce	SSN 2	3	1.99	45.0	0.03	29.8

Graphs for the tests of individual materials are shown in appendix D in figures D.37 - D.44.

6.6. Material combination test results

After completing the tests on the individual specimens, it is now the objective to see how the materials deform when they are stacked. Values for the material combinations are obtained with the same approach as discussed in previous section for individual material tests.

6.6.1. Young's Modulus in linear range (material combination test)

In appendix D the force displacement graphs and stress strain graphs for all the material combination tests are given by figures D.45-D.52. Table 6.13 gives the values obtain by these graphs. The Young's modulus for a multiple layered block can be calculated by the equivalent Young's modulus as shown in the equation below. This relation can be used to verify the results obtained from measuring the combined materials.

$$E_{eq} = \frac{h_i}{\sum \frac{h_i}{E_i}} \quad (6.13)$$

The average values obtained by the individual material tests are used in this equation. In theory the average values of for example Azobe (RAN) and Pine (RPN) obtained by the tests should lead to the same value as evaluated from the combined compression test.

Table 6.13: Young's Modulus (E_{\perp}) for material combinations in the non-linear range (w.r.t analytical approach)

Material 1	Material 2	Name	E_{\perp} [MPa]	$E_{eq\perp}$ [MPa]	Difference [%]
Azobe	Pine	RAN2B RPN1D	494.3	539.2	8.3
Azobe	Pine	RAN2C RPN2D	569.2	539.2	5.6
Azobe	Spruce	RAN1C RSN1C	246.0	261.8	6.0
Azobe	Spruce	RAN1D RSN2C	220.9	261.8	15.6
Oak	Spruce	SON1B SSN1E	294.5	319.1	7.7
Oak	Spruce	SON2A SSN2C	121.9	101.5	20.0
Oak	LVL	AOO1C ALN3D	279.8	242.5	15.4
Oak	LVL	AOO2C ALO3D	152.1	209.3	27.3

Using the conclusion of unpredictable results when using a material of high moisture content, it is not surprising that the highest difference is noticed at the combination with the highest moisture content (AOO2C ALO3D). The high difference for the combination of SON2A and SSN2C is hard to declare. A possible reason is that there is only one individual test done, this is from specimen SON1. Another possibility is damage which is not noticed in the preparation phase. Difference between the two combinations SON2A-SSN2C and SON1B-SSN1E is clarified by the same reasons, and with the fact that the two spruce specimens are not of the same type. For the combinations where multiple individual

specimens are tested, and where the moisture content is below 30%, it is safe to use the formula for the equivalent Young's modulus (in the linear range).

6.6.2. Young's Modulus in non-linear range (material combination test)

For the material combination tests in the non-linear range the same approach and equations are used. The results of the non-linear range are given in table 6.14.

Table 6.14: Young's Modulus (E_{\perp}) for material combinations in the linear range (w.r.t analytical approach)

Material 1	Material 2	Name	E_{\perp} [MPa]	$E_{eq\perp}$ [MPa]	Difference [%]
Azobe	Pine	RAN2B RPN1D	35.8	40.8	12.4
Azobe	Pine	RAN2C RPN2D	38.1	40.8	6.8
Azobe	Spruce	RAN1C RSN1C	30.4	17.1	78.5
Azobe	Spruce	RAN1D RSN2C	13.5	17.1	20.9
Oak	Spruce	SON1B SSN1E	16.1	11.3	42.2
Oak	Spruce	SON2A SSN2C	10.2	4.6	120.2
Oak	LVL	AOO1C ALN3D	20.5	20.1	2.1
Oak	LVL	AOO2C ALO3D	16.6	22.8	27.5

One would expect high difference between the equivalent Young's modulus and the one obtained by the test itself, this due the high variability in the non-linear range. Besides the test configurations discussed in the linear range, there are more notable numbers. The main reason for an unpredictable behaviour in the non-linear range is due to the stacked configuration, the larger the height (w.r.t the contact area), the higher the chance of cracking and complete failure. With a critical point of view one can conclude that the non-linear range, especially for the higher hardwoods, should be avoided at any cost.

6.6.3. Yield point (material combination test)

Table 6.15 give the yield point specifics for the material combination tests. As a stacked block is so strong as the weakest link the yield point of a combination is always close to the yield point of the softwood. Where the Azobe has a yield stress of 15.54MPa , it has a combination yield stress (with Pine) of 3.61MPa . In previous section the conclusion of over-stressing the hardwood is made, therefore the information of the softwood yield points is sufficient.

Table 6.15: Yield point for material specimen on combination compression tests

Material 1	Material 2	Name	σ_y [MPa]	ϵ_y [-]
Azobe	Pine	RAN2B RPN1D	3.61	0.011
Azobe	Pine	RAN2C RPN2D	4.31	0.013
Azobe	Spruce	RAN1C RSN1C	2.24	0.010
Azobe	Spruce	RAN1D RSN2C	1.93	0.012
Oak	Spruce	SON1B SSN1E	5.11	0.023
Oak	Spruce	SON2A SSN2C	1.48	0.016
Oak	LVL	AOO1C ALN3D	4.26	0.021
Oak	LVL	AOO2C ALO3D	2.96	0.025

Graphs for the combination tests of materials are shown in appendix D in figures D.53 - D.58.

6.7. Creep test results

Creep is the tendency of a material to deform permanently under persistent stresses. To evaluate the influence of this behaviour a test with long-term stress exposure is carried out. For creep to occur one should avoid reaching the yield strength, this to prevent failure mechanisms such as cracking. Table 6.16 gives the creep test information and the results. Here height 1 is the initial material height and height 2 is the height measured after the test.

Table 6.16: Creep test results

Material	Name	Force [kN]	Time [days]	Height 1 [mm]	Height 2 [mm]	Difference [mm]
Oak	AOO1D	150	5	200	188	12
LVL	ALN3C			40	39	1
Oak	AOO6A	150	5	175	172	3
LVL	ALO1D			40	29	11
Oak	AOO5B	150	1	172	172	0
LVL	ALO1E			40	34	6
Oak	AOO5A	70	1	174	173	1
LVL	ALN4C			40	38	2
Oak	AOO6C	70	1	177	175	2
LVL	ALO3D			40	39	1
Oak	SON2B	300	1	77	66	11
Spruce	SSN1D			50	31	19
Azobe	RAN2D	130	1	200	196	4
Spruce	RSN2D			50	33	17

In appendix D figure D.59 gives the force displacement graphs for the creep tests. From the data measured by the hydraulic compression test one could also make a displacement time graph (figure 6.15), here the x-axis is on logarithmic scale.

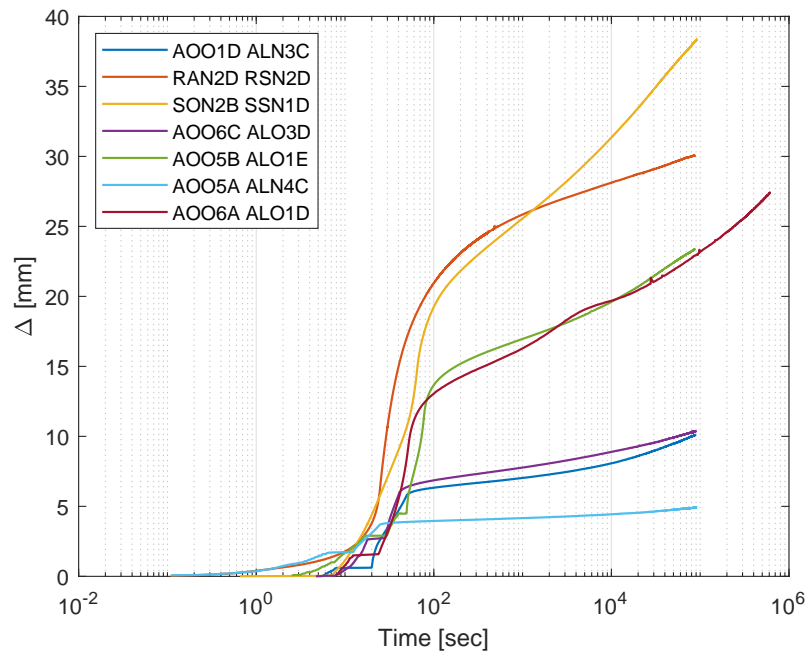


Figure 6.15: Displacement time graph for creep

From both the table as also the graph it can be concluded that the deformation is larger when the moisture content is higher. So, if one look at the combinations of Oak and LVL there are multiple results on different stress levels, besides the LVL is dry for the one and wet for the other there is not difference in the two tests. For the second test the softwood (LVL wet) is so weak that almost no force is directed to the hardwood. For the dry one however, there is pure compression (due to a relatively low softwood

height), and that the higher oak deforms more. The force of $150kN$ is close to the yield strength, therefore a relative high deformation occurred. It is safe to assume that there is hardly any creep for the stacked blocks loaded way below their yield strength. Even in case of high moisture content the creep is little, however, still more than the dry one. From the graph it is hard to determine in what section of creep behaviour the upper four lines are. The first steep part is the initial creep (elastic part), this is followed by the yield point region where deformation rate decreases with time. The next section is the range of interest for engineering purpose, here the creep is almost constant and predictable. The last region is a rapidly increasing creep which results in failure at the end. Apparently, the duration of 1 or even 5 days was not enough to recall the fourth region. Interpolation of creep data points is possible with the known data, however, the point where the last region starts is not known and therefore one doesn't know till what extend the interpolation holds. For full creep identification a longer test should be carried out, however the influence of creep with respect to other failure mechanisms is very low. The consequence of the load levels in the creep campaign is that a load above the yield point lead to over-stress failure. Correct load levels for creep are below the equivalent yield point of the stacked block.

Graphs for the creep material tests are shown in appendix D in figures D.60 - D.67.

6.8. Secant modulus

To use the values in the non-linear range the secant modulus (E_s) is introduced. The secant modulus is the slope of the line between the origin and a point of the non-linear range. The secant modulus can take different values over the non-linear range, however, for modelling purpose it is set as the maximum value of the non-linear range. The maximum point of the non-linear range is defined in previous sections and is known as the point where pure compression occurs (from test data). It is safe to assume the maximum value of the non-linear range as no cracking failure is expected for the softwood, the secant modulus for hardwoods is not needed as this range of non-linear material behaviour should be avoided at any cost. Figure 6.16 illustrates the slope for the secant modulus of the example with specimen of oak.

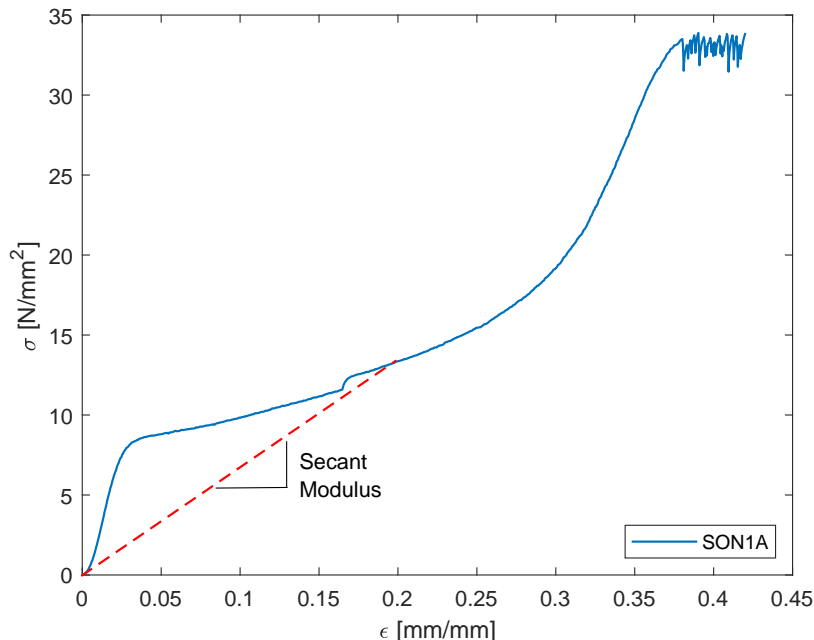


Figure 6.16: Secant modulus for SON

In table 6.17 the average values for the secant modulus per specimen is given. The secant modulus of ALO needs a clarification as it is a relatively high value, this is to the fact that is hard to predict the non-linear range. As mentioned before it is better to avoid specimens with such a high moisture

content, using the values would lead to an increase of risks.

Table 6.17: Second modulus values

Material	Name	E_s [MPa]
Azobe	RAN	324.1
Oak	AOO	39.3
Oak	SON	67.0
Pine	RPN	27.9
LVL	ALN	30.7
LVL	ALO	46.9
Spruce	RSN	9.4
Spruce	SSN 1	32.0
Spruce	SSN 2	12.4

6.9. Conclusions

From the test phase it was observed that some blocks are subject to different load distribution along their transversal length. The controlled deformation tests were carried out to assess the material properties (including also for the moisture content) of the different layers by considering larger specimens (to avoid size effects) and multiple samples (minimum 3 per type): AOO, ALN, ALO, RPN, RSN, RAN, SSN 1, SSN 2, SON. For these materials (obtained by Damen yards) it was observed that:

- Soft wood: displays a uniform deformation when loaded outside the linear range.
- Hard wood: several cracks and visible damage when loaded outside the linear range.
- Non-linear behaviour is also dependent on the size of the specimens. Due to the relatively low height of the softwood with respect to the hardwood, the softwood displays uniform deformation, where the hardwood displays cracks.
- For each layer different “nominal identical” samples were considered: there is a large variability in the material properties and in its behaviour under compression loading.
- Moisture content significantly affect the linear and non-linear material behaviour.
- Nominal Linear Young Modulus values found in literature (EN 338) were different from the one obtained during experiments. It is not safe to use nominal values.
- Yield point was also largely affected by moisture content, Moisture content below 30% display less variability of the linear behaviour.

Therefore, the single dock behaviour varies significantly even for the nominal identical layers. Since in the yard the environment is such that there is always a very high moisture content, the variability in the material behaviour must be taken into account. For hardwood it is prudent to avoid the non-linear range as it is very hard to predict its behaviour.

7

Effect of material variability on dry docking solutions

With the variability of the test results, and the model approach known it is valuable to see what the effect of these variabilities on the output of the models is.

7.1. Validation of model with test results

The model for a single dock block is validated with numerical data in chapter 5, however, now the test results are known it is also possible to have one final validation with respect to the practical results. From observations with respect to the compression test one can conclude that the deformation of the stacked block is mostly devoted to the softwood deformation. So total deformation is mainly based on the softwood, and hardly on the hardwood. Figures 7.1 and 7.2 illustrates perfectly the deformation of the stacked block compression, since the hardwood has a higher stiffness is will remain in the elastic range for a longer period, and consequently won't deform until very high pressures.

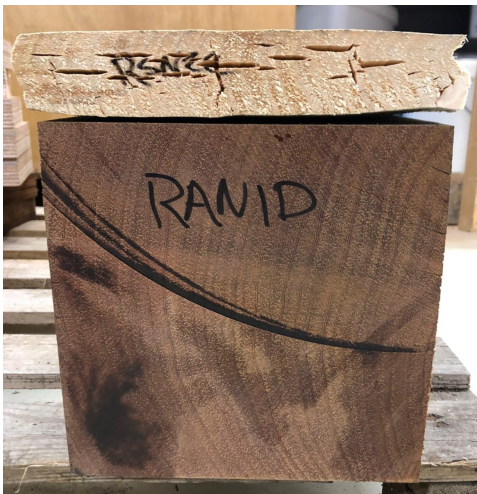


Figure 7.1: Deformation picture as result of compression a combination of Azobe and Spruce

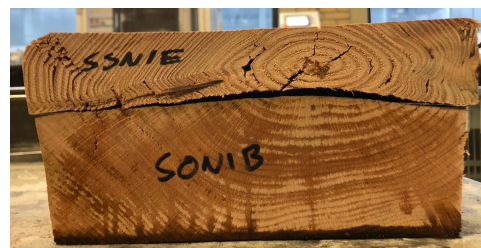


Figure 7.2: Deformation picture as result of compression a combination of Oak and Spruce

Using the model of a single dock block and the input values from the test campaign, it is possible to reproduce a specific test. By this way the model is validated by physical data obtained from test results, what means that the physics of both linear and non-linear behaviour are captured well.

Input parameters for deflection calculation as measured in the test phase:

b_{sw}	= block width of the softwood	200	[mm]
h_{sw}	= block height of the softwood	70	[mm]
l_{sw}	= block length of the softwood	200	[mm]
E_{sw}	= Young's modulus of the softwood	245	[N/mm ²]
b_{hw}	= block width of the hardwood	200	[mm]
h_{hw}	= block height of the hardwood	200	[mm]
l_{hw}	= block length of the hardwood	200	[mm]
E_{hw}	= Young's modulus of the hardwood	930	[N/mm ²]
F	= Point load	80.35	[kN]

Using following relations:

k_{d1}	= interaction parameter between soft- and hardwood	$(E_{sw}b_{sw})/h_{sw}$	[N/mm ²]
k_{d2}	= interaction parameter between hardwood and ground	$(E_{hw}/b_{hw})h_{hw}$	[N/mm ²]
I_{sw}	= Inertia for softwood	$(b_{sw}h_{sw}^3)/12$	[mm ⁴]
I_{hw}	= Inertia for hardwood	$(b_{hw}h_{hw}^3)/12$	[mm ⁴]
q	= Uniform distributed load	F/l_{sw}	[N/mm]

From table 7.1 it is shown that the combined displacement calculated with the single dock block model is very close to the actual test data. Taking the variability of the material parameters into account it is safe to say that the physics are captured with the single dock block model.

Table 7.1: Displacement results for combination of Azobe (RAN) and Pine (RPN)

Material	Individual displacement	Combined displacement	
Softwood (Pine)	1.0060	1.4380	[mm]
Hardwood (Azobe)	0.4320		[mm]
Test result (RANRPN)	-	1.4310	[mm]

7.2. Solution approach to check material variability

To evaluate the material variability it is necessary to do multiple case studies. The first study is on the moisture content, where the second one is on the different material layers. In this section the steps and equations are recalled and introduced.

1. Gather all input data: Weight distribution (W_s), block dimensions ($l_{sw}, l_{hw}, b_{sw}, b_{hw}, h_{sw}, h_{hw}$), block Young's modulus (E_{sw}, E_{hw}), block spacing, ship shear area (A_s), ship inertia (I_s), ship Young's modulus (E_s), ship shear modulus (G), frame spacing, block contact area (A).
2. Calculate the uniform distributed load (q) with equation 4.11. This uniform distributed load is used as input value for the ship model.
3. Use the equivalent Young's modulus (equation 4.12) to calculate the block spring stiffness (K) with equation 4.13.
4. Calculate the block reaction force (F_r) with the ship model (Timoshenko theory) and the according input parameters (equation 4.19).
5. Use the reaction force as input parameter for the single dock block model. This value is changed to an uniform distributed load (q) with equation 4.20.
6. Now the ship model is used to calculate the reaction forces on all dock block positions, it is time to calculate the individual timber deformations (Euler-Bernoulli theory).
7. Calculate the interaction parameters (k_{d1}, k_{d2}) with equation 4.9.
8. Use the single dock block model to calculate the deformation (W) of the individual material layers per dock block.

9. Calculate the strain (ϵ) with the deformation, using equation 6.10.
10. Check if the strain is below the yield strain point obtained by test measurements.

7.3. Material variability effect of moisture content on the obtained models

To see what the influence of the moisture content is on the results for the obtained materials, one can use the same case study as used for the validation in chapter 5 and introduce the variability due to the moisture content. From the test data conclusions one knows that the moisture content influences the Young's modulus. In this section 4 scenarios are used:

- Case 1: Hardwood with low moisture content (Azobe with MC of 20.9%) in combination with softwood of low moisture content (LVL with MC of 13.5%).
- Case 2: Hardwood with low moisture content (Azobe with MC of 20.9%) in combination with softwood of high moisture content (LVL with MC of 60.6%).
- Case 3: Hardwood with high moisture content (Azobe with MC of 25.6%) in combination with softwood of low moisture content (LVL with MC of 13.5%).
- Case 4: Hardwood with high moisture content (Azobe with MC of 25.6%) in combination with softwood of high moisture content (LVL with MC of 60.6%).

First step is to use the appropriate input values to calculate the dock block reaction force, which will be used in the analyse of a single dock block. The configuration is a Azobe hardwood with an LVL softwood. Dimensions for this analyse are the same as used in the validation in chapter 5.

Hardwood	Value	Softwood	Value	Unit
l_{hw}	800	l_{sw}	800	mm
b_{hw}	300	b_{sw}	300	mm
h_{hw}	200	h_{sw}	40	mm

With the Young's moduli as obtained from test data the equivalent Young's modulus for the ship model can be calculated. A good point to notice is the relative high equivalent Young's modulus compared to the validation in chapter 5, therefore it is expected that the maximum capacity is not likely to be exceeded. Nevertheless, the moisture content variability can be shown.

Table 7.2: Young's moduli for case study: hardwood, softwood and equivalent

Case	E_{hw} [N/mm^2]	E_{sw} [N/mm^2]	E_{eq} [N/mm^2]
Case 1	1129.9	325.3	800.1
Case 2	1129.9	57.5	275.0
Case 3	620.1	325.3	538.7
Case 4	620.1	57.5	235.7

Figure 7.3 gives the load on every single dock block as consequence of the ship resting on the block bed. The sum of the loads is in all cases equal, which validates the calculation. The dock blocks of case 1 have the highest stiffness, and results in a higher reaction force in the aft of the ship (frame 24.5). Using the deformation strain relation, and the yield strain from the test data it is possible to see if one of the blocks, in both soft- or hardwood is exceeded.

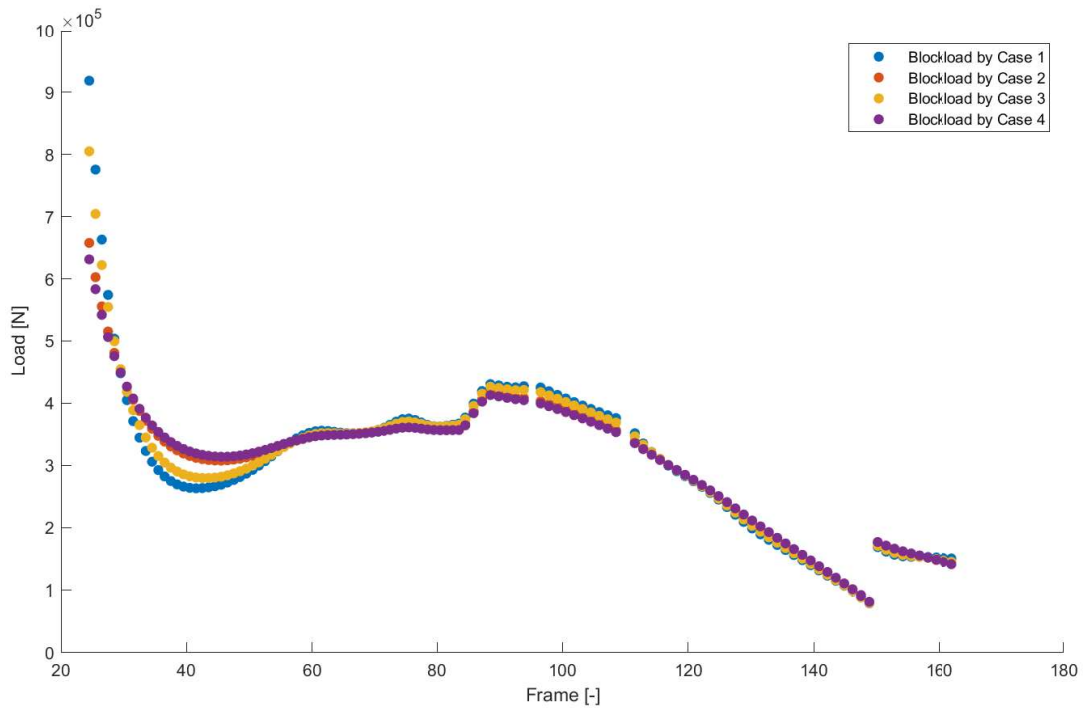


Figure 7.3: Influence of moisture content variability with respect to the dock block reaction force

Table 7.3: Yield strain point for specimens with different moisture content

Material	MC [%]	Yield strain ϵ [mm/mm]
Azobe	20.9	0.02100
Azobe	25.6	0.02030
LVL	13.5	0.02105
LVL	60.6	0.01822

Figures 7.4 and 7.5 gives the strain per layer for every single dock block as they are loaded by the force calculated by the ship model. One can clearly see the high difference in strain for the softwood in different scenarios, where the strain for the dry-dry configuration is not close to the yield point, is the wet-wet condition (looking at softwood) close to the yield point. This configuration has a high stiffness and is therefore not exceeded by at any dock block. The suggested dock plan with the Azobe and LVL combination is safe to use. The difference in softwood strain is larger compared to the hardwood strain, which can be explained due to the lower moisture content difference for these hardwood specimens.

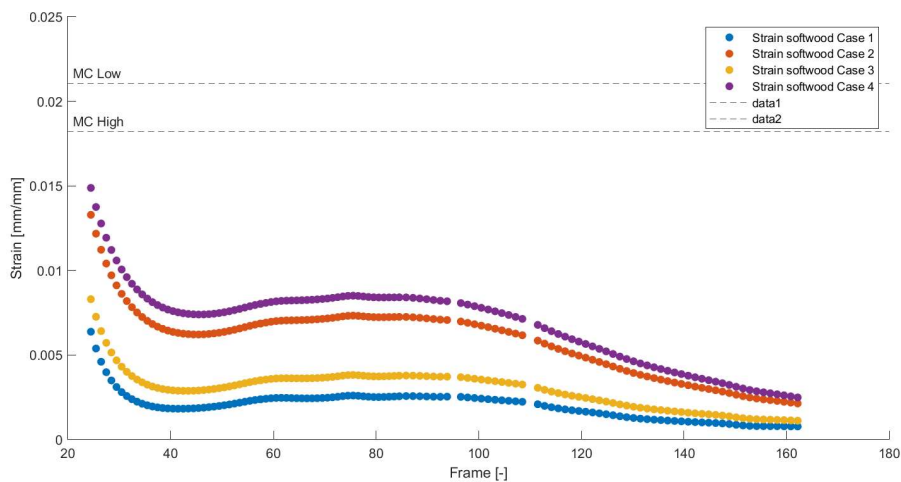


Figure 7.4: Influence of moisture content variability with respect to the dock block strain for softwood

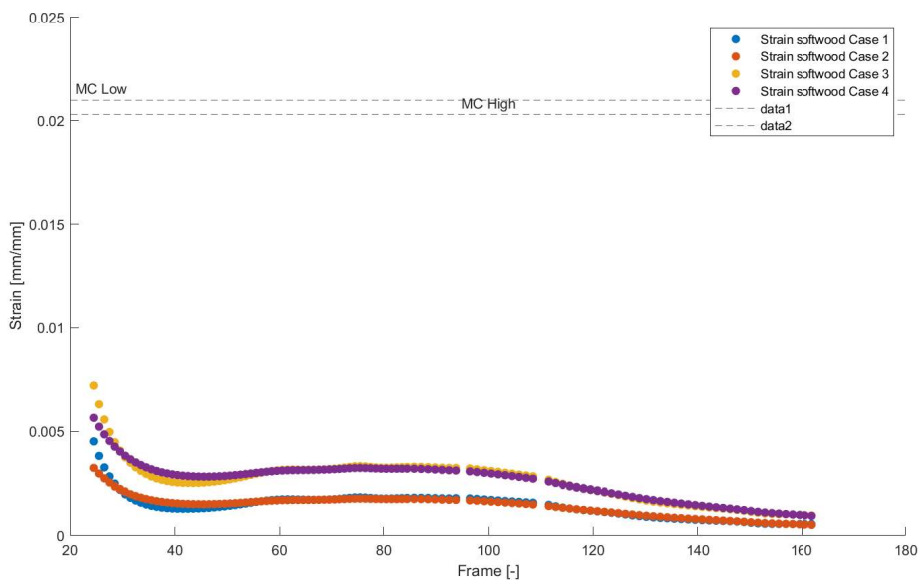


Figure 7.5: Influence of moisture content variability with respect to the dock block strain for hardwood

7.3.1. Material variability effect of moisture content on the obtained models in worst case scenario

Previous case study showed the effect of material moisture content variability on both the soft- and hardwood. The situation could occur that in engineering phase the moisture content is not taken into account, which lead to an overestimation of the Young's modulus. For the ship model one calculates the expected dock block forces with an equivalent Young's modulus with low moisture content, however the materials used appeared to have a higher moisture content as expected. The consequence is shown in figures 7.6 and 7.7, where the softwood in the aft of the ship exceeds the proportional limit of the yield point. For this particular configuration it wouldn't lead to block failure as the configuration was very stiff regardless the moisture content. In practice this difference between the yield for every single block, and the yield point may be closer, which could eventually lead to failure of a block as the capacity is overestimated.

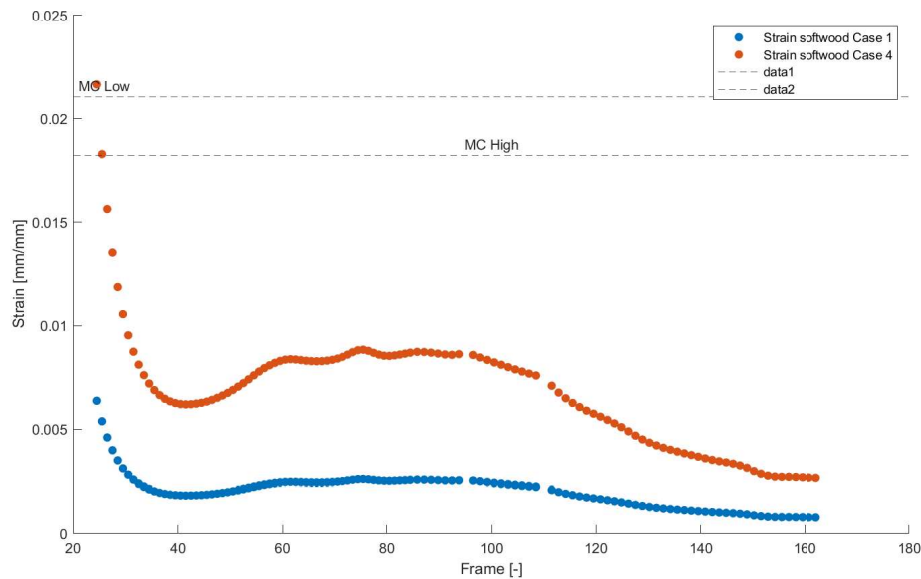


Figure 7.6: Influence of moisture content variability with respect to the dock block strain for softwood in a worst case scenario

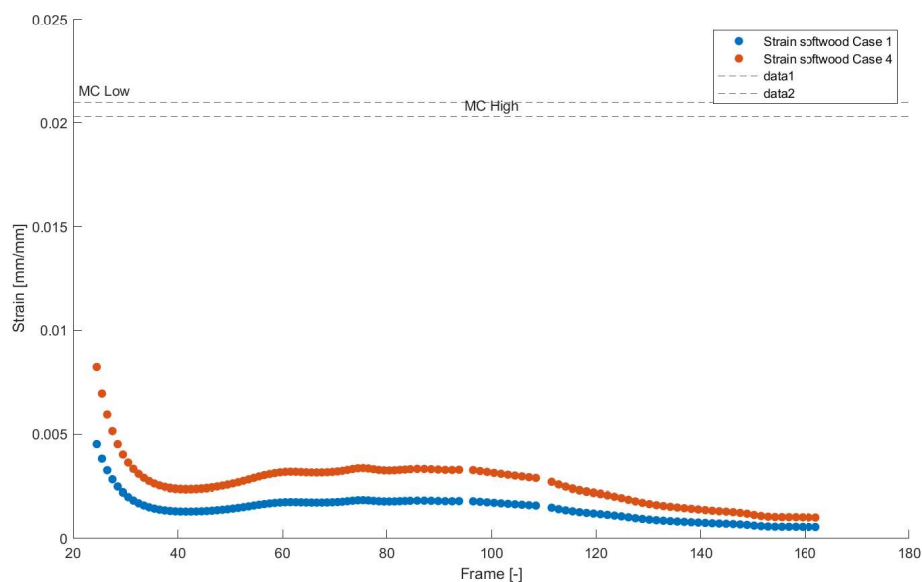


Figure 7.7: Influence of moisture content variability with respect to the dock block strain for hardwood in a worst case scenario

Moisture content highly influence the response of the dock block behaviour as the strength decreases by an increasing moisture content. Variability due to the moisture content can't be avoided from practical point of view, however, knowing the consequences it is preferable account for possible worst case scenarios.

7.4. Material variability effect of different material layers on the obtained models

Multiple configurations are evaluated to see what the response is on a single dock block. The same ship configuration and dock plan is used, only the block dimensions and belonging characteristics are changed. The influence of the moisture content is already showed, so the average test data with respect to humidity is used. Configurations represents the dimensions as they are used in the yards of Damen.

First subsection represents linear material properties, where the second subsection makes use of a secant softwood Young's modulus to represent the non-linear behaviour.

7.4.1. Material variability effect of different material layers with linear properties

With the linear material properties measured one can do a study on different dock block configurations. The values are shown in 7.4 where the length and width of the block is still the same as for the validation case. The effect is illustrated by using the three standard dock block configurations as used at the Damen yards:

- Combination of Oak and LVL used at Amels (AOO ALN). With equivalent Young's modulus of 242.5 N/mm^2 .
- Combination of Oak and Spruce used at Schiedam (SON SSN). With equivalent Young's modulus of 216.4 N/mm^2
- Combination of Azobe and Spruce used at Vlissingen-Oost (RAN RSN). With equivalent Young's modulus of 261.9 N/mm^2

The reaction force of the three combinations are shown in 7.8. As the equivalent Young's modulus for the three configurations is more or less equal it results in an equal spreading of the reaction force.

Table 7.4: Input values for the effect on different material layers with linear characteristics

Hardwood	E_{hw} [N/mm^2]	h_{hw} [mm]	MC [-]	Softwood	E_{sw} [N/mm^2]	h_{sw} [mm]	MC [-]
Oak (AOO)	228.5	200	20.7	LVL (ALN)	349.9	40	14.2
Oak (SON)	404.4	150	36.9	Spruce (SSN)	90.4	50	17.2
Azobe (RAN)	930.4	200	23.3	Spruce (RSN)	67.6	50	25.7

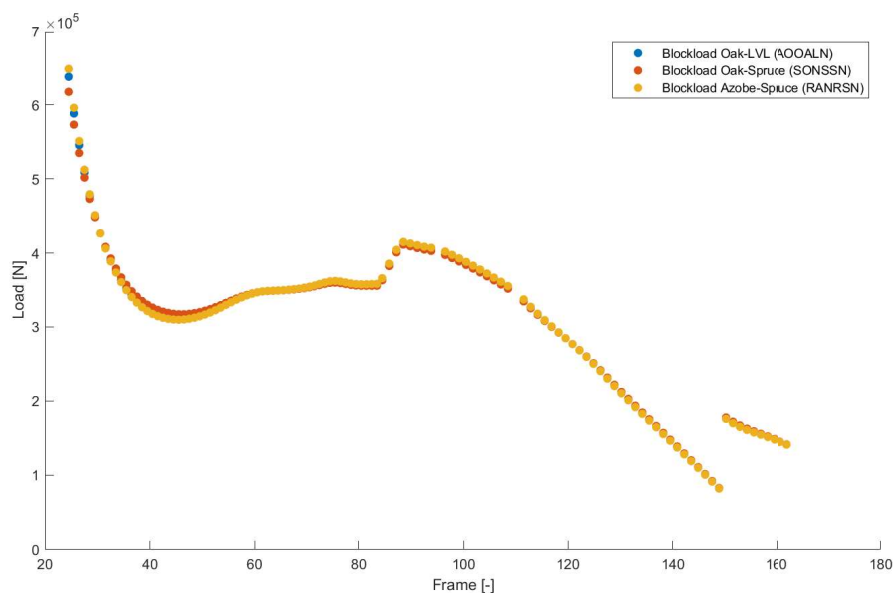


Figure 7.8: Influence of different material layers on dock block reaction force response

With the reaction force per dock block the single dock block analysis can be done. Figures 7.9 and 7.10 gives the strain for the soft- and hardwood layers per configuration. The limit illustrated is the one obtained from measuring. This limit is the average yield strain limit for soft- and hardwood. It is clear that all three configurations are sufficiently strong enough when only the linear material properties are accounted. Furthermore, one can conclude that the configuration of Oak and LVL is the weakest, this

can be clarified by the relatively low stiffness of the hardwood. This configuration almost exceeds the limit of the hardwood strain.

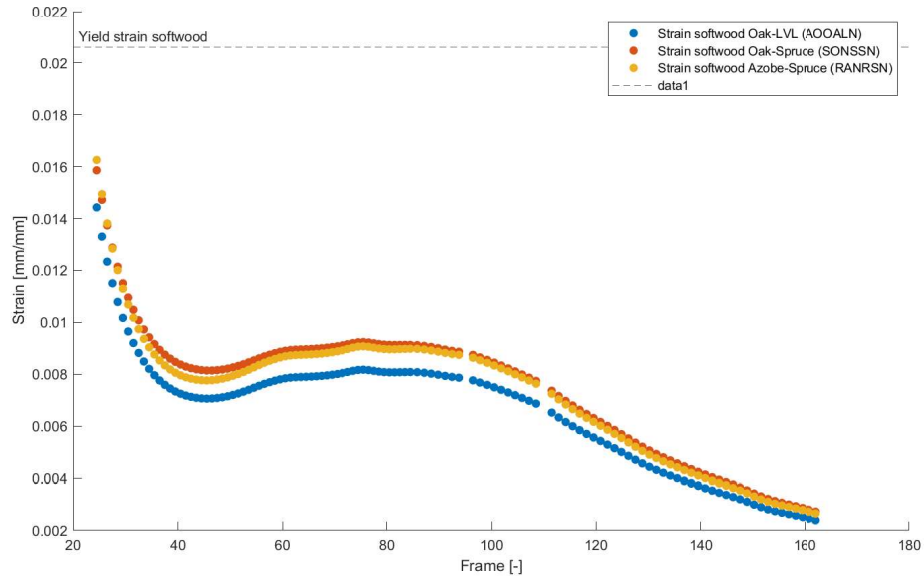


Figure 7.9: Influence of different material layers on dock block softwood strain response

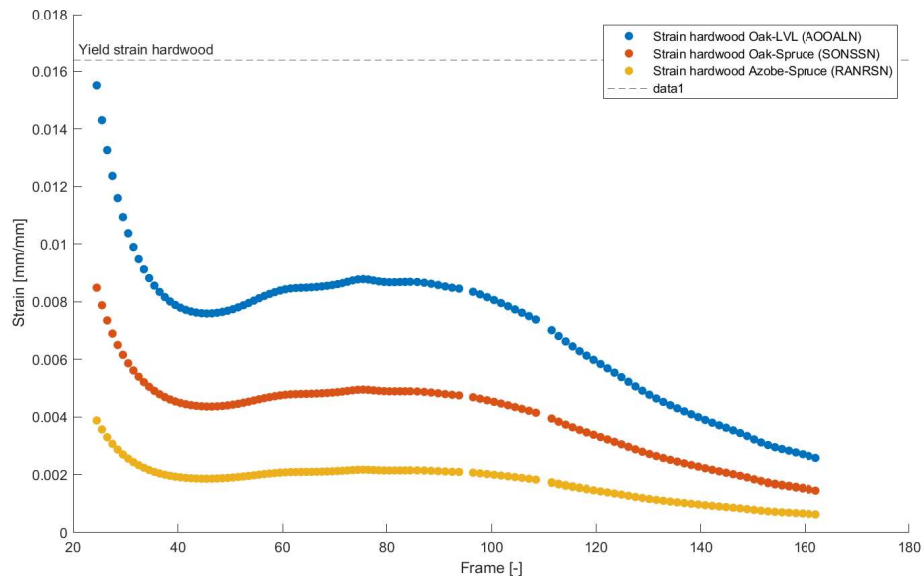


Figure 7.10: Influence of different material layers on dock block hardwood strain response

7.4.2. Material variability effect of different material layers on the obtained models with non-linear material properties

With the properties of table 7.5, and the same configurations as in previous subsection, it is evaluated what the effect is of the non-linear material behaviour. The fourth configuration is the same as used in the validation chapter, this to give a reference between the configuration used at engineering, and the actual configuration at the yards. Figure 7.11 gives the load graph for the 4 configurations.

Table 7.5: Input values for the effect on different material layers with non-linear characteristics

Hardwood	E_{hw} [N/mm^2]	h_{hw} [mm]	MC [-]	Softwood	(Secant) E_{sw} [N/mm^2]	h_{sw} [mm]	MC [-]
Oak (AOO)	228.5	200	20.7	LVL (ALN)	30.7	40	14.2
Oak (SON)	404.4	150	36.9	Spruce (SSN)	12.4	50	17.2
Azobe (RAN)	930.4	200	23.3	Spruce (RSN)	9.4	50	25.7
Oak	600	200	-	Spruce	10	50	-

As the Young’s modulus for the softwood is changed to a secant modulus, is the equivalent Young’s modulus also changing. For AOOALN is $E_{eq} = 110.2 N/mm^2$, SONSSN $E_{eq} = 45.4 N/mm^2$, RANRSN $E_{eq} = 45.2 N/mm^2$ and Oak Spruce $E_{eq} = 46.9 N/mm^2$. As the last three are close to each other it result in a almost equal load distribution. The most important conclusion for the load with non-linear material properties is that the load in the aft of the ship is lower, this as consequence of a lower stiffness. The lower stiffness lead to a better distribution of the load in the aft, due to the overhang.

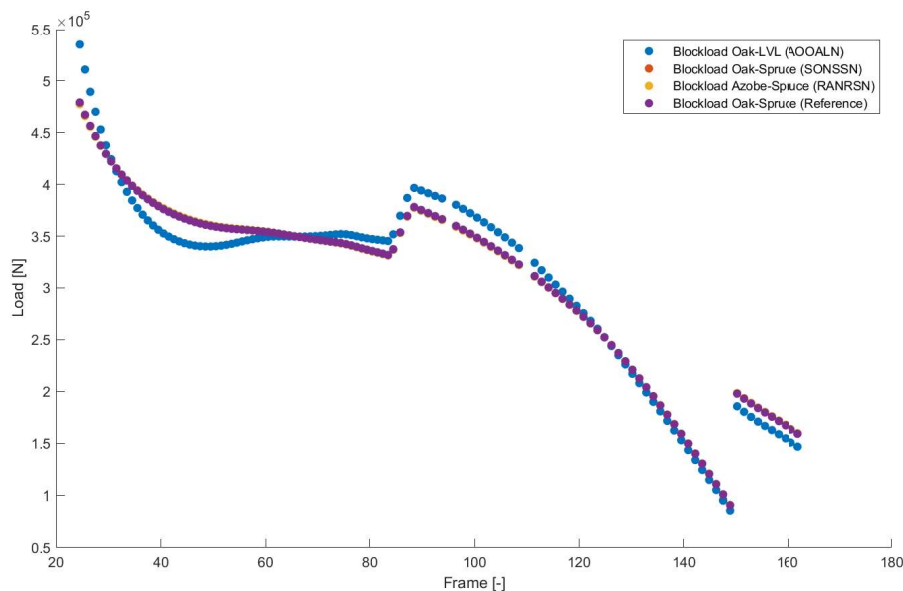


Figure 7.11: Influence of different material layers on dock block reaction force response with non-linear softwood properties

With the load per single dock block one can do the analyse of the strain of the individual material layers, and compare this with the linear simulation. Figures 7.12 and 7.13 illustrates the non-linear effect on the strain of both the soft- and hardwood. First conclusion is that for the softwood almost every configuration, and every dock block is exceeding the maximum limit. As softwood is a sacrificial material this is not a problem in the end. The hardwood is not exceeding the yield strain limit, therefore it is safe to use all 4 configurations in the obtained dockplan. The lower hardwood strain is a consequence of the better load distribution over the block line. Taking non-linear material behaviour into account directly lead to a lower equivalent block stiffness, which eventually results in a lower reaction force in case of a large overhang.

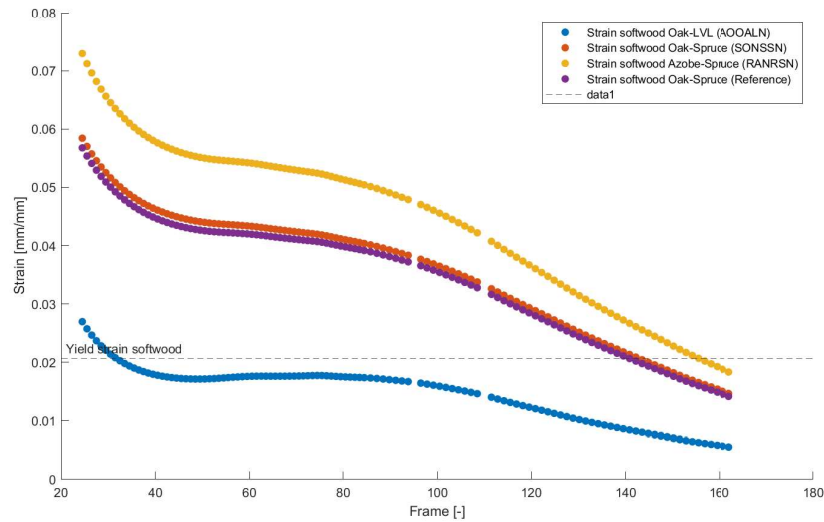


Figure 7.12: Influence of different material layers on dock block softwood strain response with non-linear softwood properties

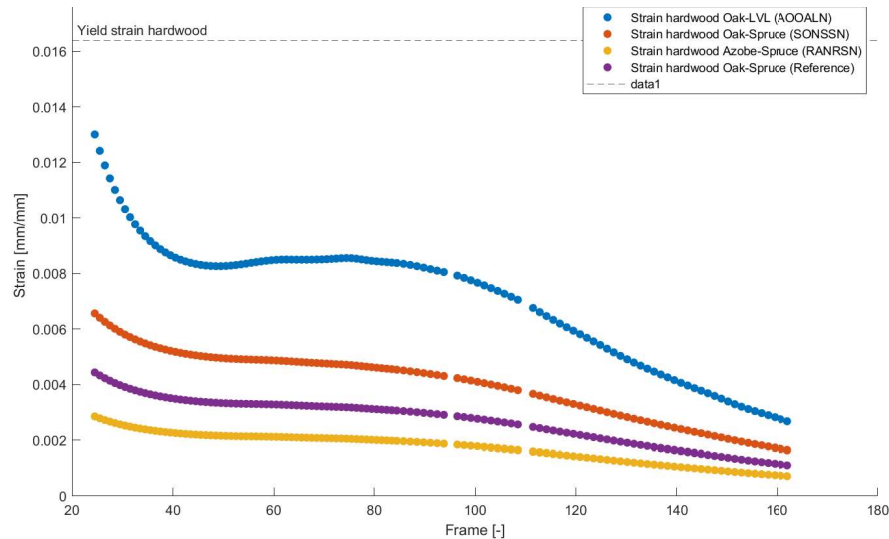


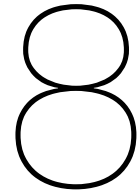
Figure 7.13: Influence of different material layers on dock block hardwood strain response with non-linear softwood properties

7.5. Conclusion

Validation with measured data justifies the assumptions made in the model phase. This last validation shows that the model of two elastic layers captures the physics of compression.

For the variability study on the effect of the moisture content, one can conclude that it is very important to account for this uncertainty. Engineering with literature values representing a low humidity is optimistic and will lead to an underestimation of the deformation of a block. If the design is close to the maximum this can cause a lot of problems in case the moisture content is lower as expected.

Variability of different layers showed that the influence of the non-linear material behaviour, for the softwood, should be introduced as a secant modulus. With the secant modulus it is possible to account for over-stress failure of the softwood, and see what the influence on the complete dock plan is. Hardwood strain values can be evaluated by means of averaged test data.



Conclusions and Recommendations

8.1. Conclusions

In chapter 1, the following research questions are formulated. They are answered one by one in this section. First all sub-questions and then the main research question. Finally, the additional conclusions are formulated.

1. What materials are involved in dock blocks and what properties influence the load acting on the block and how is this calculated and distributed?
 - In the analysis of dock blocks and the materials used, a high variety of configurations and values can be found within the Damen company. There are 2 types of hardwood that are used as a dock block layer: oak and azobe. Spruce is usually used for as softwood layer, but the configuration with LVL (laminated veneer lumber) or pine is also an possibility.
 - Material assessment regarding compression perpendicular to the grain found that for a timber, the deformation is highly dependent on the Young's modulus, moisture content and dimensions to capture non-linear material behaviour.
 - Characterization of material properties with respect to the perpendicular loading is scarce in the literature. In addition, the high variability due to moisture content is an important parameter that must be taken into account when using properties such as Young's modulus or yield point.
2. How should one model the interaction between the individual material layers to get a representation of the physical compression effect?
 - The objective to predict the deformation of the individual material layers (involving non-linear phenomena) is a coherence of changing parameters and time-wise optimal modelling. By taking this into account and reviewing multiple studies, an analytical approach emerges as the most appropriate solution method for this problem.
 - The use of the analytical solution method of the double Winkler foundation with the Euler-Bernoulli beam fundamentals leads to a fast and accurate solution method to account for these non-linearities. The two elastic layers represent the interaction between the rigid floor and the hardwood, and the interaction between the hardwood and softwood during compression.
 - Consequence of using a double elastic layer is the coupled fourth order differential system of equations which are mathematically complex. Solving leads to an expression of the deformation along the longitudinal length of the beam. This expression depends on the flexural rigidity (EI), the load (q) characterized by the ship model, and the interaction parameters representing the stiffness of the elastic layers (k_d).
 - Validation of the single dock block model as described by a double elastic layer lead to safe assumptions based on limit cases. The block may be assumed as a free-free finite boundary problem with a fully effective contact area.

3. How should one model the interaction between the ship and the dock block to get a realistic but still practical result?
 - The objective of this model is to predict the load on a single dock block as a consequence of the docked ship resting on the block line. Reviewing empirical, numerical and analytical studies, all with results of a case study [7] [16], pointed out that an analytical approach is a fast and realistic approach.
 - The preliminary concept of a Euler-Bernoulli beam supported by springs, representing the dock blocks, underestimates the ship's shear bending effect. Validation with the Timoshenko beam theory lead to more realistic results in the mid and fore of the ship, but still underestimates the load in the aft. On average the under- and overestimation of the Timoshenko theory is 15.5%.
 - Increased local stiffness due to transverse bulkheads is not covered in any of the analytical approaches and lead to large differences.
 - With the inertia and shear area known per frame location, the prediction of the load is very accurate in the aft of the ship (12.8%).
 - On average the load estimation of the new obtained tool has a minimal increase of accuracy. The prediction in the aft of the ship, where the load are the highest, has a high accuracy.
4. What are the similarities and differences between the test results and the theoretical values of mechanical properties?
 - From the test campaign it is observed that softwood displays a uniform deformation when loaded outside the linear range. Due to a relatively low height with respect to the width and length a pure compression curve is noticed at some point.
 - Hardwood displays several cracks and visible damage after exceeding the yield point, due to the larger height of the specimens. Where softwood is unlikely have complete failure as consequence of pure compression is hardwood failure noticed in this plastic range. Exceeding the yield point for the hardwood layer should be avoided at any cost.
 - However nominal identical specimens where considered the variability in material properties was very high.
 - Moisture content significantly affect the linear and non-linear behaviour, since the yard environment is such that there is always a very high moisture content, it should be considered in the engineering phase.
 - Nominal linear Young's modulus values found in literature where different from the ones obtained during experiments. All measured values are significantly lower as expected, and therefore, it is not safe to use nominal values. The yield point was also largely affected by the moisture content. For both properties it is concluded that a high moisture content result in a lower strength capacity.
 - Moisture content below 30% display less variability of linear behaviour. Since properties in the non-linear range already display a large variability it leads to highly unpredictable results in combination with a high moisture content.
5. What affect has the non-linear material behaviour in the obtained tool with respect to the linear tool used at the DSNS engineering?
 - Using only values in the linear range for both the soft- and hardwood leads to a strong underestimation of the actual deformation of the individual material layers.
 - In the new tool both material layers are evaluated by means of strain, which give a insight in the work-ability range of the hardwood.
 - The use of the secant modulus gives a lower equivalent stiffness of the dock block, which leads to more spreading of the reaction forces. The secant modulus captures the non-linear material range for the softwood layer and should be used in the calculations.

- Variability of the moisture content has major influence on the distribution of the load on the keel line. Neglecting moisture content variability can lead to a large underestimation of the actual hardwood deformation. In the worst case scenario, where both soft- and hardwood moisture content is designed to be low moisture content, but found to be high, there may be more complete block failures.

How does non-linear material behaviour influence the drydock block load and how can this be predicted?

- Single dock block behaviour varies significantly even for nominal identical layers.
- Variability due to moisture content is a non-linear material behaviour which highly influence the prediction of the block load and the deformation of each material layer.
- Using low moisture content values results in high strength and stiffness values. The higher the stiffness of the block the larger the resulting reaction force from the ship model.
- Using measured data one can deal with the variability of the material properties and the variability due to the moisture content. Variability is taken into account by using mean values obtained from multiple test samples.
- The new obtained tool has a high accuracy with respect to the locations where the load is the highest (aft of the ship).
- Non-linear material behaviour is covered by using a secant modulus in the softwood layer. The influence of this non-linear behaviour is significant in the prediction of the load, and the prediction of the maximum capacity.
- The influence of the non-linear compression behaviour hardly affects the results. The model of the double Winkler foundation makes it easier to evaluate the behaviour of the hardwood.

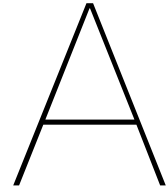
In conclusion, the new proposed tool displays the non-linear material behaviour of the interaction of the individual layers and the rigid ground. The tool gives an accurate representation of the physical compression behaviour of a stacked block where both the soft- and hardwood are displayed by their deformation and equivalent strain. For Damen, this means that an accurate prediction of the single block capacity is made for each configuration, with knowledge of the variability of the specimens and the associated moisture content. For science, the double elastic foundation is a good representation of the non-linear material behaviour. The ship block interaction model underestimates the load prediction when a transverse bulkhead is located, further development is necessary.

8.2. Recommendations

Using the combination of the single dock block model and the ship model to predict the load on a block and estimate the deformation gives reasonable results in this research. However, since the load at some location is over- or underestimated, further research is recommended. To increase the accuracy of the model, recommendations are made in this section.

- Conduct more case studies to understand the effect of the overhang over the first few blocks. Now only one FE analysis is known that could potentially lead to wrong assumptions in the validation phase.
- Taking full advantage of the measured data will take more time. Here, uncertainties and trends could be visualized by running many more test series on nominally identical specimens.
- Field studies on the actual deformation of a dock block are needed to see if the obtained solutions by FE models or analytical models represent the real-life situation. Proposed strategy could be to use dock blocks of completely new layers of materials and measure the deformation immediately after the docking, and right after loosening (when the dock is filled with water again).

- The so-called critical period, when the ship is in the docking phase and the aft of the ship touches the first dock block, resulting in a change of the metacentric height should be evaluated. In this dynamic behaviour the highest loads on the dock blocks is expected.
- Creep and fatigue test campaigns are recommended to see what the influence of the compression is after a long duration or after frequently re-using the hardwood.



Common strength properties

The information used for the explanation of the properties comes from the Wood Handbook [32].

Poisson's ratio The Poisson's ratio is the ratio of the transverse to axial strain. This happens if a specimen is loaded axially, then the deformation perpendicular to the direction of the load is proportional to the deformation parallel to the load direction. Just as the strength the Poisson's ratio is affected by moisture content and density.

Modulus of Rigidity The modulus of rigidity is often noticed as the shear modulus, this refers to the resistance to deflection caused by shear stress G_{ij} .

$$G_{mean} = E_{\parallel}/16 \quad (\text{A.1})$$

Modulus of rupture Reflects the maximum load-carrying capacity of a member in bending and is proportional to maximum moment borne by the specimen. Modulus of rupture is an accepted criterion of strength, although it is not a true stress because the formula by which it is computed is valid only to the elastic limit.

Work to maximum load in bending Ability to absorb shock with some permanent deformation and more or less injury to a specimen. Work to maximum load is a measure of the combined strength and toughness of wood under bending stresses.

Compressive strength parallel to grain Maximum stress sustained by a compression parallel-to-grain specimen having a ratio of length to least dimension of less than 11.

Compression strength parallel to grain:

$$f_{c,\parallel} = 5(f_m)^{0.45} \quad (\text{A.2})$$

Compressive stress perpendicular to grain Reported as stress at proportional limit. There is no clearly defined ultimate stress for this property.

$$f_{c,\perp} = \begin{cases} 0.007\rho & \text{softwoods} \\ 0.015\rho & \text{hardwoods} \end{cases} \quad (\text{A.3})$$

Shear strength parallel to grain Ability to resist internal slipping of one part upon another along the grain. Values presented are average strength in radial and tangential shear planes.

$$f_v = \min \begin{cases} 3.8 \\ 0.2(f_m)^{0.8} \end{cases} \quad (\text{A.4})$$

Impact bending In the impact bending test, a hammer of given weight is dropped upon a beam from successively increased heights until rupture occurs or the beam deflects 152 mm (6 in.) or more. The

height of the maximum drop, or the drop that causes failure, is a comparative value that represents the ability of wood to absorb shocks that cause stresses beyond the proportional limit.

Tensile strength perpendicular to grain Resistance of wood to forces acting across the grain that tend to split a member. Values presented are the average of radial and tangential observations.

Hardness Generally defined as resistance to indentation using a modified Janka hardness test, measured by the load required to embed a 11.28-mm (0.444-in.) ball to one-half its diameter. Values presented are the average of radial and tangential penetrations.

Tensile strength parallel to grain Maximum tensile stress sustained in direction parallel to grain. Relatively few data are available on the tensile strength of various species

$$f_{t,\parallel} = 0.6f_m \quad (\text{A.5})$$

B

Modelling of dock block and ship behaviour

B.1. Derivation of the expression for the deformation of the beam on elastic foundation

In order to solve the general expression, the homogeneous part needs to be solved by using the characteristic equation of the differential equation.

$$\frac{d^4 W}{dx^4} + 4\alpha^4 W = \frac{q(x)}{EI} \quad (\text{B.1})$$

Where:

$$\alpha = \sqrt[4]{\frac{k_d}{4EI}}$$

$$r^4 + 4\alpha^4 = 0 \quad (\text{B.2})$$

Where the roots are:

$$r_1 = (\alpha + i\alpha), \quad r_2 = (\alpha - i\alpha), \quad r_3 = (-\alpha + i\alpha), \quad r_4 = (-\alpha - i\alpha)$$

Using the equation for the characteristic equation and substituting this in the expression for the homogeneous equation one finds the following equation:

$$W_h(x) = A_1 e^{r_1 x} + A_2 e^{r_2 x} + A_3 e^{r_3 x} + A_4 e^{r_4 x} \quad (\text{B.3})$$

Using Euler's expressions:

$$e^{i\alpha x} = \cos(\alpha x) + i\sin(\alpha x), \quad e^{-i\alpha x} = \cos(\alpha x) - i\sin(\alpha x)$$

$$W_h(x) = e^{-\alpha x} [B_1 \cos(\alpha x) + B_2 \sin(\alpha x)] + e^{\alpha x} [B_3 \cos(\alpha x) + B_4 \sin(\alpha x)] \quad (\text{B.4})$$

Where:

$$B_1 = A_3 + A_4, \quad B_2 = iA_3 - iA_4, \quad B_3 = A_1 - A_2, \quad B_4 = iA_1 - iA_2$$

Finally, after mathematical manipulations, the expression for the homogeneous solution is written in equation B.5:

$$W_h(x) = \cosh(\alpha x) [C_1 \cos(\alpha x) + C_2 \sin(\alpha x)] + \sinh(\alpha x) [C_3 \cos(\alpha x) + C_4 \sin(\alpha x)] \quad (\text{B.5})$$

Where:

$$e^{\alpha x} = \cosh(\alpha x) + \sinh(\alpha x), \quad e^{-\alpha x} = \cosh(\alpha x) - \sinh(\alpha x)$$

$$C_1 = B_1 + B_3,$$

$$C_2 = B_2 + B_4$$

$$C_3 = -B_1 + B_3,$$

$$C_4 = -B_2 + B_4$$

Expression B.5 can also be written in terms without cosinus and sinus:

$$W_h(x) = C_1 \exp\left(\frac{(-k_d E^3 I^3)^{1/4} x}{EI}\right) + C_2 \exp\left(-\frac{(-k_d E^3 I^3)^{1/4} x}{EI}\right) + C_3 \exp\left(i \frac{(-k_d E^3 I^3)^{1/4} x}{EI}\right) + C_4 \exp\left(-i \frac{(-k_d E^3 I^3)^{1/4} x}{EI}\right) \quad (\text{B.6})$$

$$W_p(x) = \frac{q}{k_d} \quad (\text{B.7})$$

B.2. Matlab script for single dock block model

3-6-21 11:25 C:\Users\bartj\OneD...\Dockblock model.m 1 of 4

```
%Matlab model for a single dock block as described in the Thesis:
%Non-linear block load corrections for dry docking by B. Jacobse

clc
clearvars
close all

syms W1(x) W2(x) E1 E2 I1 I2 kd1 kd2 q
%Introducing the used symbolics
%W1(x) [mm] : function for the deflection of the toplayer with respect to x
%W2(x) [mm] : function for the deflection of the bottom layer with respect to x
%EI1 [MPa] : flexural rigidity of the softwood
%EI2 [MPa] : flexural rigidity of the hardwood
%kd1 [N/mm2]: interaction paramters between the soft- and hardwood
%kd2 [N/mm2]: interaction paramters between hardwood and rigid ground
%q [N/mm] : uniform distributed load

%Order differential equation for the softwood:
ode1 = E1*I1*diff(W1,x,x,x,x)+kd1*(W1-W2) == 0;
%Order differential equation for the hardwood:
ode2 = E2*I2*diff(W2,x,x,x,x)-kd1*(W1-W2)+kd2*W2 == 0;
%Solve function for the coupled system of ODEs (homogeneous solution)
odes = [ode1; ode2];
S = dsolve(odes);

%Particular solution for the softwood layer
W1_part = ((q * (kd1 + kd2)) / (kd1 * kd2));
%Particular solution for the hardwood layer
W2_part = (q/kd2);

%Total solution for the deflection, slope, moment ans shear:
W1Sol(x) = S.W1+W1_part;
S1Sol(x) = diff(S.W1,x);
M1Sol(x) = -E1*I1*diff(S.W1,x,x);
V1Sol(x) = -E1*I1*diff(S.W1,x,x,x);
W2Sol(x) = S.W2+W2_part;
S2Sol(x) = diff(S.W2,x);
M2Sol(x) = -E2*I2*diff(S.W2,x,x);
V2Sol(x) = -E2*I2*diff(S.W2,x,x,x);

%Introduce variables which can be changed per case:
F = 559800; % [N] Force acting on a single dock block
%Softwood layer:
b1 = 300; % [mm] Width of the blocklayer
h1 = 50; % [mm] Height of the blocklayer
L1 = 600; % [mm] Length of the blocklayer
E1 = 10; % [MPa] Young's modulus of the blocklayer
%Hardwood layer:
b2 = 300; % [mm] Width of the blocklayer
h2 = 200; % [mm] Height of the blocklayer
L2 = 600; % [mm] Length of the blocklayer
E2 = 600; % [MPa] Young's modulus of the blocklayer
```

Figure B.1: Matlab code for single dock block pressure and deflection 1

3-6-21 11:25 C:\Users\bartj\OneD...\Dockblock model.m 2 of 4

```

%Introduce constants which (not variable):
I1 = (b1*h1^3)/12; %[mm4] Moment of inertia for blocklayer
I2 = (b2*h2^3)/12; %[mm4] Moment of inertia for blocklayer
A1 = L1*b1; %[mm2] Contactarea for blocklayer
A2 = L2*b2; %[mm2] Contactarea for blocklayer
Cs = 1; %[-] Correction factor for kd1
Ch = 1; %[-] Correction factor for kd2
kd1 = Cs*E1*b1/(h1); %[N/mm2] interaction parameter
kd2 = Ch*E2*b2/(h2); %[N/mm2] interaction parameter
q = F/L1; %[N/mm] Change the pointload to a uniform distributed load

%Substitute constants in the total solution
W1(x) = subs(W1Sol);
W2(x) = subs(W2Sol);
S1(x) = subs(S1Sol);
S2(x) = subs(S2Sol);
M1(x) = subs(M1Sol);
M2(x) = subs(M2Sol);
V1(x) = subs(V1Sol);
V2(x) = subs(V2Sol);

%Set boundary conditions Can be changed to Free-Free when the practical
%case implies this type of stacked block
%Pinned-Pinned
cond1 = W1(0) == 0; %Boundary condition at x = 0 -> no deflection
cond2 = M1(0) == 0; %Boundary condition at x = 0 -> no moment
cond3 = W2(0) == 0; %Boundary condition at x = 0 -> no deflection
cond4 = M2(0) == 0; %Boundary condition at x = 0 -> no moment
cond5 = W1(L1) == 0; %Boundary condition at x = L -> no deflection
cond6 = M1(L1) == 0; %Boundary condition at x = L -> no moment
cond7 = W2(L2) == 0; %Boundary condition at x = L -> no deflection
cond8 = M2(L2) == 0; %Boundary condition at x = L -> no moment

%Free-Free
% cond1 = M1(0) == 0; %Boundary condition at x = 0 -> no moment
% cond2 = V1(0) == 0; %Boundary condition at x = 0 -> no shear
% cond3 = M2(0) == 0; %Boundary condition at x = 0 -> no moment
% cond4 = V2(0) == 0; %Boundary condition at x = 0 -> no shear
% cond5 = M1(L1) == 0; %Boundary condition at x = L -> no moment
% cond6 = V1(L1) == 0; %Boundary condition at x = L -> no shear
% cond7 = M2(L2) == 0; %Boundary condition at x = L -> no moment
% cond8 = V2(L2) == 0; %Boundary condition at x = L -> no shear

%Substitute solution of beam equation in the boundary conditions
syms C1 C2 C3 C4 C5 C6 C7 C8
sol = solve([cond1, cond2, cond3, cond4, cond5, cond6, cond7, cond8], [C1, C2, C3, C4, C5, C6, C7, C8]);
C1sol = double(sol.C1);
C2sol = double(sol.C2);
C3sol = double(sol.C3);
C4sol = double(sol.C4);
C5sol = double(sol.C5);

```

Figure B.2: Matlab code for single dock block pressure and deflection 2

3-6-21 11:25 C:\Users\bartj\OneD...\Dockblock model.m 3 of 4

```

C6sol = double(sol.C6);
C7sol = double(sol.C7);
C8sol = double(sol.C8);

C1 = C1sol; C2 = C2sol; C3 = C3sol; C4 = C4sol; C5 = C5sol; C6 = C6sol; C7 = C7sol; C8 = C8sol;
W1(x) = real(subs(W1));
W2(x) = real(subs(W2));
S1(x) = real(subs(S1));
S2(x) = real(subs(S2));
M1(x) = real(subs(M1));
M2(x) = real(subs(M2));
V1(x) = real(subs(V1));
V2(x) = real(subs(V2));

xvec1=0:L1/100:L1;
xvec2=0:L2/100:L2;

Displacement_Beam1 = W1;
Displacement_Beam2 = W2;
Slope_Beam1 = S1;
Slope_Beam2 = S2;
Moment_Beam1 = M1;
Moment_Beam2 = M2;
Shear_Beam1 = V1;
Shear_Beam2 = V2;

Pressure_Beam1 = (W1*E1)/(h1);
Pressure_Beam2 = (W2*E2)/(h2);

Displacement1 = zeros(length(xvec1),1);
Displacement2 = zeros(length(xvec2),1);
Slope1 = zeros(length(xvec1),1);
Slope2 = zeros(length(xvec2),1);
Moment1 = zeros(length(xvec1),1);
Moment2 = zeros(length(xvec2),1);
Shear1 = zeros(length(xvec1),1);
Shear2 = zeros(length(xvec2),1);
Pressure1 = zeros(length(xvec1),1);
Pressure2 = zeros(length(xvec2),1);

for i = 1:length(xvec1)
    x = xvec1(i);
    Displacement1(i) = double(subs(Displacement_Beam1));
    Slope1(i) = double(subs(Slope_Beam1));
    Moment1(i) = double(subs(Moment_Beam1));
    Shear1(i) = double(subs(Shear_Beam1));
    Pressure1(i) = double(subs(Pressure_Beam1));
end

for i = 1:length(xvec2)
    x = xvec2(i);
    Displacement2(i) = double(subs(Displacement_Beam2));

```

Figure B.3: Matlab code for single dock block pressure and deflection 3

3-6-21 11:25 C:\Users\bartj\OneD...\Dockblock model.m 4 of 4

```

    Slope2(i)      = double(subs(Slope_Beam2));
    Moment2(i)    = double(subs(Moment_Beam2));
    Shear2(i)     = double(subs(Shear_Beam2));
    Pressure2(i)  = double(subs(Pressure_Beam2));
end

%-----
%Make plot (if one is interested in the slope, shear and moment it can be
%displayed by plots p3 - p8)
tiledlayout(1,1);
nexttile
p1= plot(xvec1,Displacement1,'color','b','linewidth',1.0);
hold on
p2= plot(xvec2,Displacement2,'color','r','linewidth',1.0);
xlabel('X [mm]')
ylabel('W [mm]')
legend('W1','W2','Location','northeast')
hold off
% nexttile
% p3= plot(xvec1,Slope1,'color','b','linewidth',1.0);
% hold on
% p4= plot(xvec2,Slope2,'color','r','linewidth',1.0);
% xlabel('X [mm]')
% ylabel('Phi [-]')
% legend('Phi1','Phi2','Location','northeast')
% hold off
% nexttile
% p5= plot(xvec1,Moment1,'color','b','linewidth',1.0);
% hold on
% p6= plot(xvec2,Moment2,'color','r','linewidth',1.0);
% xlabel('X [mm]')
% ylabel('M [Nmm]')
% legend('M1','M2','Location','northeast')
% hold off
% nexttile
% p7= plot(xvec1,Shear1,'color','b','linewidth',1.0);
% hold on
% p8= plot(xvec2,Shear2,'color','r','linewidth',1.0);
% xlabel('X [mm]')
% ylabel('V [N]')
% legend('V1','V2','Location','northeast')
% hold off
set(gcf,'color','w');

Property = {'Displacement'; 'Moment'; 'Shear'; 'Pressure'};
Softwood = [max(Displacement1); max(Moment1) ; max(Shear1); max(Pressure1)];
Hardwood = [max(Displacement2); max(Moment2) ; max(Shear2); max(Pressure2)];
Unit = {'mm' ; 'Nmm' ; 'N' ; 'N/mm2'};
T = table(Softwood,Hardwood, Unit, 'RowNames',Property)

```

Figure B.4: Matlab code for single dock block pressure and deflection 4

B.3. Matlab script for complete model

B.3.1. Run file for the model

8-6-21 15:23 C:\Users\bartj\On...\run_reactionforce.m 1 of 2

```
%Model to predict the block load by B.Jacobse
%Runfile for the strain and reaction force for the block load prediction.
%Do not change any of the other files!

%Files which need to be located in the same folder are:
% run_reactionforce
% get_Input_Frf
% get_Frf
% get_Pressure_Frf
% ODE_blocks_Frf
% Excel file with the input data at the exact right columns

%Output will be saved by the filename given in the last 2 lines!!

%PS: The waitbar indicates how long the script will run.
clear all;
close all;
clc;

%% Input file location
% Change the filename to the correct folder where all the Matlab files and
% Excel files are located
filename = 'C:\Users\bartj\OneDrive\Documenten\Master
ODE\Thesis\Test\Weightdistribution_input_timoshenko_simplev4.csv';

%% get data
data = get_Input_Frf(filename);

%% calculate W, Phi, M and V
[W,Wres,Frf] = get_Frf(data);

%% Calculate the reaction force at each block frame location
Results_Frf = table(data.Blockframe,Frf','VariableNames', {'Frame','Blockload
[N]'});

%% Export results to Excel file
filename = 'Results_Frf.xlsx';
writetable(Results_Frf,filename,'Sheet',1,'Range','A1');

%% calculate Strain
ODE_blocks_Frf;
progress = 0;
h = waitbar(progress,'Loading your data');
for i = 1:length(data.Shipframe)
P(i,:) = get_Pressure_Frf(data,Frf,i,W1Sol,W2Sol,S1Sol,S2Sol,M1Sol,M2Sol,V1Sol,
V2Sol);
progress = (i/length(data.Shipframe));
waitbar(progress,h);
end
xVec = -1:max(data.Shiplocation)/100:max(data.Shiplocation);

%% Calculate the reaction force and strain at each block frame location
Results_Strain = table(data.Blockframe,Frf',P(:,1),P(:,2),'VariableNames',
```

Figure B.5: Matlab code for complete analyse - Runfile page 1/2

8-6-21 15:23 C:\Users\bartj\On...\run_reactionforce.m 2 of 2

```
{'Frame','Blockload [N]','Strain SW [mm/mm]','Strain HW [mm/mm]'});  
  
%% Export results to Excel file  
filename = 'Results_Strain.xlsx'; %output filename which will be automatically  
updated in the folder  
writetable(Results_Strain,filename,'Sheet',1,'Range','A1');
```

Figure B.6: Matlab code for complete analyse - Runfile page 2/2

B.3.2. Input file for the model

8-6-21 15:23 C:\Users\bartj\OneDri...\get_Input_Frf.m 1 of 2

```
function [data] = get_Input(filename)

dlim = ',';

[fid,msg] = fopen(filename,'rt');

    if fid<0
        error('FOPEN could not read the file because:\n%s',msg)
    end

S = textscan(fid, [ repmat('%s',[1,25]), '%q' ] ...
            , 'Delimiter',dlim, 'EmptyValue',0 , 'Headerlines', 1);

fclose(fid);

data.Shipframe      = str2double(S{1}); %Input for ship framenummer [-]
data.Shiplocation  = str2double(S{2}); %Input for ship location [m]
data.Shipinertia   = str2double(S{5}); %Input for the inertia of the ship [m4]
data.Shipstiffness = str2double(S{6}); %Input for the stiffness of the ship
(210e9) [N/m2]

data.Blockframe    = str2double(S{7}); %Input for block frame number [-]
data.Blocklocation = str2double(S{8}); %Input for block location in [m]
data.Weight        = str2double(S{9}); %Input for weightdistribution (per segment)
[ton/m]
data.Load          = str2double(S{10}); %Input for loaddistribution (per segment)
[N/m]
data.Blockpresence = str2double(S{11}); %Check if a block is in the segment (if
yes, 1 otherwise 0)
data.Blocklength_sw = str2double(S{12});
data.Blockwidth     = str2double(S{13});
data.Blocklength_hw = str2double(S{14});

data.Contactarea   = str2double(S{15}); %Input for the block contact area with the
ship [m4]
data.Blockstiffness = str2double(S{16}); %Input for the stiffness of the block
[N/m2]
data.Ehw           = str2double(S{17}); %Input for the Young's modulus of the
hardwood [N/mm2]
data.Esw           = str2double(S{18}); %Input for the Young's modulus of the
softwood [N/mm2]
data.h_hw          = str2double(S{19}); %Input for the height of the hardwood
layer [mm]
data.h_sw          = str2double(S{20}); %Input for the height of the softwood
layer [mm]
data.stress_hw     = str2double(S{21}); %Input for the maximum allowable hardwood
pressure [N/mm2]
data.stress_sw     = str2double(S{22}); %Input for the maximum allowable softwood
pressure [N/mm2]
data.Effblocklength = str2double(S{23}); %Input for the effective block length [mm]
data.G             = str2double(S{24}); %Input G [N/m2]
data.Ashear        = str2double(S{25}); %Input Shear of ship [m2]
```

Figure B.7: Matlab code for complete analyse - Inputfile

B.3.3. Reaction force file for the model

8-6-21 15:24 C:\Users\bartj\OneDrive\Doc...\get_Frf.m 1 of 3

```
function [W,Wres,Frf] = get_Frf(data)

syms x
q = data.Load; % [N/m]
I = data.Shipinertia; % [m4]
E = data.Shipstiffness; % [N/m2]
k = data.Blockstiffness; % [N/m2]
x0 = data.Blocklocation; % [m]
x1 = data.Shiplocation; % [m]
L = max(data.Shiplocation); % [m]
K = 5/6; % [-]
G = data.G; % [N/m2]
Ashear = data.Ashear; % [m4]

syms('A',[length(data.Shipframe),1]);
syms('B',[length(data.Shipframe),1]);
syms('C',[length(data.Shipframe),1]);
syms('D',[length(data.Shipframe),1]);

vars = [0];
eqn = [0];

n = length(data.Shipframe);

for i = 1:n
%Timoshenko beam equations:
W(i) = (q(i)*x^4/24 + A(i)*x^3/6 + B(i)*x^2/2 + C(i)*x + D(i))/(E(i)*I(i))- 1/
(K*Ashear(i)*G(i))*((q(i)*x^2/2)+A(i)*x);
Phi(i) = (q(i)*x^3/6 + A(i)*x^2/2 + B(i)*x + C(i))/(E(i)*I(i));
M(i) = (-q(i)*x^2/2 - A(i)*x - B(i));
V(i) = -q(i)*x - A(i);

end

for i = 1:n
if i == 1
%Boundary condition at free-free end (i=1)
eqn_array(i,1) = subs(V(i),x,0) == 0;
eqn_array(i,2) = subs(M(i),x,0) == 0;
eqn_array(i,3) = 0;
eqn_array(i,4) = 0;

%Interface condition when there is no block and i=odd
else
if data.Blockpresence(i) == 0
%tot hier

V_cur = V(i);
V_prev = V(i-1);
M_cur = M(i);
M_prev = M(i-1);
Phi_cur = Phi(i);
Phi_prev = Phi(i-1);
```

Figure B.8: Matlab code for complete analyse - Reaction force file page 1/3

8-6-21 15:24 C:\Users\bartj\OneDrive\Doc...\get Frf.m 2 of 3

```

        W_cur = W(i);
        W_prev = W(i-1);

        eqn_array(i,1) = subs(V_cur,x,data.Blocklocation(i)) == subs(V_prev,x,data.
Blocklocation(i));
        eqn_array(i,2) = subs(M_cur,x,(data.Blocklocation(i))) == subs(M_prev,x,
(data.Blocklocation(i)));
        eqn_array(i,3) = subs(Phi_cur,x,(data.Blocklocation(i))) == subs(Phi_prev,x,
(data.Blocklocation(i)));
        eqn_array(i,4) = subs(W_cur,x,(data.Blocklocation(i))) == subs(W_prev,x,
(data.Blocklocation(i)));

        %Interface condition when there is a block and i=odd
        else

            V_cur = V(i);
            V_prev = V(i-1);
            M_cur = M(i);
            M_prev = M(i-1);
            Phi_cur = Phi(i);
            Phi_prev = Phi(i-1);
            W_cur = W(i);
            W_prev = W(i-1);

            eqn_array(i,1) = subs(V_cur,x,data.Blocklocation(i))-subs(V_prev,x,data.
Blocklocation(i)) == k(i)*subs(W_cur,x,(data.Blocklocation(i)));
            eqn_array(i,2) = subs(M_cur,x,(data.Blocklocation(i))) == subs(M_prev,x,
(data.Blocklocation(i)));
            eqn_array(i,3) = subs(Phi_cur,x,(data.Blocklocation(i))) == subs(Phi_prev,
x,(data.Blocklocation(i)));
            eqn_array(i,4) = subs(W_cur,x,(data.Blocklocation(i))) == subs(W_prev,x,
(data.Blocklocation(i)));

            end
        end

        int = [A(i); B(i); C(i); D(i)];
        vars = [vars; int];
    end
    %Boundary condition at free-free end (i=last one)
    eqn_array(n+1,1) = subs(V(length(data.Shipframe)),x,L) == 0;
    eqn_array(n+1,2) = subs(M(length(data.Shipframe)),x,L) == 0;
    eqn_array(n+1,3) = 0;
    eqn_array(n+1,4) = 0;

    for i = 1:length(eqn_array)

        inteq = [eqn_array(i,1); eqn_array(i,2); eqn_array(i,3); eqn_array(i,4)];
        eqn = [eqn; inteq];
    end

    vars(1) = [];
    eqn(1) = [];

```

Figure B.9: Matlab code for complete analyse - Reaction force file page 2/3

8-6-21 15:24 C:\Users\bartj\OneDrive\Doc...\get Frf.m 3 of 3

```

eqn(4) = [];
eqn(3) = [];
eqn(length(eqn)-1) = [];
eqn(length(eqn)) = [];

%Substitute the boundary and interface conditions into the Euler Bernoulli
equations
[Ma,F] = equationsToMatrix(eqn,vars);
%Solve the matrices to find the intergration constants
coefficients = linsolve(Ma,F);

subvars1 = reshape(vars,4,length(data.Shipframe));
subvars2 = reshape(coefficients,4,length(data.Shipframe));

%Substitute the coefficients in the Euler Bernoulli equation to get a final
%expression dependent of only x
for i = 1:length(data.Shipframe)
    W(i) = subs(W(i),[subvars1(1,i) subvars1(2,i) subvars1(3,i) subvars1(4,i)],
[subvars2(1,i) subvars2(2,i) subvars2(3,i) subvars2(4,i)]);
    M(i) = subs(M(i),[subvars1(1,i) subvars1(2,i) subvars1(3,i) subvars1(4,i)],
[subvars2(1,i) subvars2(2,i) subvars2(3,i) subvars2(4,i)]);
    Phi(i) = subs(Phi(i),[subvars1(1,i) subvars1(2,i) subvars1(3,i) subvars1(4,i)],
[subvars2(1,i) subvars2(2,i) subvars2(3,i) subvars2(4,i)]);
    V(i) = subs(V(i),[subvars1(1,i) subvars1(2,i) subvars1(3,i) subvars1(4,i)],
[subvars2(1,i) subvars2(2,i) subvars2(3,i) subvars2(4,i)]);
end

%Calculate the reaction force at each block location
for i = 1:length(data.Blocklocation)
    Wres(i) = double(subs(W(i),x,data.Blocklocation(i)));
    Frf(i) = double(subs(W(i),x,data.Blocklocation(i)))*k(i);
end

```

Figure B.10: Matlab code for complete analyse - Reaction force file page 3/3

B.3.4. Strain file for the model

8-6-21 15:25 C:\Users\bartj\One...\get_Pressure_Frf.m 1 of 2

```
function [P] = get_Pressure_Frf(data,Frf,i,W1Sol,W2Sol,S1Sol,S2Sol,M1Sol,M2Sol,V1Sol,V2Sol)

syms W1(x) W2(x) C1 C2 C3 C4 C5 C6 C7 C8

b1 = data.Blockwidth(i)*1e3;
h1 = data.h_sw(i); %[mm]
I1 = (b1*h1^3)/12; %[mm4]
% L1 = data.Blocklength(i)*1e3; %[mm]
L1 = data.Effblocklength(i); %[mm]
A1 = L1*b1; %[mm2]
E1 = data.Esw(i); %[MPa]
k1 = E1*b1/h1; %[N/mm2]
%Second material layer:
b2 = data.Blockwidth(i)*1e3; %[mm]
h2 = data.h_hw(i); %[mm]
I2 = (b2*h2^3)/12; %[mm4]
% L2 = data.Blocklength(i)*1e3; %[mm]
L2 = data.Effblocklength(i); %[mm]
A2 = L2*b2; %[mm2]
E2 = data.Ehw(i); %[MPa]
k2 = E2*b2/h2; %[N/mm2] A2*E2/b2

F = Frf(i); %[N]
% F = data.reactionforce(i);
q = F/L1; %[N/mm]

%Substitute constants in the total solution
W1(x) = subs(W1Sol);
S1(x) = subs(S1Sol);
M1(x) = subs(M1Sol);
V1(x) = subs(V1Sol);
W2(x) = subs(W2Sol);
S2(x) = subs(S2Sol);
M2(x) = subs(M2Sol);
V2(x) = subs(V2Sol);

%Set boundary conditions
%Free-Free
cond1 = M1(0) == 0;
cond2 = V1(0) == 0;
cond3 = M2(0) == 0;
cond4 = V2(0) == 0;
cond5 = M1(L1) == 0;
cond6 = V1(L1) == 0;
cond7 = M2(L2) == 0;
cond8 = V2(L2) == 0;

%Substitute solution of beam equation in the boundary conditions
syms C1 C2 C3 C4 C5 C6 C7 C8
sol = solve([cond1, cond2, cond3, cond4, cond5, cond6, cond7, cond8], [C1, C2, C3, C4, C5, C6, C7, C8]);
C1sol = double(sol.C1);
```

Figure B.11: Matlab code for complete analyse - Strain file page 1/2

8-6-21 15:25 C:\Users\bartj\One...\get Pressure Frf.m 2 of 2

```
C2sol = double(sol.C2);
C3sol = double(sol.C3);
C4sol = double(sol.C4);
C5sol = double(sol.C5);
C6sol = double(sol.C6);
C7sol = double(sol.C7);
C8sol = double(sol.C8);

C1 = C1sol; C2 = C2sol; C3 = C3sol; C4 = C4sol; C5 = C5sol; C6 = C6sol; C7 = C7sol; C8 = C8sol;
W1(x) = real(subs(W1));
W2(x) = real(subs(W2));
S1(x) = real(subs(S1));
S2(x) = real(subs(S2));
M1(x) = real(subs(M1));
M2(x) = real(subs(M2));
V1(x) = real(subs(V1));
V2(x) = real(subs(V2));

xvec1=0:L1/10:L1;
xvec2=0:L2/10:L2;

Displacement_Beam1 = double(subs(W1,x,xvec1));
Displacement_Beam2 = double(subs(W2,x,xvec2));
Pressure_Beam1 = ((max(Displacement_Beam1)*k1)/(b1));
Pressure_Beam2 = ((max(Displacement_Beam2)*k2)/(b2));
Strain_Beam1 = (max(Displacement_Beam1)/(h1+h2));
Strain_Beam2 = (max(Displacement_Beam2)/(h2));

% P = [Pressure_Beam1 Pressure_Beam2];
P = [Strain_Beam1 Strain_Beam2];
```

Figure B.12: Matlab code for complete analyse - Strain file page 2/2

B.3.5. ODE file for the model

8-6-21 15:26 C:\Users\bartj\OneDr...\ODE_blocks Frf.m 1 of 1

```
syms W1(x) W2(x) E1 E2 I1 I2 k1 k2 q W1_part W2_part C1 C2 C3 C4 C5 C6 C7 C8 L1 L2
ode1 = E1*I1*diff(W1,x,x,x,x)+k1*(W1-W2) == 0;
ode2 = E2*I2*diff(W2,x,x,x,x)-k1*(W1-W2)+k2*W2 == 0;
odes = [ode1; ode2];
S = dsolve(odes);

W1_part = ((q * (k1 + k2)) / (k1 * k2));
W2_part = (q/k2);

W1Sol(x) = S.W1+W1_part;
S1Sol(x) = diff(S.W1,x);
M1Sol(x) = -E1*I1*diff(S.W1,x,x);
V1Sol(x) = -E1*I1*diff(S.W1,x,x,x);
W2Sol(x) = S.W2+W2_part;
S2Sol(x) = diff(S.W2,x);
M2Sol(x) = -E2*I2*diff(S.W2,x,x);
V2Sol(x) = -E2*I2*diff(S.W2,x,x,x);
```

Figure B.13: Matlab code for complete analyse - ODE file

C

Validation

Table C.1: Weight distribution per frame and location for the patrol ship

Frame [-]	x [m]	Weight [ton/m]	Frame [-]	x [m]	Weight [ton/m]
-1	-0.6	0.553	44	26.4	41.405
0	0	19.486	45	27	34.73
1	0.6	19.265	46	27.6	41.183
2	1.2	22.577	47	28.2	43.717
3	1.8	25.425	48	28.8	46.442
4	2.4	26.703	49	29.4	40.947
5	3	27.981	50	30	44.875
6	3.6	29.321	51	30.6	48.122
7	4.2	31.282	52	31.2	48.838
8	4.8	30.93	53	31.8	49.554
9	5.4	23.867	54	32.4	51.613
10	6	24.541	55	33	60.52
11	6.6	25.216	56	33.6	66.833
12	7.2	30.069	57	34.2	64.948
13	7.8	30.871	58	34.8	63.05
14	8.4	31.682	59	35.4	65.406
15	9	15.655	60	36	72.261
16	9.6	18.242	61	36.6	72.337
17	10.2	19.855	62	37.2	67.488
18	10.8	21.327	63	37.8	61.715
19	11.4	22.8	64	38.4	56.246
20	12	24.305	65	39	55.932
21	12.6	25.434	66	39.6	55.66
22	13.2	26.995	67	40.2	55.176
23	13.8	31.683	68	40.8	54.416
24	14.4	32.915	69	41.4	54.432
25	15	32.068	70	42	54.694
26	15.6	34.171	71	42.6	52.76
27	16.2	32.068	72	43.2	53.302
28	16.8	30.141	73	43.8	53.597
29	17.4	31.212	74	44.4	85.696
30	18	23.312	75	45	88.71
31	18.6	32.282	76	45.6	93.062
32	19.2	35.243	77	46.2	59.741
33	19.8	36.536	78	46.8	54.252
34	20.4	34.847	79	47.4	47.278
35	21	31.606	80	48	46.32
36	21.6	32.295	81	48.6	53.757
37	22.2	33.899	82	49.2	61.682
38	22.8	34.422	83	49.8	61.62
39	23.4	34.705	84	50.4	60.324
40	24	35.702	85	51	58.828
41	24.6	35.034	86	51.6	58.442
42	25.2	37.326	87	52.2	57.306
43	25.8	39.053	88	52.8	56.828

Table C.2: Weight distribution per frame and location for the patrol ship

Frame [-]	x [m]	Weight [ton/m]	Frame [-]	x [m]	Weight [ton/m]
89	53.4	56.35	134	80.4	21.145
90	54	55.872	135	81	20.583
91	54.6	49.732	136	81.6	20.013
92	55.2	47.213	137	82.2	19.451
93	55.8	42.204	138	82.8	18.889
94	56.4	41.822	139	83.4	18.328
95	57	41.44	140	84	17.766
96	57.6	46.624	141	84.6	17.205
97	58.2	54.042	142	85.2	12.225
98	58.8	53.41	143	85.8	11.861
99	59.4	52.778	144	86.4	13.931
100	60	52.146	145	87	16.002
101	60.6	51.096	146	87.6	16.191
102	61.2	50.515	147	88.2	16.045
103	61.8	49.935	148	88.8	16.65
104	62.4	48.952	149	89.4	17.884
105	63	48.505	150	90	19.119
106	63.6	48.059	151	90.6	12.632
107	64.2	47.612	152	91.2	12.564
108	64.8	47.165	153	91.8	12.084
109	65.4	42.556	154	92.4	12.021
110	66	42.045	155	93	11.959
111	66.6	45.446	156	93.6	22.194
112	67.2	31.278	157	94.2	21.511
113	67.8	30.746	158	94.8	20.827
114	68.4	30.213	159	95.4	20.143
115	69	36.493	160	96	19.716
116	69.6	35.428	161	96.6	18.716
117	70.2	33.848	162	97.2	17.716
118	70.8	26.857	163	97.8	16.716
119	71.4	38.059	164	98.4	10.387
120	72	37.421	165	99	10.008
121	72.6	36.736	166	99.6	9.629
122	73.2	36.1	167	100.2	8.173
123	73.8	35.464	168	100.8	7.797
124	74.4	34.828	169	101.4	7.421
125	75	34.192	170	102	7.045
126	75.6	36.198	171	102.6	3.615
127	76.2	22.184	172	103.2	3.255
128	76.8	21.79	173	103.8	2.895
129	77.4	21.396	174	104.4	2.535
130	78	21.002	175	105	2.176
131	78.6	20.608	176	105.6	0.046
132	79.2	20.416	177	106.2	0
133	79.8	20.022			

Table C.3: Input values for deflection calculation of dock block material layers

Block Frame [–]	F_r [N]	l_{sw}, l_{hw} [mm]	b_{sw}, b_{hw} [mm]	h_{sw} [mm]	h_{hw} [mm]	A_{eff} [mm ²]	E_{sw} [MPa]	E_{hw} [MPa]
24.5	561300	800	300	50	200	180000	10	600
25.5	549580	800	300	50	200	180000	10	600
26.5	539190	800	300	50	200	180000	10	600
27.5	526530	800	300	50	200	180000	10	600
28.5	515430	800	300	50	200	180000	10	600
29.5	504390	800	300	50	200	180000	10	600
30.5	492490	800	300	50	200	180000	10	600
31.5	478390	800	300	50	200	180000	10	600
32.5	463840	800	300	50	200	180000	10	600
33.5	447550	800	300	50	200	180000	10	600
34.5	429480	800	300	50	200	180000	10	600
35.5	410830	800	300	50	200	180000	10	600
36.5	392960	800	300	50	200	180000	10	600
37.5	380020	800	300	50	200	180000	10	600
38.5	367200	800	300	50	200	180000	10	600
39.5	358030	800	300	50	200	180000	10	600
40.5	358050	800	300	50	200	180000	10	600
41.5	364490	800	300	50	200	180000	10	600
42.5	375030	800	300	50	200	180000	10	600
43.5	388820	800	300	50	200	180000	10	600
44.5	396610	800	300	50	200	180000	10	600
45.5	390400	800	300	50	200	180000	10	600
46.5	375210	800	300	50	200	180000	10	600
47.5	357950	800	300	50	200	180000	10	600
48.5	339340	800	300	50	200	180000	10	600
49.5	326430	800	300	50	200	180000	10	600
50.5	310620	800	300	50	200	180000	10	600
51.5	311690	800	300	50	200	180000	10	600
52.5	316150	800	300	50	200	180000	10	600
53.5	330570	800	300	50	200	180000	10	600
54.5	352090	800	300	50	200	180000	10	600
55.5	373720	800	300	50	200	180000	10	600
56.5	391470	800	300	50	200	180000	10	600
57.5	407560	800	300	50	200	180000	10	600
58.5	425230	800	300	50	200	180000	10	600
59.5	440840	800	300	50	200	180000	10	600
60.5	278750	800	300	50	200	180000	10	600
61.5	274650	800	300	50	200	180000	10	600
62.5	269150	800	300	50	200	180000	10	600
63.5	263060	800	300	50	200	180000	10	600
64.5	256070	800	300	50	200	180000	10	600
65.5	250900	800	300	50	200	180000	10	600
66.5	247630	800	300	50	200	180000	10	600
67.5	246330	800	300	50	200	180000	10	600
68.5	247610	800	300	50	200	180000	10	600
69.5	246920	800	300	50	200	180000	10	600
70.5	250150	800	300	50	200	180000	10	600
71.5	250500	800	300	50	200	180000	10	600
72.5	253350	800	300	50	200	180000	10	600
73.5	257320	800	300	50	200	180000	10	600
74.5	261800	800	300	50	200	180000	10	600

Continued on next page

Table C.3 – continued from previous page

Block Frame [–]	F_r [N]	l_{sw}, l_{hw} [mm]	b_{sw}, b_{hw} [mm]	h_{sw} [mm]	h_{hw} [mm]	A_{eff} [mm ²]	E_{sw} [MPa]	E_{hw} [MPa]
75.5	263920	800	300	50	200	180000	10	600
76.5	266090	800	300	50	200	180000	10	600
77.5	274690	800	300	50	200	180000	10	600
78.5	281500	800	300	50	200	180000	10	600
79.5	293670	800	300	50	200	180000	10	600
80.5	306000	800	300	50	200	180000	10	600
81.5	302460	800	300	50	200	180000	10	600
82.5	285130	800	300	50	200	180000	10	600
83.5	270260	800	300	50	200	180000	10	600
84.5	395150	800	300	50	200	183760	10	600
85.83	387220	800	300	50	200	193760	10	600
87.17	386220	800	300	50	200	203760	10	600
88.5	353410	800	300	50	200	210000	10	600
89.83	369030	800	300	50	200	210000	10	600
91.17	388130	800	300	50	200	210000	10	600
92.5	380870	800	300	50	200	210000	10	600
93.83	435200	800	300	50	200	210000	10	600
96.5	434590	800	300	50	200	210000	10	600
97.83	424850	800	300	50	200	210000	10	600
99.17	398090	800	300	50	200	210000	10	600
100.5	346110	800	300	50	200	210000	10	600
101.83	348470	800	300	50	200	210000	10	600
103.17	347780	800	300	50	200	210000	10	600
104.5	324820	800	300	50	200	210000	10	600
105.83	354390	800	300	50	200	210000	10	600
107.17	375380	800	300	50	200	210000	10	600
108.5	352980	800	300	50	200	210000	10	600
111.5	384890	800	300	50	200	210000	10	600
112.83	397080	800	300	50	200	209960	10	600
114.17	371520	800	300	50	200	209860	10	600
115.5	312400	800	300	50	200	209700	10	600
116.83	329580	800	300	50	200	209420	10	600
118.17	311590	800	300	50	200	209000	10	600
119.5	281060	800	300	50	200	208400	10	600
120.83	297410	800	300	50	200	207620	10	600
122.17	294540	800	300	50	200	206600	10	600
123.5	274780	800	300	50	200	205320	10	600
124.83	297440	800	300	50	200	203720	10	600
126.17	305250	800	300	50	200	201780	10	600
127.5	272940	800	300	50	200	199440	10	600
128.83	276210	800	300	50	200	196720	10	600
130.17	264060	800	300	50	200	193600	10	600
131.5	236680	800	300	50	200	190120	10	600
132.83	239300	800	300	50	200	186240	10	600
134.17	228960	800	300	50	200	181980	10	600
135.5	208930	800	300	50	200	177320	10	600
136.83	211060	800	300	50	200	172280	10	600
138.17	203810	800	300	50	200	166840	10	600
139.5	187960	800	300	50	200	160980	10	600
140.83	188150	800	300	50	200	154660	10	600
142.17	182140	800	300	50	200	147880	10	600
143.5	172960	800	300	50	200	140620	10	600

Continued on next page

Table C.3 – continued from previous page

Block Frame [-]	F_r [N]	l_{sw}, l_{hw} [mm]	b_{sw}, b_{hw} [mm]	h_{sw} [mm]	h_{hw} [mm]	A_{eff} [mm ²]	E_{sw} [MPa]	E_{hw} [MPa]
144.83	169190	800	300	50	200	132880	10	600
146.17	158830	800	300	50	200	124720	10	600
147.5	148840	800	300	50	200	116180	10	600
148.83	142150	800	300	50	200	107420	10	600
150.17	159950	800	300	50	200	240000	10	600
151.5	152580	800	300	50	200	240000	10	600
152.83	147110	800	300	50	200	240000	10	600
154.17	141780	800	300	50	200	240000	10	600
155.5	134820	800	300	50	200	240000	10	600
156.83	129120	800	300	50	200	240000	10	600
158.17	122700	800	300	50	200	240000	10	600
159.5	110510	800	300	50	200	240000	10	600
160.83	95552	800	300	50	200	240000	10	600
162.17	78648	800	300	50	200	240000	10	600

D

Test results

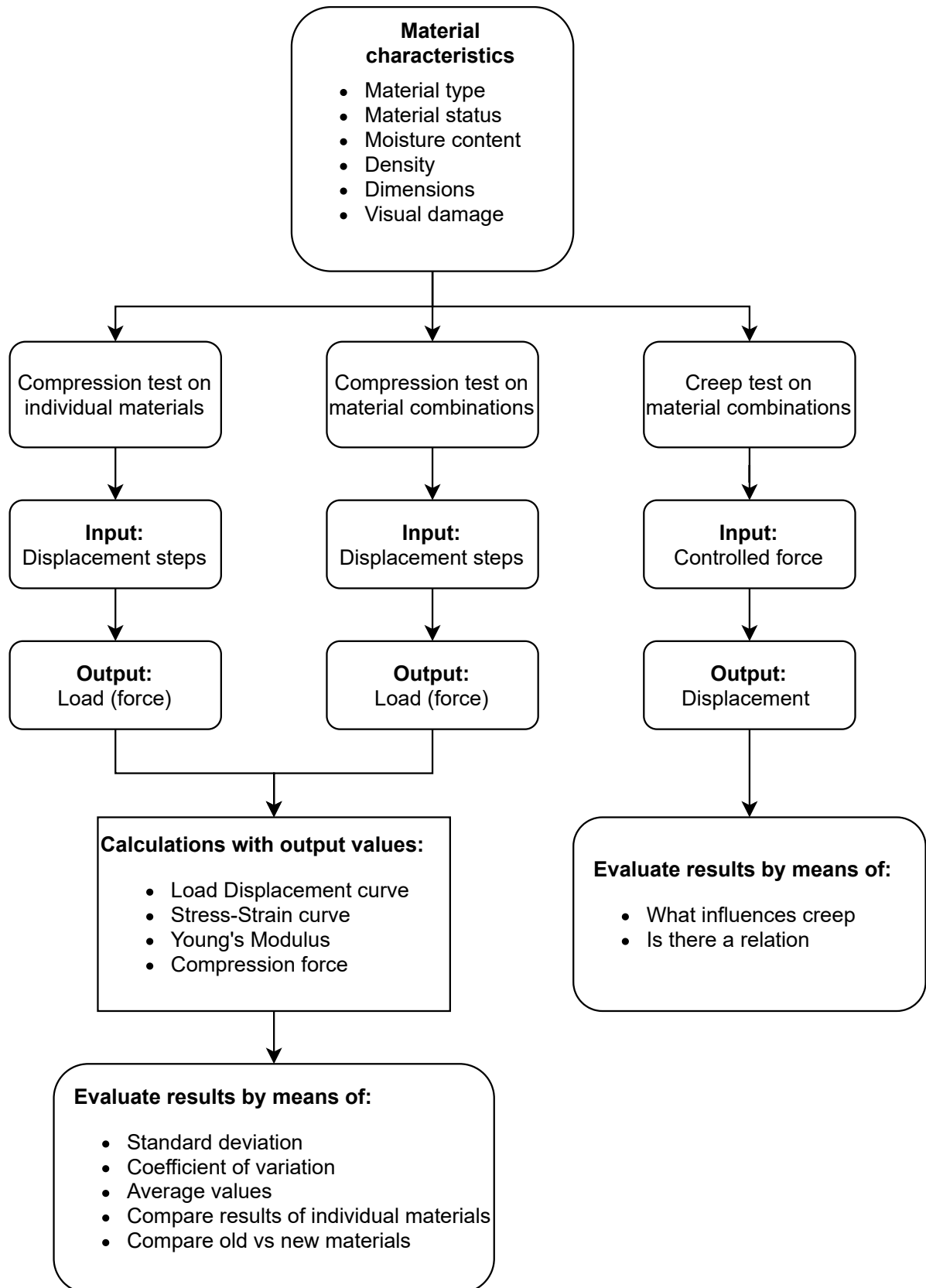


Figure D.1: Flowchart for test plan








Test Name	Dimensions (l x b x h) [mm]	Number of tests	Sketch
AOO Amels Oak Old Hardwood	200 x 200 x 200	4	
SON Schiedam Oak New Hardwood	200 x 200 x 75	1	
RAN Ritthem Azobe New Hardwood	200 x 200 x 200	3	
ALN Amels LVL New Softwood	200 x 200 x 40	8	
ALO Amels LVL Old Softwood	200 x 200 x 40	6	
RPN Ritthem Pine New Softwood	200 x 200 x 70	5	
RSN Ritthem Spruce New Softwood	200 x 200 x 50	5	
SSN Schiedam Spruce New Softwood	200 x 200 x 50	6	

Figure D.2: Test overview individual material tests






Test Name	Dimensions (l x b x h) [mm]	Number of tests	Sketch
AOO - ALN Amels Oak Old Amels LVL New	200 x 200 x 240	1	
AOO - ALO Amels Oak Old Amels LVL Old	200 x 200 x 240	1	
RAN - RSN Ritthem Azobe New Ritthem Spruce New	200 x 200 x 250	2	
RAN - RPN Ritthem Azobe New Ritthem Pine New	200 x 200 x 270	2	
SON - SSN Schiedam Oak New Schiedam Spruce New	200 x 200 x 125	2	

Figure D.3: Test overview material combination tests





Test Name	Dimensions (l x b x h) [mm]	Duration of test [days]	Applied Load [kN]	Sketch
1: AOO - ALN 2: AOO - ALN Amels Oak Old Amels LVL New	200 x 200 x 240 200 x 200 x 240	1 5	70 150	
1: AOO - ALO 2: AOO - ALO 3: AOO - ALO Amels Oak Old Amels LVL Old	200 x 200 x 240 200 x 200 x 240 200 x 200 x 240	1 1 5	70 250 150	
RAN - RSN Ritthem Azobe New Ritthem Spruce New	200 x 200 x 250	1	130	
SON - SSN Schiedam Oak New Schiedam Spruce New	200 x 200 x 125	1	300	

Figure D.4: Test overview creep tests

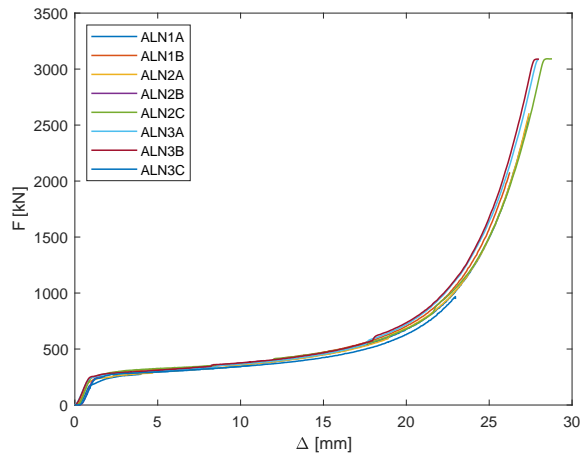


Figure D.5: ALN force displacement graph

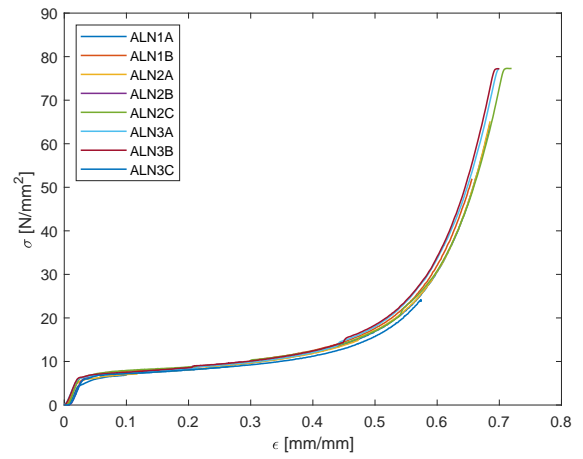


Figure D.6: ALN stress strain graph

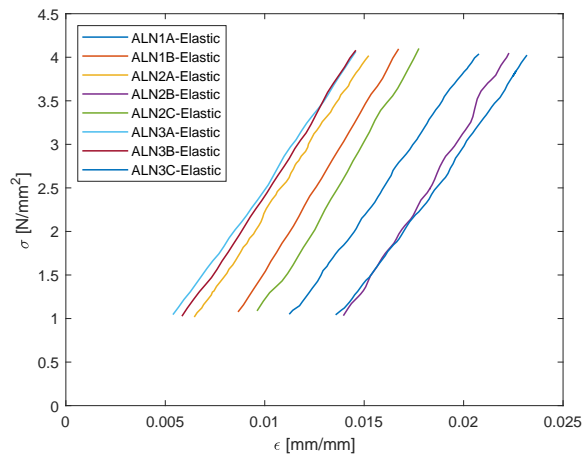


Figure D.7: ALN stress strain graph for elastic range

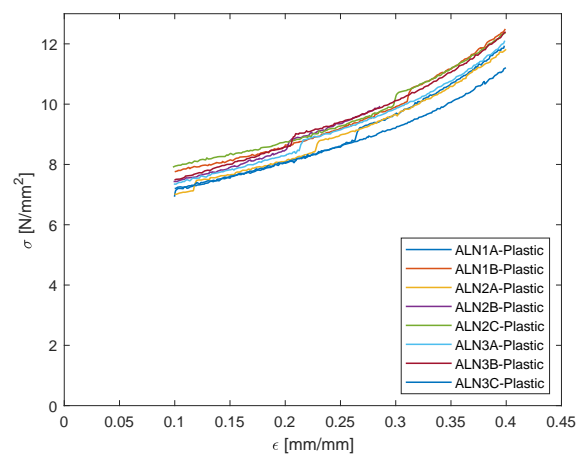


Figure D.8: ALN stress strain graph for plastic range

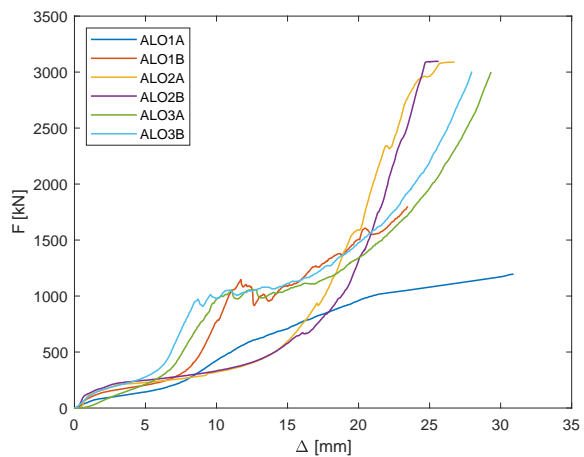


Figure D.9: ALO force displacement graph

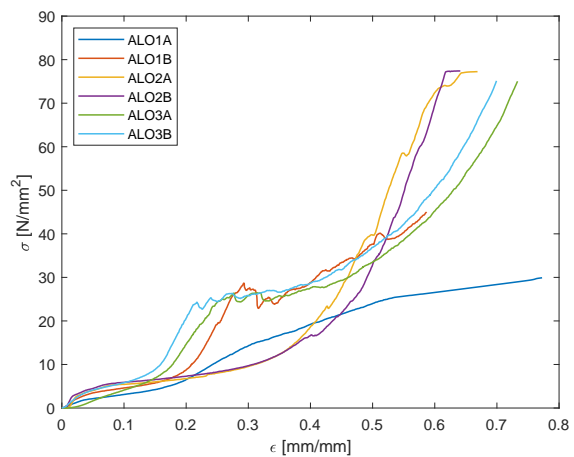


Figure D.10: ALO stress strain graph

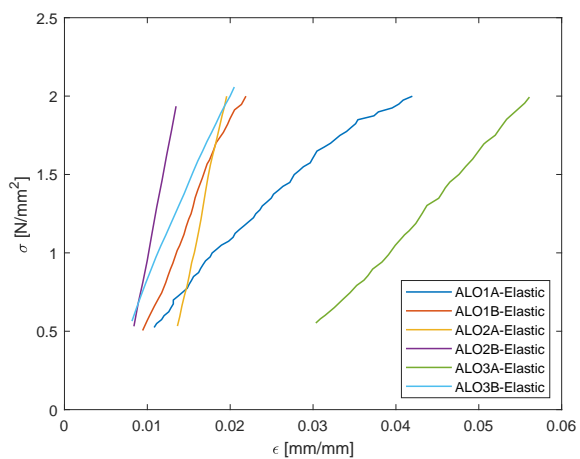


Figure D.11: ALO stress strain graph for elastic range

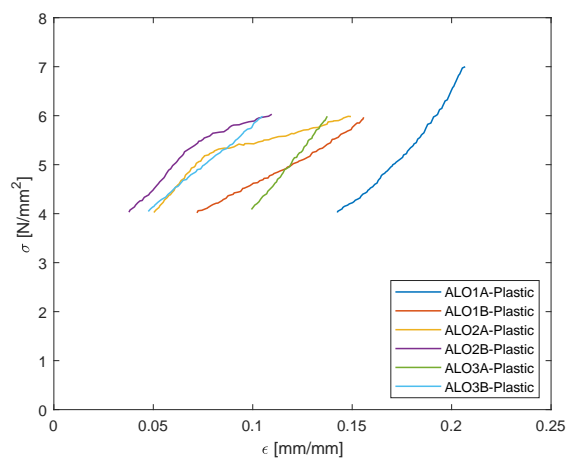


Figure D.12: ALO stress strain graph for plastic range

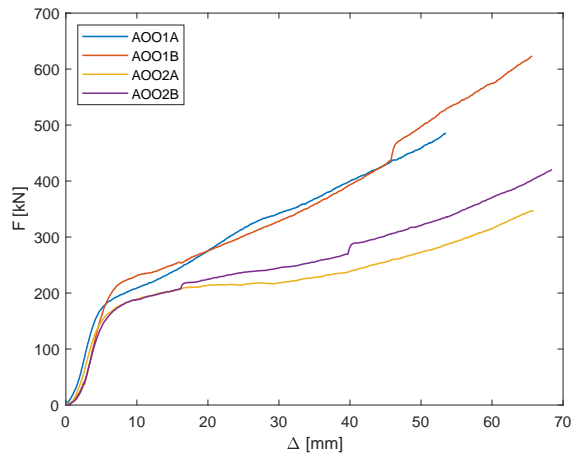


Figure D.13: AOO force displacement graph

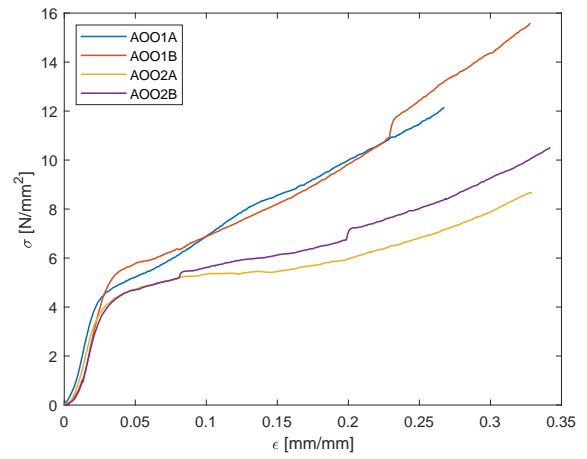


Figure D.14: AOO stress strain graph

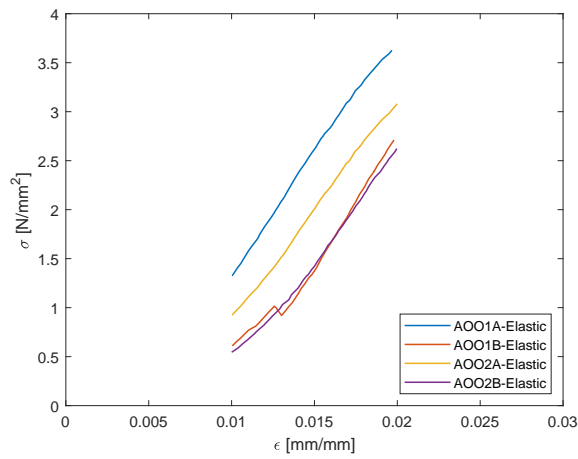


Figure D.15: AOO stress strain graph for elastic range

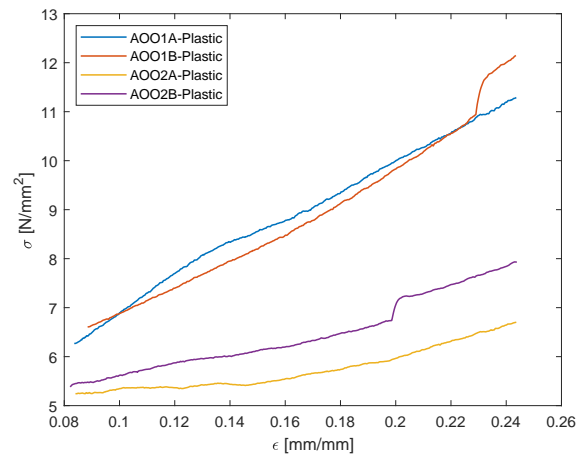


Figure D.16: AOO stress strain graph for plastic range

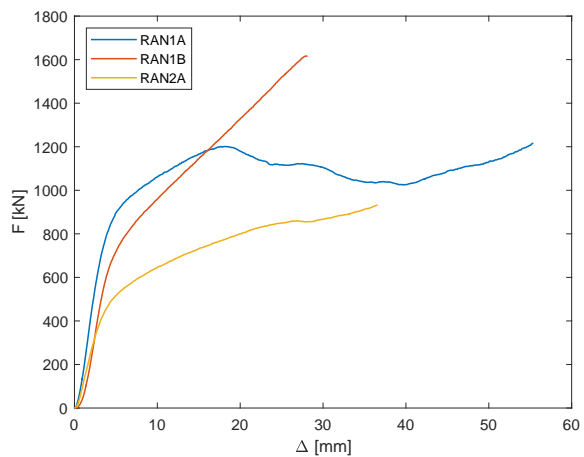


Figure D.17: RAN force displacement graph

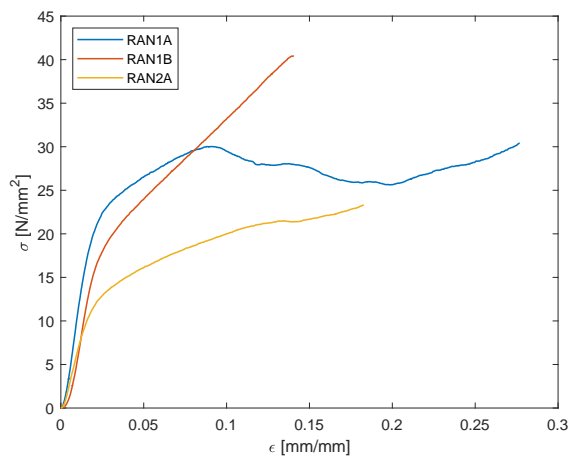


Figure D.18: RAN stress strain graph

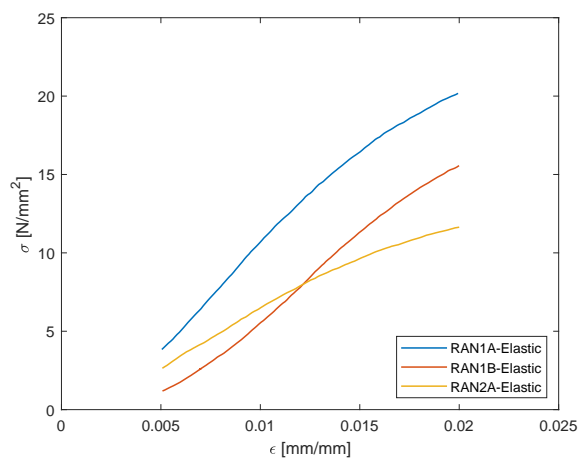


Figure D.19: RAN stress strain graph for elastic range

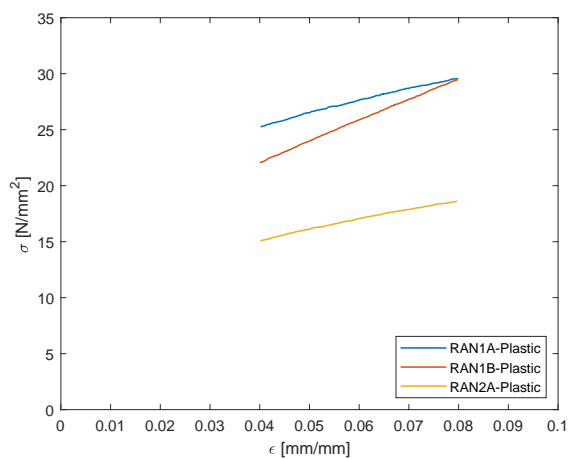


Figure D.20: RAN stress strain graph for plastic range

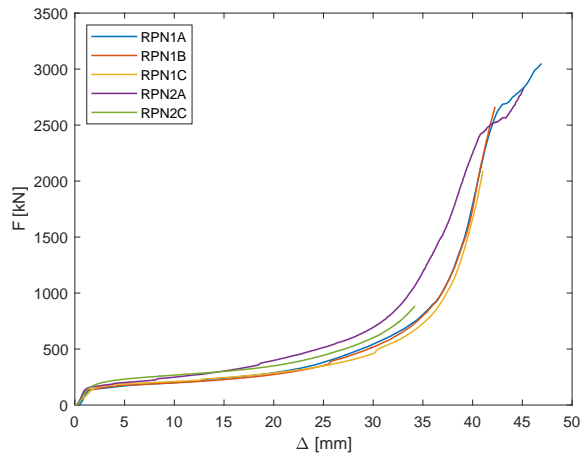


Figure D.21: RPN force displacement graph

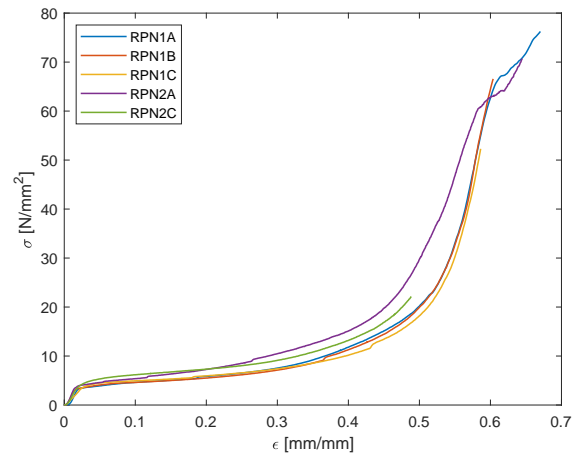


Figure D.22: RPN stress strain graph

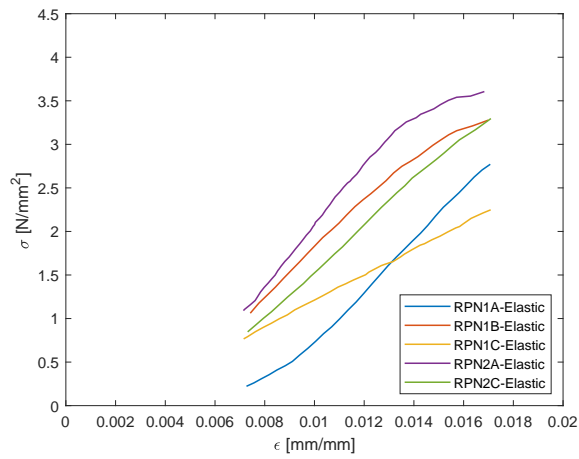


Figure D.23: RPN stress strain graph for elastic range

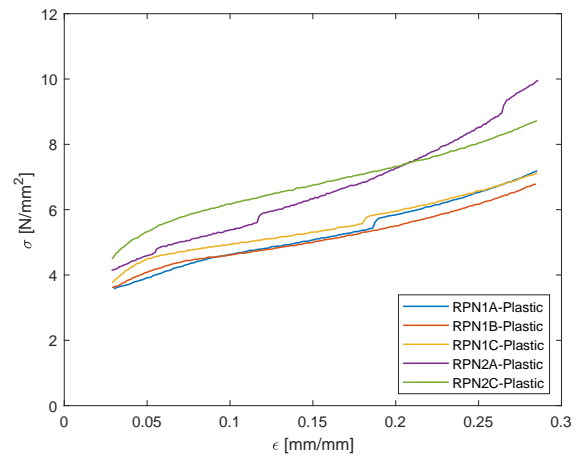


Figure D.24: RPN stress strain graph for plastic range

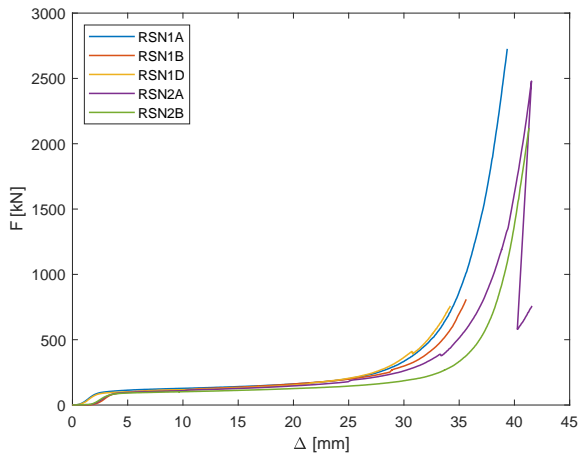


Figure D.25: RSN force displacement graph

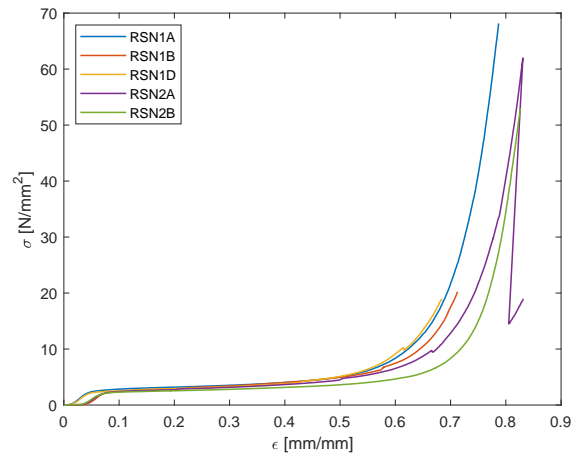


Figure D.26: RSN stress strain graph

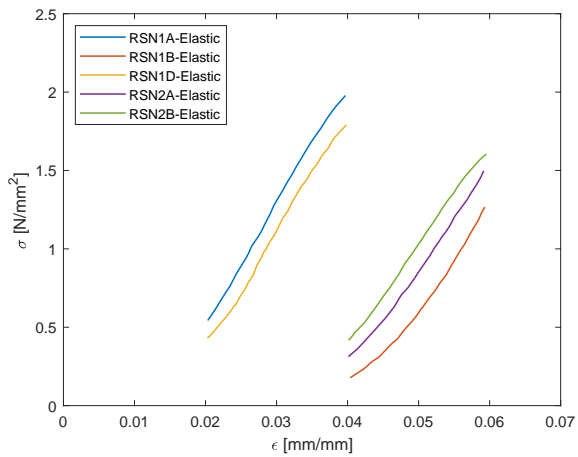


Figure D.27: RSN stress strain graph for elastic range

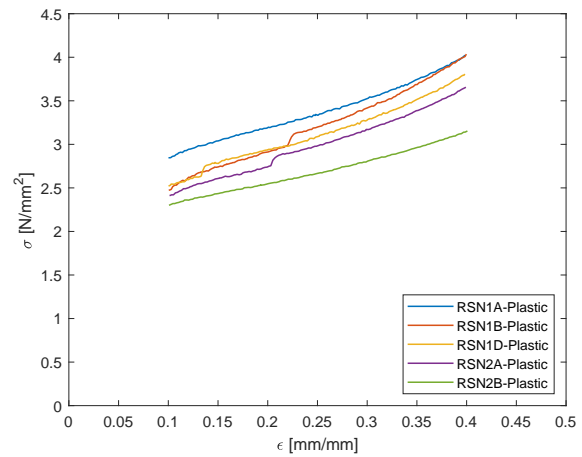


Figure D.28: RSN stress strain graph for plastic range

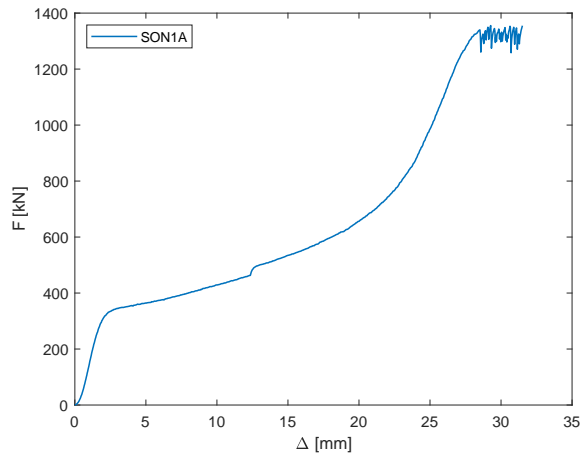


Figure D.29: SON force displacement graph

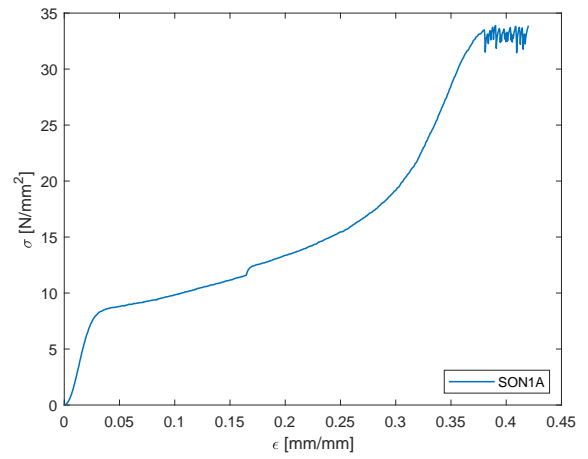


Figure D.30: SON stress strain graph

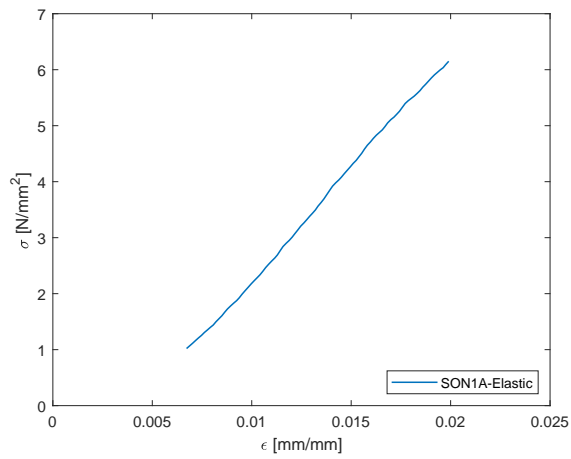


Figure D.31: SON stress strain graph for elastic range

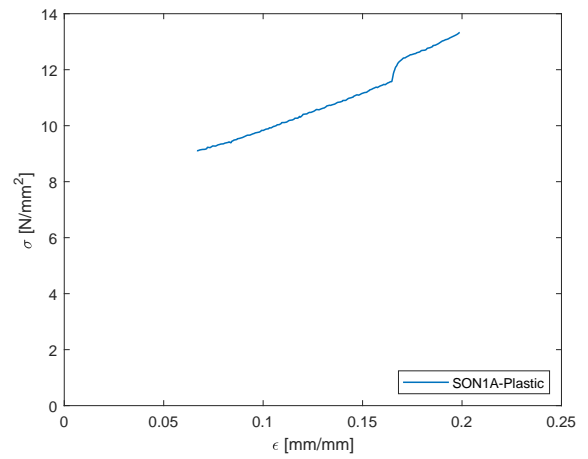


Figure D.32: SON stress strain graph for plastic range

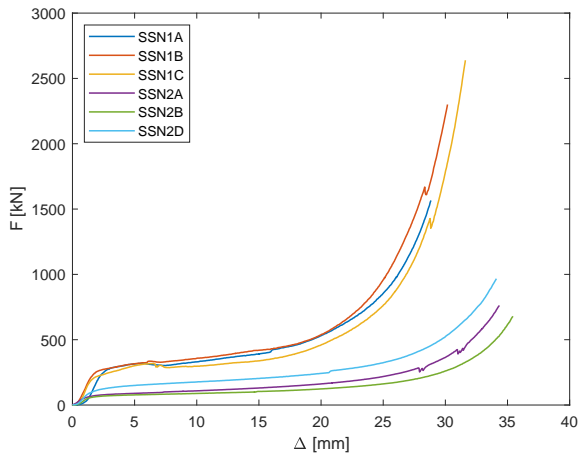


Figure D.33: SSN force displacement graph

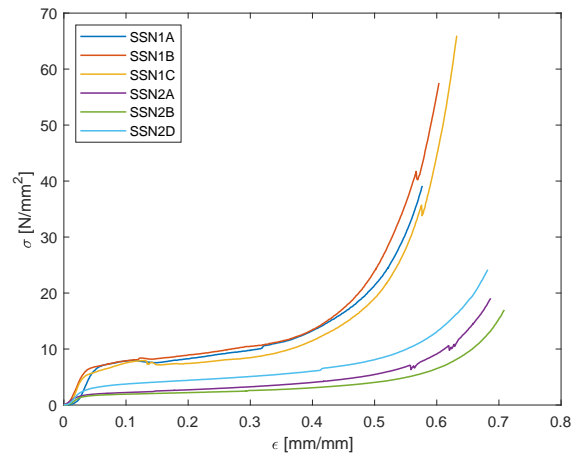


Figure D.34: SSN stress strain graph

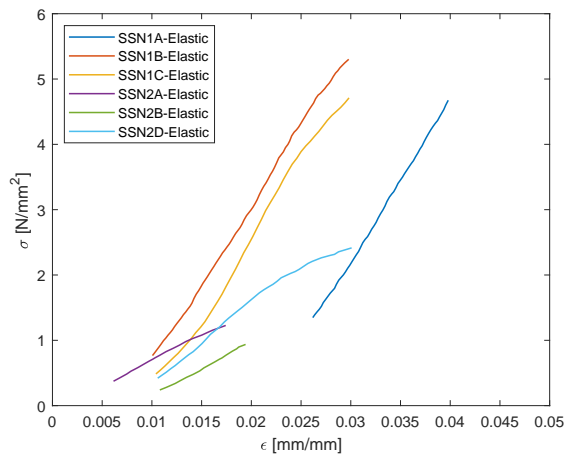


Figure D.35: SSN stress strain graph for elastic range

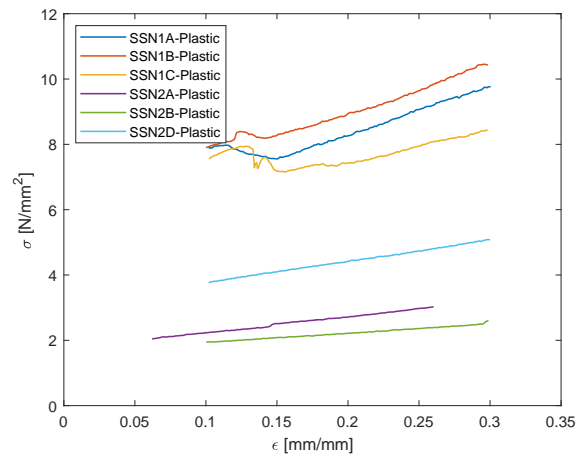


Figure D.36: SSN stress strain graph for plastic range



Figure D.37: Compression of Azobe (RAN)

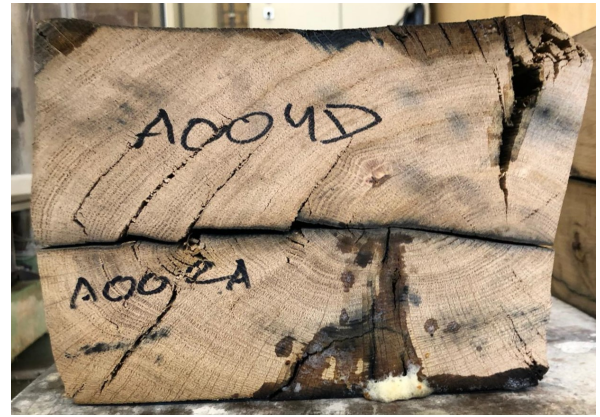


Figure D.38: Compression of Oak (A00)

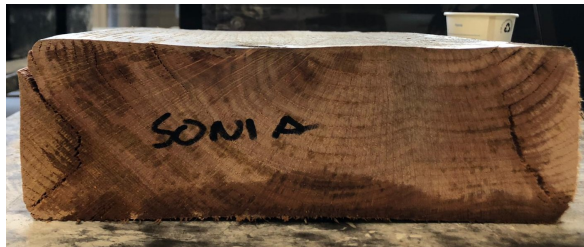


Figure D.39: Compression of Oak (SON)



Figure D.40: Compression of Pine (RPN)



Figure D.41: Compression of LVL (ALN ALO)



Figure D.42: Compression of Spruce (RSN)



Figure D.43: Compression of Spruce (SSN1)



Figure D.44: Compression of Spruce (SSN2)

Table D.1: Characteristic values for individual materials

Material	Name	$MC[\%]$	$\rho[kg/m^3]$	$\rho_{12\%}[kg/m^3]$	$E_{\perp lin}[MPa]$	$E_{\perp nonlin}[MPa]$
Azobe	RAN1A	20.9	438.2	399.2	1129.9	109.0
Azobe	RAN1B	20.9	1140.1	1038.5	1041.5	186.3
Azobe	RAN2A	25.6	1151.0	994.0	620.1	88.9
Oak	AOO1A	19.0	781.5	726.7	246.1	30.4
Oak	AOO1B	19.0	763.2	709.7	223.5	32.4
Oak	AOO2A	22.3	695.6	623.7	226.5	8.3
Oak	AOO2B	22.3	744.4	667.4	217.8	14.9
Oak	SON1A	36.9	412.2	309.6	404.4	32.5
Pine	RPN1A	26.5	1024.4	876.1	276.5	13.1
Pine	RPN1B	26.5	672.1	574.9	243.8	10.7
Pine	RPN1C	26.5	660.7	565.1	147.9	11.0
Pine	RPN2A	25.2	655.7	568.8	297.7	20.7
Pine	RPN2C	25.2	719.3	624.0	258.7	13.8
LVL	ALN1A	13.8	670.7	658.6	325.3	16.0
LVL	ALN1B	13.8	508.8	499.6	376.8	15.7
LVL	ALN2A	14.4	508.1	495.8	350.9	15.4
LVL	ALN2B	14.4	526.3	513.4	367.1	14.1
LVL	ALN2C	14.4	526.9	514.0	379.0	14.7
LVL	ALN3A	14.3	515.0	503.0	330.5	15.4
LVL	ALN3B	14.3	520.0	507.9	353.9	15.9
LVL	ALN3E	14.3	520.6	508.5	316.2	13.0
LVL	ALO1A	38.0	516.3	382.1	49.5	49.7
LVL	ALO1B	38.0	991.9	734.1	127.5	22.3
LVL	ALO2A	52.2	1046.9	625.5	252.5	17.5
LVL	ALO2B	52.2	759.1	453.6	277.1	29.3
LVL	ALO3A	61.0	749.4	382.3	57.5	47.0
LVL	ALO3B	61.0	1058.8	540.1	120.0	33.0
Spruce	RSN1A	27.2	733.6	622.0	77.0	3.6
Spruce	RSN1B	27.2	511.8	433.9	58.2	4.9
Spruce	RSN1D	27.2	495.6	420.2	74.6	3.9
Spruce	RSN2A	24.3	481.4	422.3	63.8	4.0
Spruce	RSN2B	24.3	481.4	422.3	64.3	2.7
Spruce	SSN1A	15.2	1158.8	1121.6	246.5	11.4
Spruce	SSN1B	15.2	637.8	617.3	242.0	12.8
Spruce	SSN1C	15.2	655.6	634.6	238.5	3.9
Spruce	SSN2A	17.2	652.6	618.6	77.0	4.9
Spruce	SSN2B	17.2	400.0	379.2	83.7	2.9
Spruce	SSN2D	17.2	391.3	371.0	110.5	6.5

Table D.2: Yield point values for individual materials

Material	Name	σ_y [MPa]	ϵ_y [-]	F_y [kN]	Δ_y [mm]
Azobe	RAN1A	19.699	0.020	787.968	4.062
Azobe	RAN1B	15.162	0.021	606.499	4.201
Azobe	RAN2A	11.766	0.021	470.659	4.168
Oak	AOO1A	3.505	0.021	140.211	4.154
Oak	AOO1B	4.470	0.030	178.808	6.047
Oak	AOO2A	3.039	0.022	121.556	4.315
Oak	AOO2B	3.078	0.024	123.136	4.865
Oak	SON1A	6.924	0.024	276.972	1.771
Pine	RPN1A	3.304	0.021	132.151	1.474
Pine	RPN1B	3.261	0.018	130.435	1.257
Pine	RPN1C	3.877	0.030	155.099	2.105
Pine	RPN2A	3.686	0.017	147.447	1.224
Pine	RPN2C	3.814	0.021	152.575	1.455
LVL	ALN1A	3.519	0.021	140.757	0.842
LVL	ALN1B	4.132	0.019	165.274	0.755
LVL	ALN2A	4.340	0.018	173.593	0.723
LVL	ALN2B	4.439	0.025	177.556	1.017
LVL	ALN2C	4.882	0.022	195.275	0.876
LVL	ALN3A	5.102	0.020	204.099	0.792
LVL	ALN3B	5.263	0.020	210.518	0.800
LVL	ALN3E	4.429	0.027	177.176	1.064
LVL	ALO1A	1.833	0.037	73.311	1.500
LVL	ALO1B	1.931	0.023	77.257	0.907
LVL	ALO2A	2.480	0.023	99.189	0.935
LVL	ALO2B	2.694	0.018	107.750	0.729
LVL	ALO3A	2.964	0.075	118.552	3.001
LVL	ALO3B	2.923	0.029	116.918	1.177
Spruce	RSN1A	1.928	0.040	77.109	2.017
Spruce	RSN1B	2.347	0.081	93.875	4.066
Spruce	RSN1D	1.771	0.041	70.851	2.044
Spruce	RSN2A	1.630	0.064	65.199	3.194
Spruce	RSN2B	1.419	0.058	56.762	2.903
Spruce	SSN1A	5.079	0.044	203.170	2.181
Spruce	SSN1B	5.046	0.030	201.845	1.509
Spruce	SSN1C	3.869	0.028	154.766	1.376
Spruce	SSN2A	2.845	0.040	113.786	1.996
Spruce	SSN2B	1.058	0.023	42.305	1.144
Spruce	SSN2D	2.068	0.027	82.709	1.343

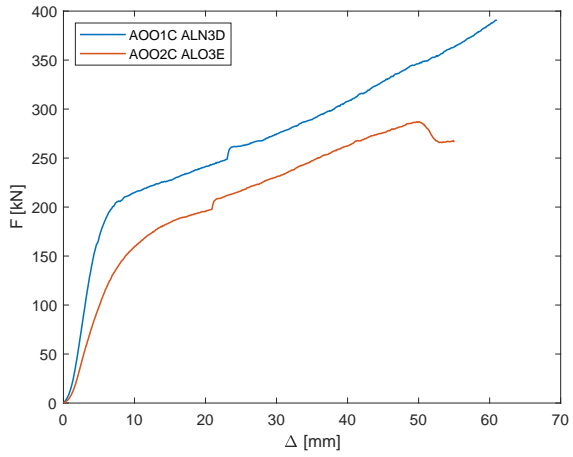


Figure D.45: AOOALN and AOOALO force displacement graph

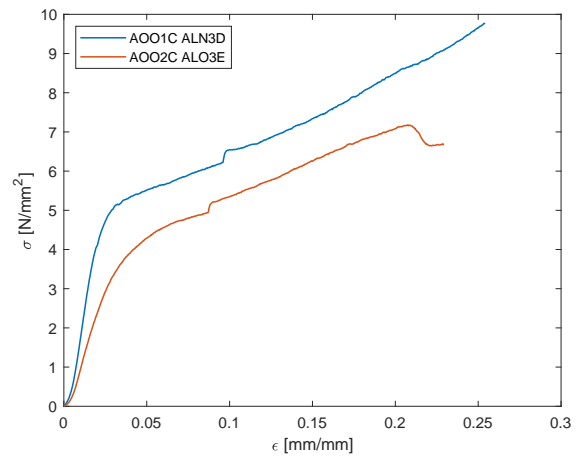


Figure D.46: AOOALN and AOOALO stress strain graph

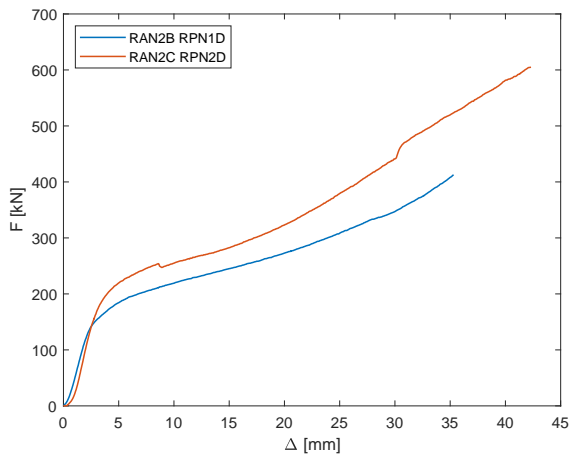


Figure D.47: RANRPN force displacement graph

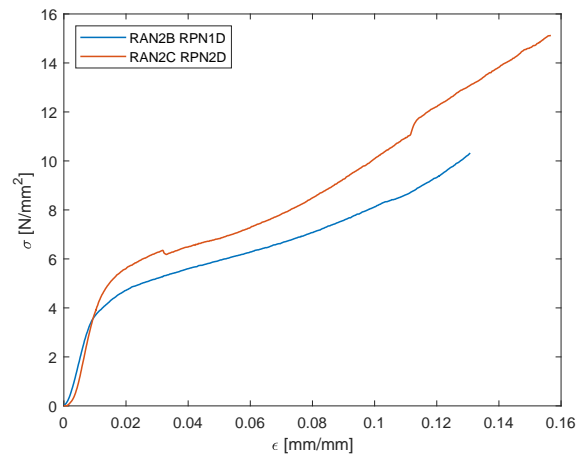


Figure D.48: RANRPN stress strain graph

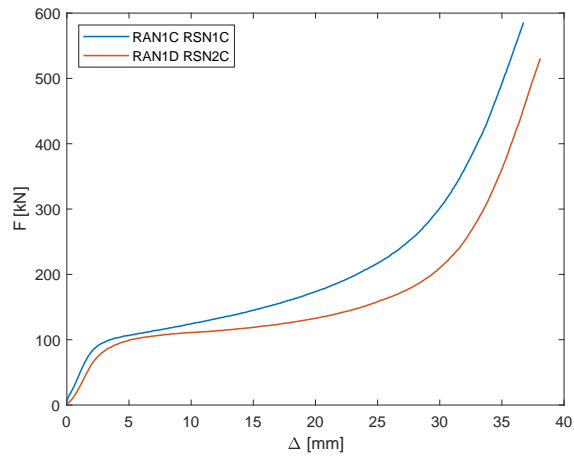


Figure D.49: RANRSN force displacement graph

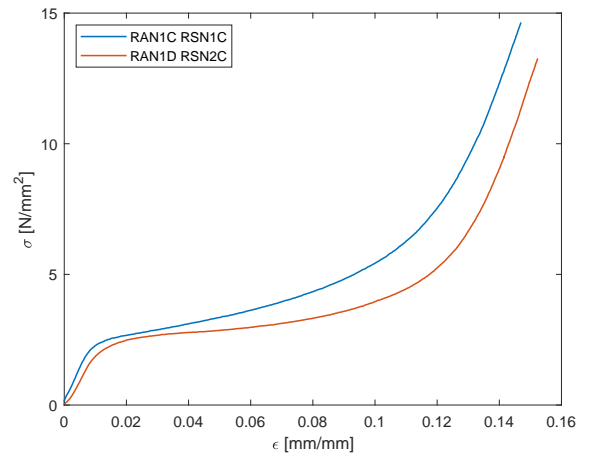


Figure D.50: RANRSN stress strain graph

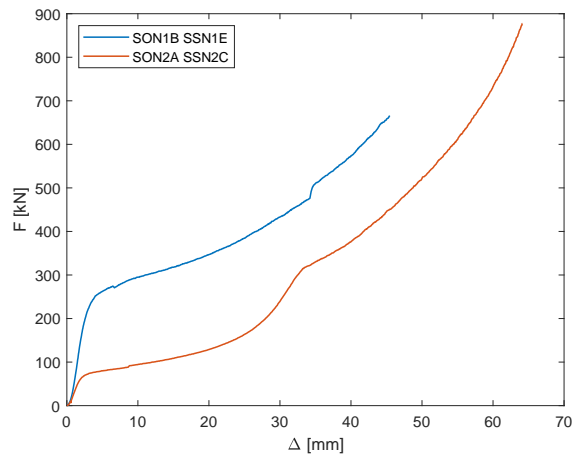


Figure D.51: SONSSN force displacement graph

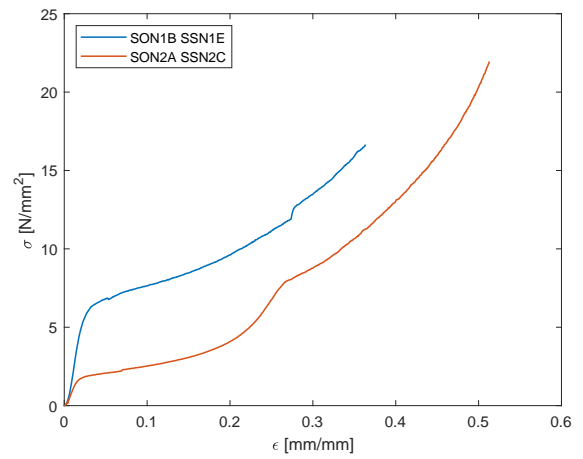


Figure D.52: SONSSN stress strain graph

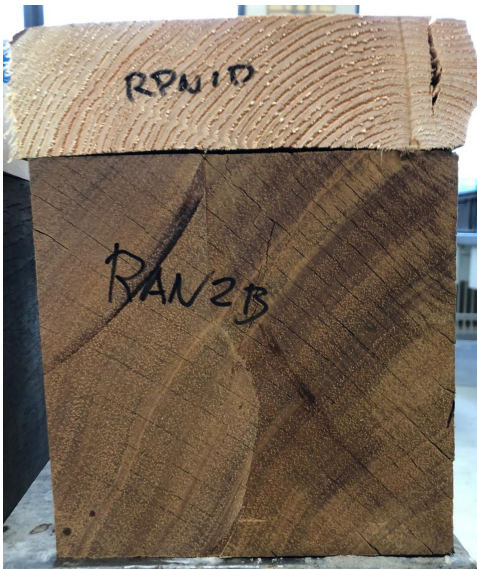


Figure D.53: Compression of Azobe and Pine (RAN RPN)

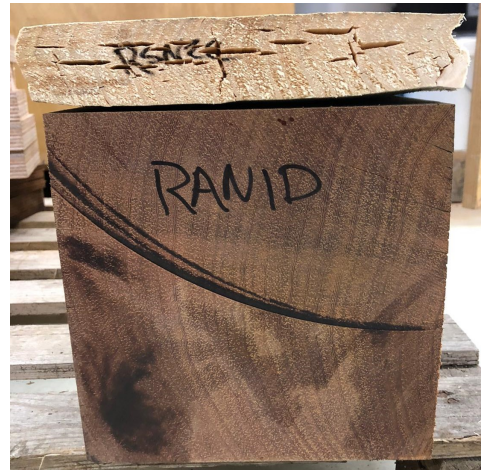


Figure D.54: Compression of Azobe and Spruce (RAN RSN)



Figure D.55: Compression of Oak and LVL (A00 ALN)



Figure D.56: Compression of Oak and LVL (A00 ALO)



Figure D.57: Compression of Oak and Spruce 1 (SON SSN1)



Figure D.58: Compression of Oak and Spruce 2 (SON SSN2)

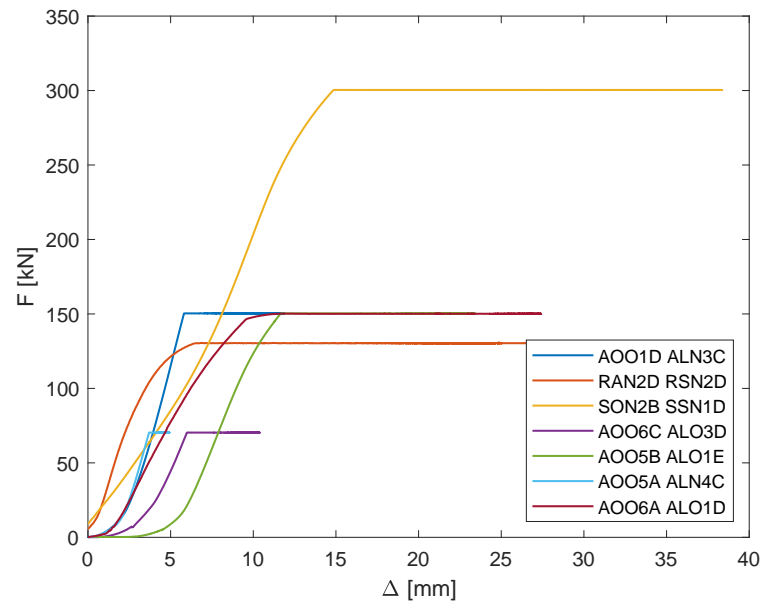


Figure D.59: Force displacement graph for creep



Figure D.60: Creep 1 AOO1D ALN3C



Figure D.61: Creep 2 AOO6A ALO1D



Figure D.62: Creep 3 AOO5B ALO1E



Figure D.63: Creep 4 AOO5A ALN4C



Figure D.64: Creep 5 AOO6C ALO3D



Figure D.65: Creep 6 SON2B SSN1D

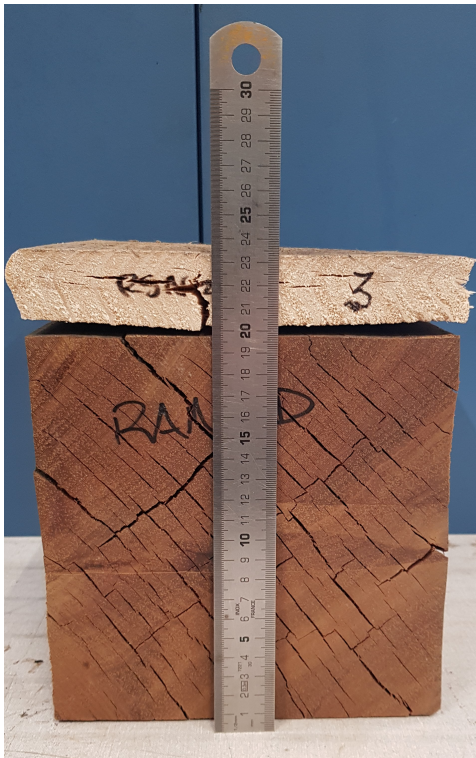


Figure D.66: Creep 7 RAN2D RSN2D



Figure D.67: Creep 8 AOO2D ALO1E Fail

Bibliography

- [1] 2020. URL <https://www.myseatime.com/blog/detail/a-complete-guide-of-bringing-a-ship-to-dry-dock>.
- [2] 2020. URL <https://www.shmgroup.com/blog/dry-docking-procedure-scope-and-advantages/>.
- [3] 2020. URL https://en.wikipedia.org/wiki/Finite_element_method.
- [4] 2021. URL <https://www.marineinsight.com/guidelines/dry-dock-types-of-dry-docks-requirements-for-dry-dock/>.
- [5] Kathem Hassan Ali, Tajdar Hussain, and Arman Kamali. *Compression perpendicular to grain in timber*. Linnaeus University, 2014.
- [6] Olivier Andre Bauchau and J. I Craig. *Aerospace Structural Analysis*. Springer Netherland, 2009.
- [7] Simon Bedert. *Evaluatiemethodiek ten behoeve van het dokken van een schip*. Katholieke Hogeschool Sint-Lieven, 2012.
- [8] Hans Joachim Blass and Rainer Görlacher. *Compression perpendicular to the grain*. Universität Karlsruhe.
- [9] Hans Joachim Blaß and Carmen Sandhaas. *Timber Engineering - Principles for Design*. KIT Scientific Publishing, 2017.
- [10] P Boresi. *Advanced mechanics of materials*. John Wiley Sons, inc., 1924.
- [11] J.S. Breeveld. *Modelling the interaction between structure and soil for shallow foundations*. Delft University of Technology.
- [12] BSI. *Structural timber - Strength classes*. British Standards Institution, 2003.
- [13] Paul S. Crandall. *Floating Dry Docks Their History and Characteristics*. Crandall Dry Dock Engineers, 1964.
- [14] Paul S Crandall. *Problems of dry docking unusual ships*. SNAME, 1966.
- [15] Paul S Crandall. *Dockmaster's manual*. Crandall Dry Dock Engineers, Inc., 1986.
- [16] DAMEN and Emiel Vanhaesebrouck. *Accurate method for predicting dry dock block reactions on a yacht*. Ghent University, 2018.
- [17] M.M. Dolganov. *Onderzoek naar de spreiding van spanning in hout, loodrecht op de vezelrichting, bij verschillende hoogtes van een balk*. Delft University of Technology, 2014.
- [18] F. Elgar. *The Distribution of Pressure Over the Bottom of a Ship in Drydock and Over the Dock Blocks*. SNAME Transactions. SNAME Transactions, 1899.
- [19] G. Falsone. *The Use of Generalised Functions in the Discontinuous Beam Bending Differential Equations*. University of Messina, 2002.
- [20] G. Falsone, P. Colajanni, and A. Recupero. *Simplified Formulation of Solution for Beams on Winkler Foundation allowing Discontinuities due to Loads and Constraints*. University of Messina, 2009.
- [21] V Fogang. *TIMOSHENKO BEAM THEORY EXACT SOLUTION FOR BENDING, SECOND-ORDER ANALYSIS, AND STABILITY*. Creative Commons CC BY, 2020.

- [22] European Committee for Standardization. *Structural timber and glued laminated timber*. Comité Européen de Normalisation (CEN), 2003.
- [23] Y. C. K. Gordon and J. R. William. *A New Method for Computing Keel Block Loads*. The Society of Naval Architecture and Marine Engineering, 1952.
- [24] Cristopher Percival Hall. *Behaviour of wood under compression perpendicular to grain loading*. The University of British Columbia, 1980.
- [25] Robbert E. Heger. *The docking report*. Heger Dry Dock Engineers, 1995.
- [26] INC Heger dry dock. *Dockmaster Training Manual*. Heger dry dock, INC, 2005.
- [27] Charles Hek. *De druksterkte van hardhout onder een hoek met de vezelrichting*. Delft University of Technology, 2014.
- [28] M. Hentenyi. *Beams on elastic foundation*. The university of Michigan, 1979.
- [29] Richard D. Hepburn. *Potential Failure of Surface Ship and Submarine Drydock Blocking Systems Due to Seismic Loadings and Recommended Design Improvements*. The Society of Naval Architects and Marine Engineers, 1988.
- [30] Richard Daniel Hepburn. *Non-Linear Material three degree of freedom analysis of submarine drydock blocking system*. Massachusetts institute of technology, 1988.
- [31] I. Jiang and K. Grubbs. *DRYDOCK: An Interactive Computer Program for Predicting Dry Dock Block Reactions*. SNAME Transactions. Designers & Planners, 1987.
- [32] Forest Products Laboratory. *Wood Handbook*. Forest Products Laboratory, 2010.
- [33] Lloyd's Register Group Limited. *Rules and Regulations for the Classification of Naval Ships*. Ship structures. Lloyd's Register Group Limited, 2020.
- [34] W.H. Macalulay. *Messenger of Mathematics*. Cambridge and Dublin Messenger of Mathematics, 1919.
- [35] B Madsen. *Structural behaviour of timber*. Amer Society of Civil Engineers, 1995.
- [36] A.V. Metrikine. *Dynamics, Slender Structures and an Introduction to Continuum Mechanics*. Delft University of Technology.
- [37] Jeffrey J. Morrell, Guy G. Helsing, and Robert D. Graham. *MARINE WOOD MAINTENANCE MANUAL: A GUIDE FOR PROPER USE OF DOUGLAS-FIR IN MARINE EXPOSURES*. The Forest Research Laboratory, 1984.
- [38] U.S. DEPARTMENT OF THE NAVY. *The National Shipbuilding Research Program*. Strength Properties of Drydocking Timbers and Blocks. U.S. DEPARTMENT OF THE NAVY, 1991.
- [39] Willem Nobel. *De druksterkte van een kesp - Druk loodrecht op de vezel*. Delft University of Technology, 2014.
- [40] P. M. Palermo and J. S. Brock. *Investigation of pressures on keel blocks during drydocking of USS midway*. Navy Department, 1956. URL <http://www.hegerdrydock.com/libraryPdf/Investigation>.
- [41] P Pruijsers. *Dokken op secundaire blokkenlijn*. DSNS, 2013.
- [42] G.J.P Ravenshorst. *Species independent strength grading of structural timber*. Delft University of Technology, 2015.
- [43] Carmen Sandhaas. *MECHANICAL BEHAVIOUR OF TIMBER JOINTS WITH SLOTTED-IN STEEL PLATES*. TU Delft, 2012.

-
- [44] DNV GL SE. *Section 8 Bottom Structures - G Docking Calculation*. Rules for Classification and Construction. DNV GL SE, 2016.
- [45] M Shokrieh. *A comparative study for beams on elastic foundation models to analysis of mode-I delamination in DCB specimens*. Iran University of Science and Technology, 2010.
- [46] A Simone. *An Introduction to the Analysis of Slender Structures*. Delft University of Technology, 2011.
- [47] Brandon M. Taravella. *Best method for predicting dry dock block reactions*. University of New Orleans, 2003.
- [48] Brandon M. Taravella. *Accuracy Assessment of Methods for Predicting Dry Dock Block Reactions*. Marine Technology, 2005.
- [49] I Teodoru. *The Modified Vlasov Foundation Model: An Attractive Approach for Beams Resting on Elastic Supports*. Technical University of Iasi, 2010.
- [50] Ansel C Ugural and Saul K Fenster. *Advanced mechanics of materials and applied elasticity*. Pearson Education, 5 edition, 2012.
- [51] VVNH and G.J.P. Ravenshorst, 2020. URL https://www.houtdatabase.nl/infobladen/Infoblad_Houteigenschappen-Sterktegegevens.pdf.
- [52] Miao Yu. *Closed-form solution of beam on Pasternak foundation under inclined dynamic load*. Technical University of Huazhong, 2017.